BRUKER

Bruker microCT

3D Morphometry and Microdensitometry for Dental and Other Life Science Research

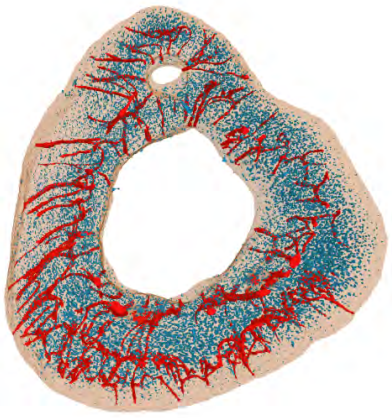

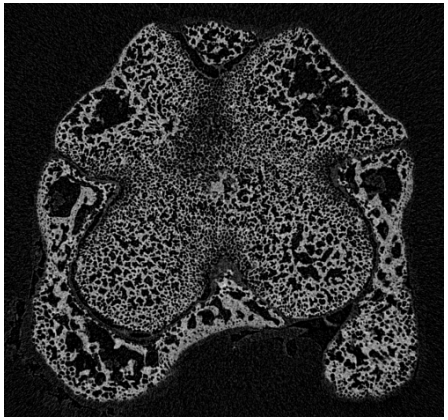

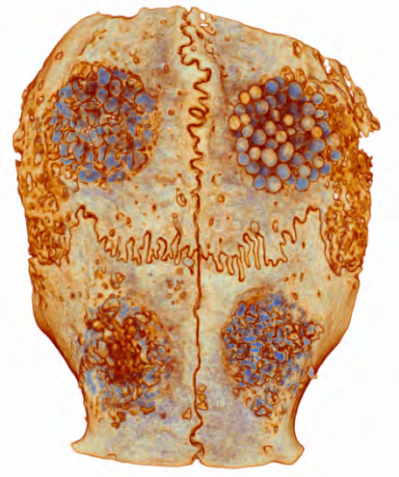

Overview

1. Principles of Micro-Computed X-ray Tomography (“micro-CT”)
   - Scanning Workflow of uCT
   - Mechanical Setup
   - X-ray Attenuation
   - How reconstruction works
   - Analysis Workflow
2. SkyScan 1172
3. Solutions for Life Science Applications
4. New Features in DataViewer, CTVox, CTAN

What is tomography?

1. **“Scan”**
A set of x-ray “projection” images are taken over a rotation of the imaging axis of 180 or 360 degrees

2. **“Reconstruction”**
The“projection” images are processed by the filtered Feldkamp cone-beam method to create the stack of crossection slices

3. **“Analysis and visualisation”**
The reconstructed crossection slices are processed into 3d models for morphometric measurements and virtual visual inspection

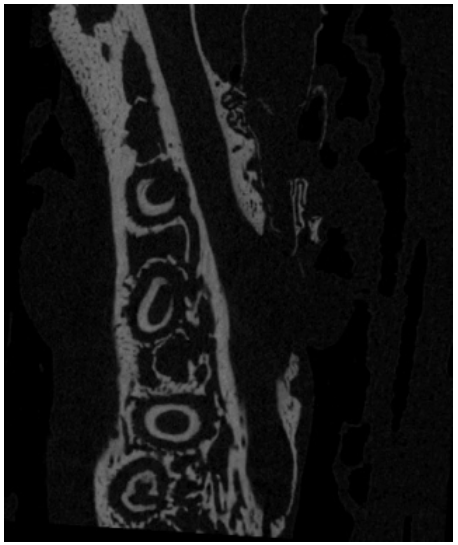

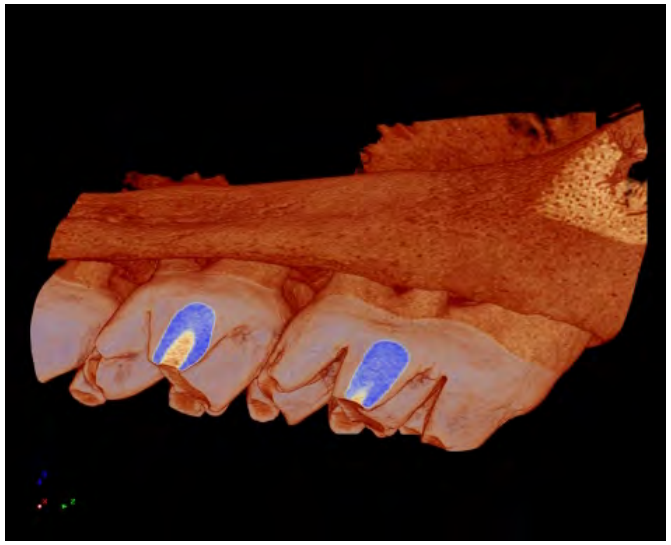

The *in vivo* and *ex vivo* methods of microCT

In the **"*ex vivo*"** scanner type, the sample rotates on a stage around a vertical axis, allowing angular projection images over 360 degrees

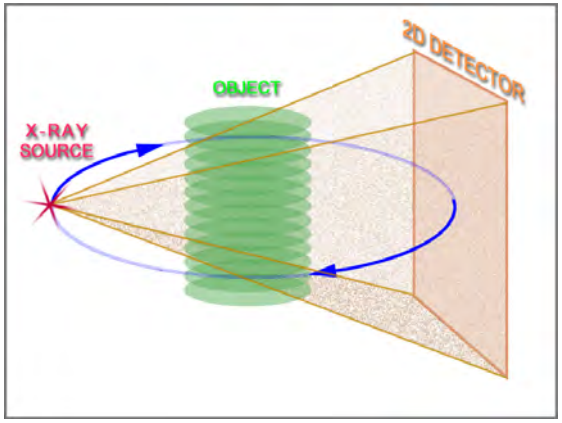

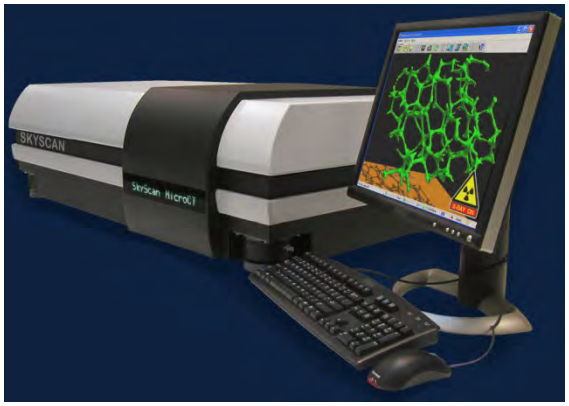

In the **"*in vivo*"** scanner type, the sample – e.g. a live mouse or rat – lies still on a horizontal bed, while x-ray source and camera rotate around the sample bed,
over 360 degrees

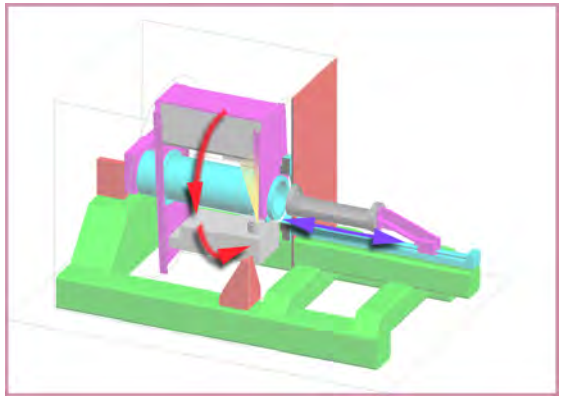

Trabecular and cortical
VOI selection

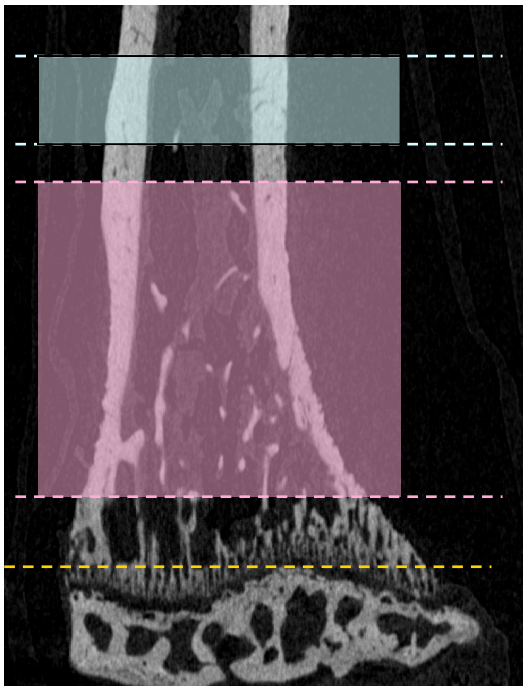

Cortical VOI

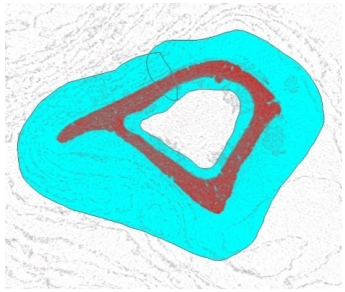

Trabecular VOI

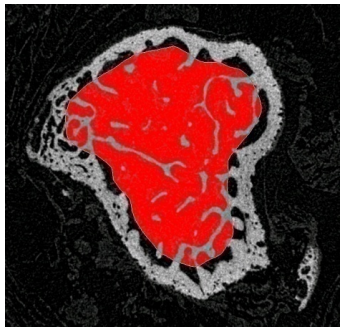

Growth plate reference

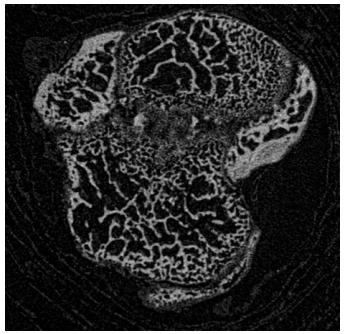

Micro-CT analysis pathway

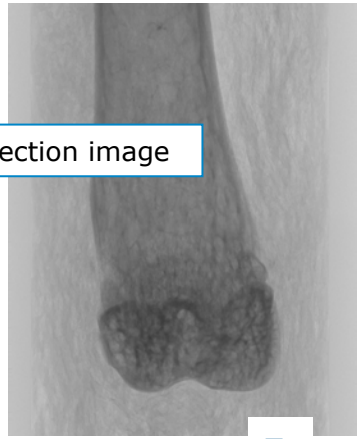

Projection image

reconstruction

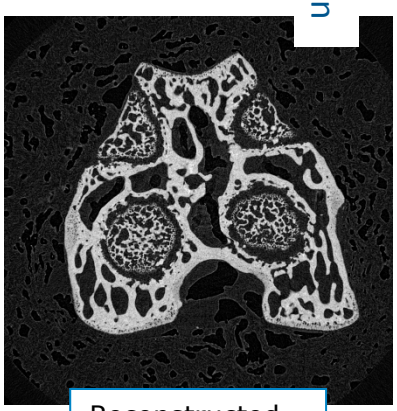

Reconstructed crossection

Volume-rendering

Surface-rendering

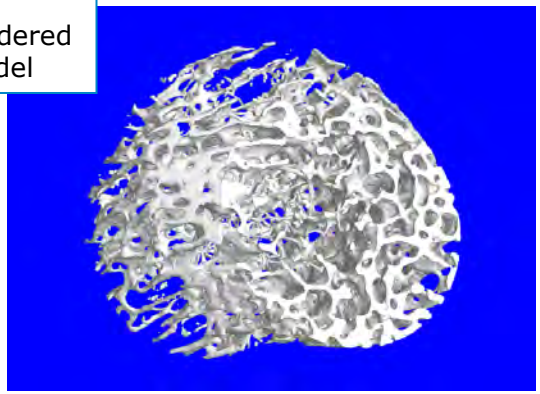

3D rendered model

thresholding

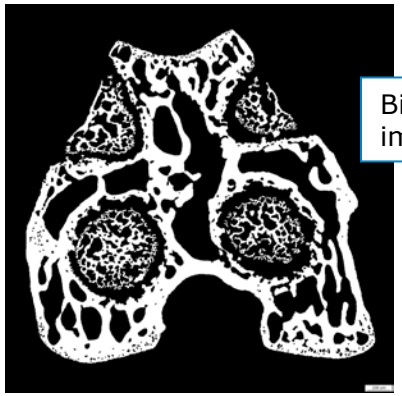

Binary image

3D Morpho-metric data

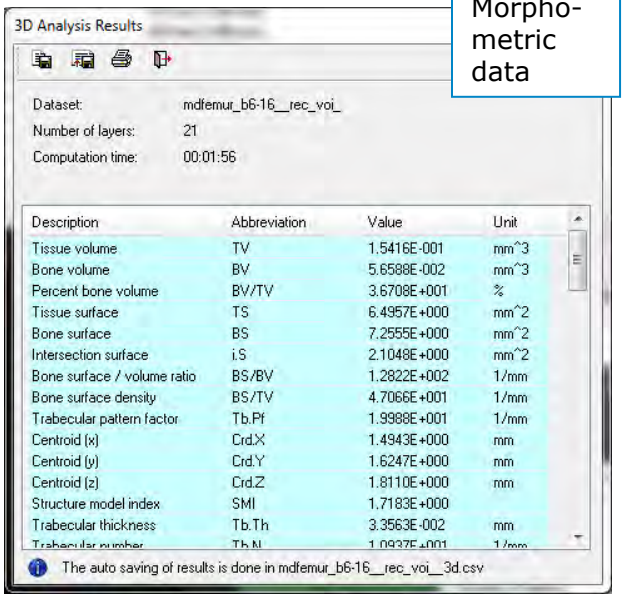

3D Morphometry

BMD histogram

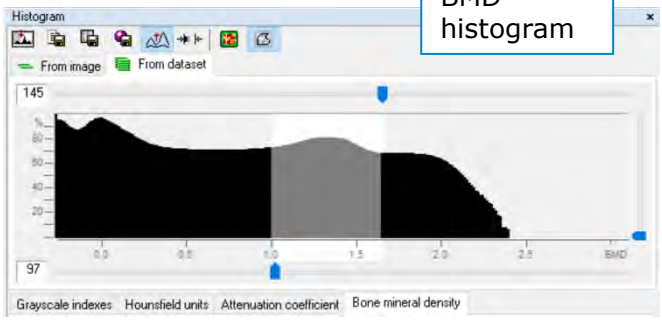

BMD calibrated densitometry

X-ray attenuation

Röntgen: The attenuation of x-rays of wavelength λ is

$$\mathbf{I/I_0 = \exp(-\mu x)} \quad , \quad \mathbf{(1)}$$

where I_0 is the intensity of the unattenuated x-ray beam,
I is the beam's intensity after traversing
x thickness of (homogeneous) material (in cm) with
μ being the linear attenuation coefficient (in cm^{-1}).

In terms of the mass attenuation coefficient μ/ρ (units cm^2/g)

$$\mathbf{I/I_0 = \exp[(-\mu/\rho)\,\rho\, x)]} \quad . \quad \mathbf{(2)}$$

In terms of what happens in each thickness element d*x*

$$\mathbf{dI/I = -(\mu/\rho)\,\rho\, dx} \quad . \quad \mathbf{(3)}$$

Slide courtesy of Dr. Stuart Stock, Northwestern University

Adding the increments of the attenuation along the direction of x-ray propagation yields the more general form

$$I = I_0 \exp\left[-\int \mu(s)\, ds\right] \quad , \quad (4)$$

where μ(s) is the linear absorption coefficient at position s along ray s. The problem is assigning the correct value of μ to each position along this ray (and along all the other rays traversing the sample) knowing only the values of the line integral for the various orientations of s, i.e.,

$$\int \mu(s)\, ds = \ln(I_0/I) \quad . \quad (5)$$

For compounds or mixtures and wt. fractions w_i

$$\langle\mu\rangle = \sum w_i (\mu/\rho)_i \langle\rho\rangle \quad . (6)$$

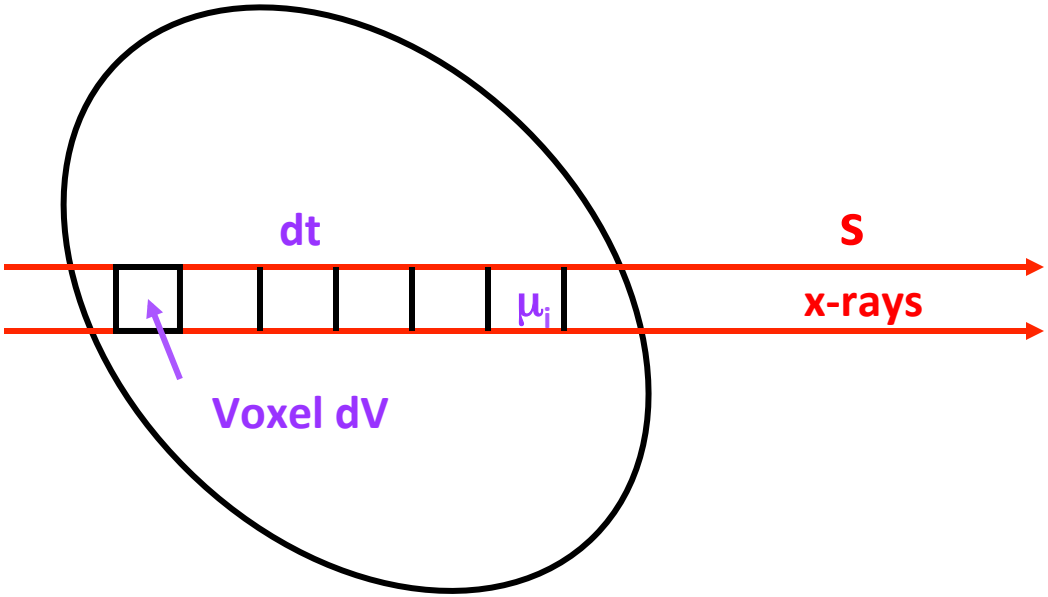

Slide courtesy of Dr. Stuart Stock, Northwestern University

Cartoon of back projection reconstruction

Absorption profiles from an idealized specimen.

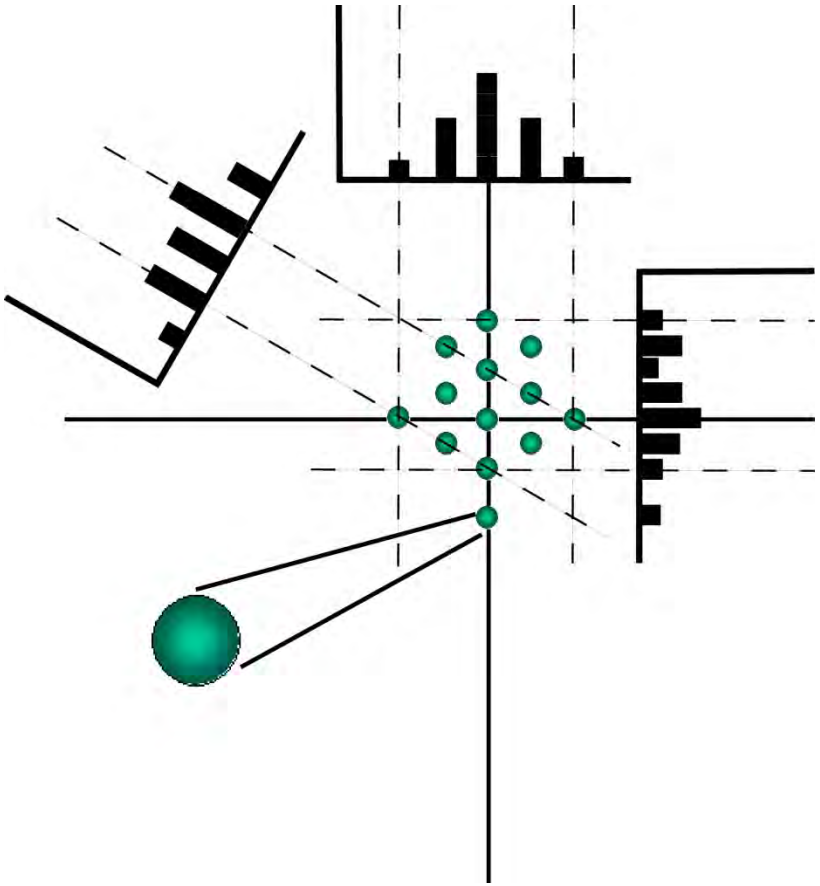

Slide courtesy of Dr. Stuart Stock, Northwestern University

Back projection (2)

First profile projected

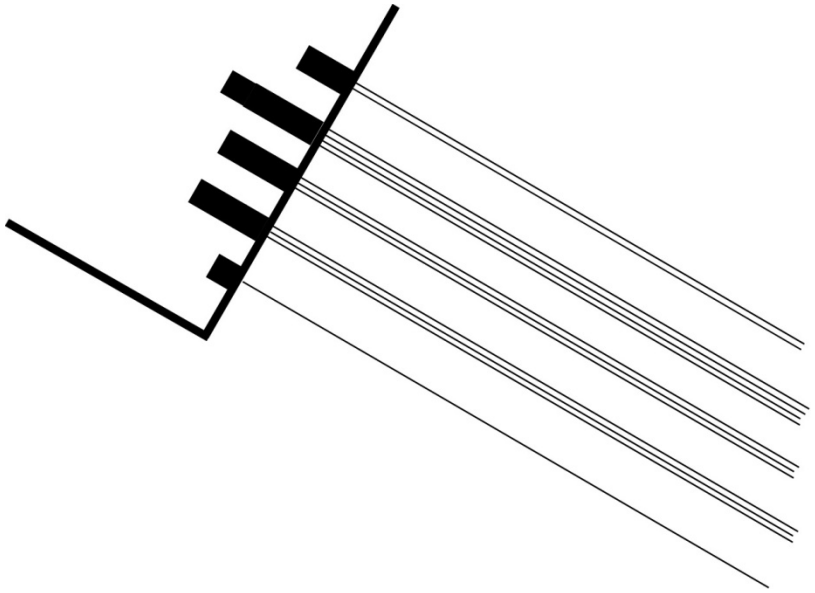

Second profile projected

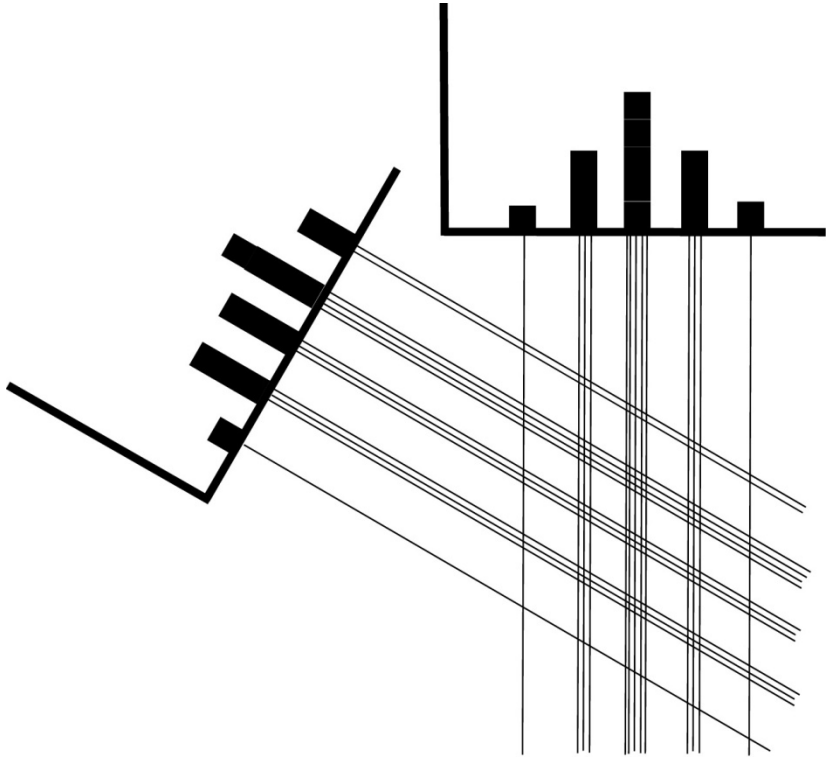

Slide courtesy of Dr. Stuart Stock, Northwestern University

Back projection (3)

Third profile projected

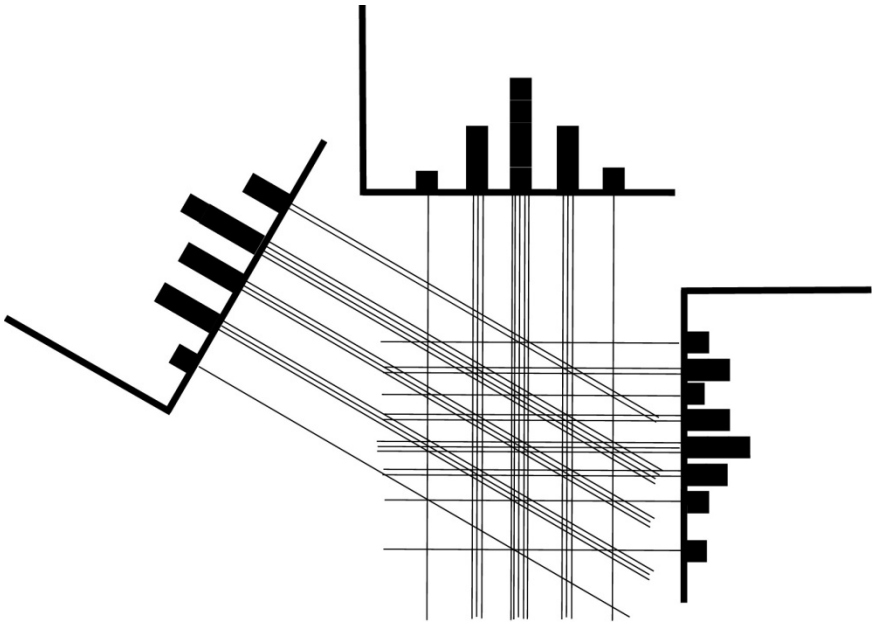

Objects identified

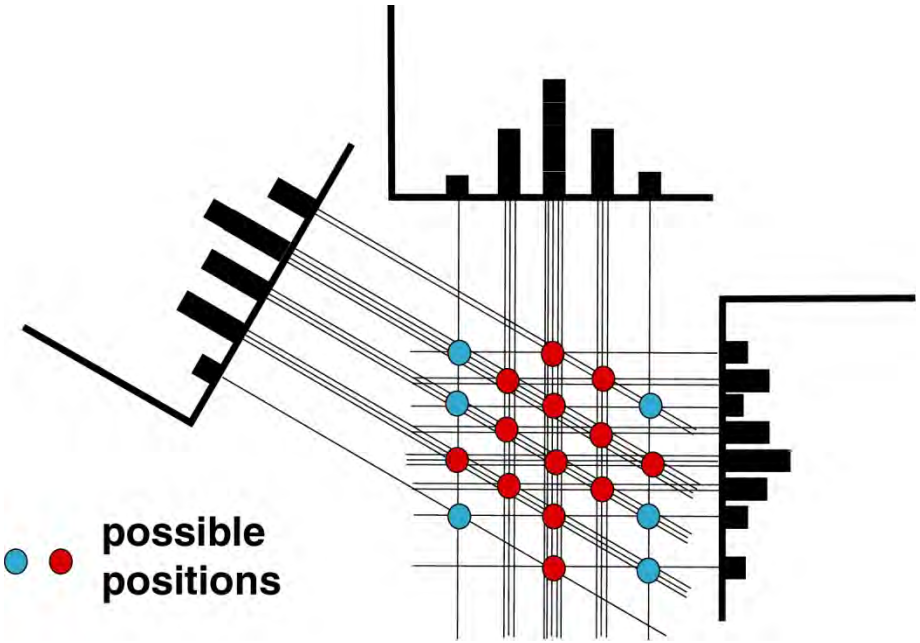

Slide courtesy of Dr. Stuart Stock, Northwestern University

Relative error in thickness measurements from partial volumes – threshold one-half of voxel

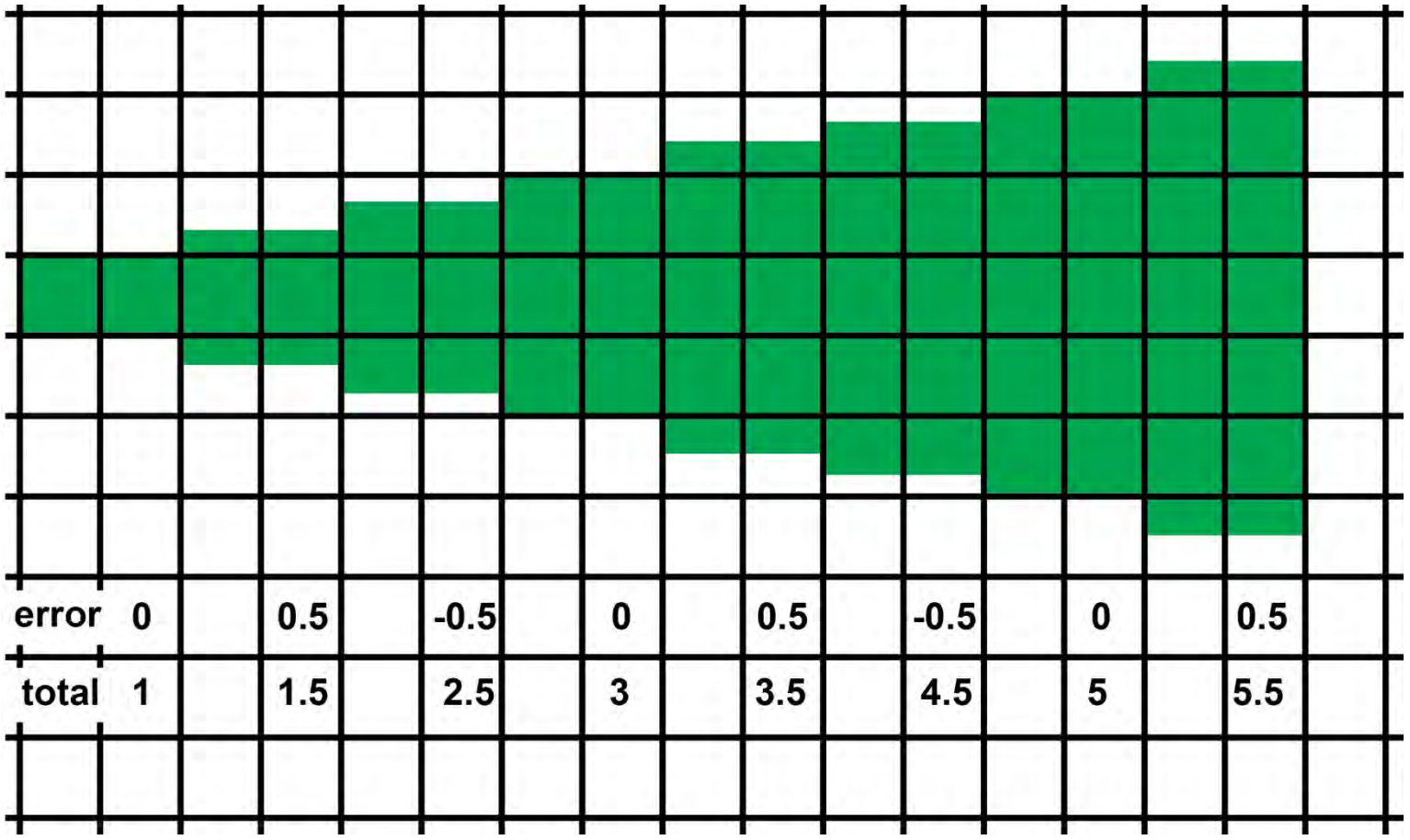

Slide courtesy of Dr. Stuart Stock, Northwestern University

Importance of Contrast Resolution

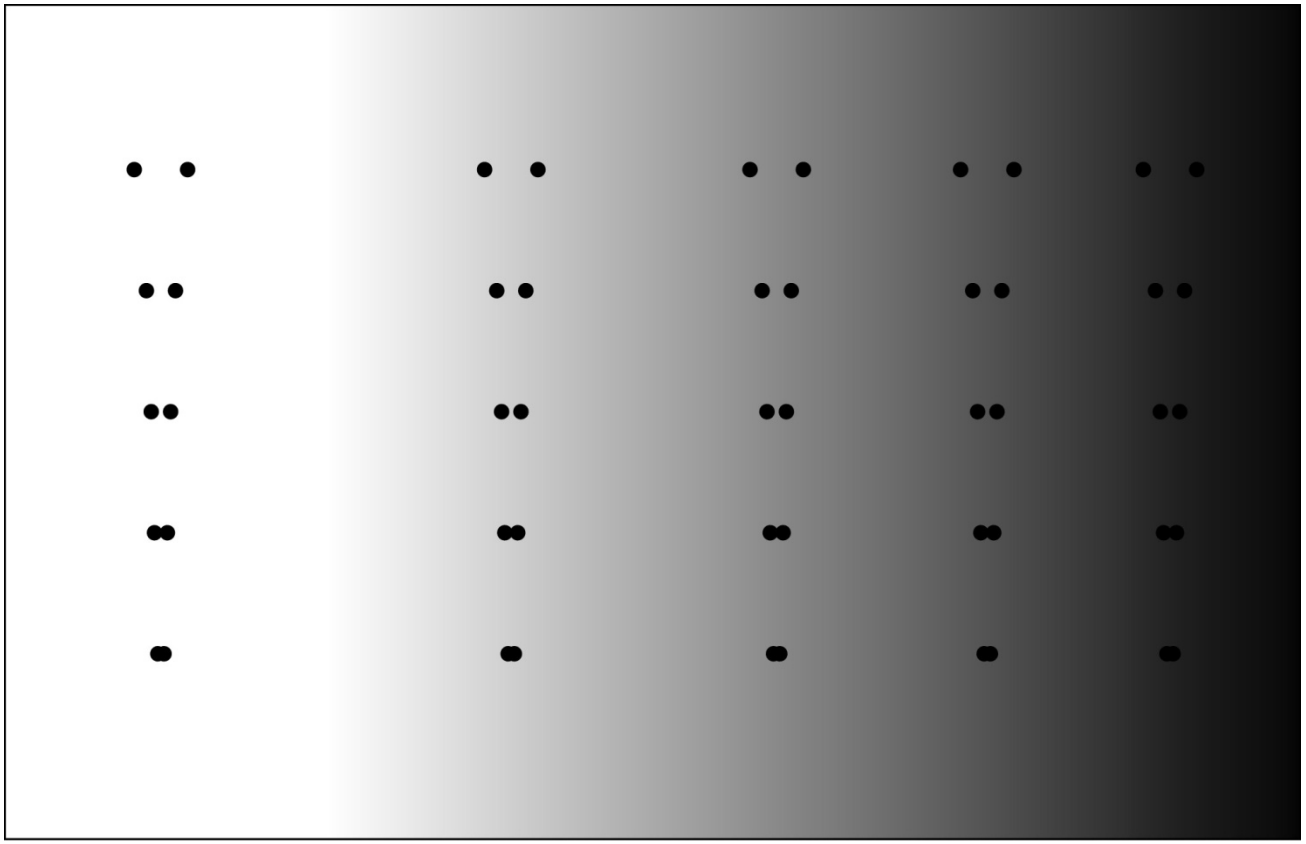

Reproduced from SR Stock, MicroComputed Tomography Methodology and Applications, In press 2008. © CRC Press/Taylor and Francis

X-ray density contrast in biological samples

Photoelectric absorption (τ) is very strongly dependent on the atomic number Z of the absorbing material.

$$\tau \propto \frac{Z^4}{E^{3.5}}$$

X-ray density therefore is primarily determined by a materials *elemental composition* and the position of these elements in the periodic table

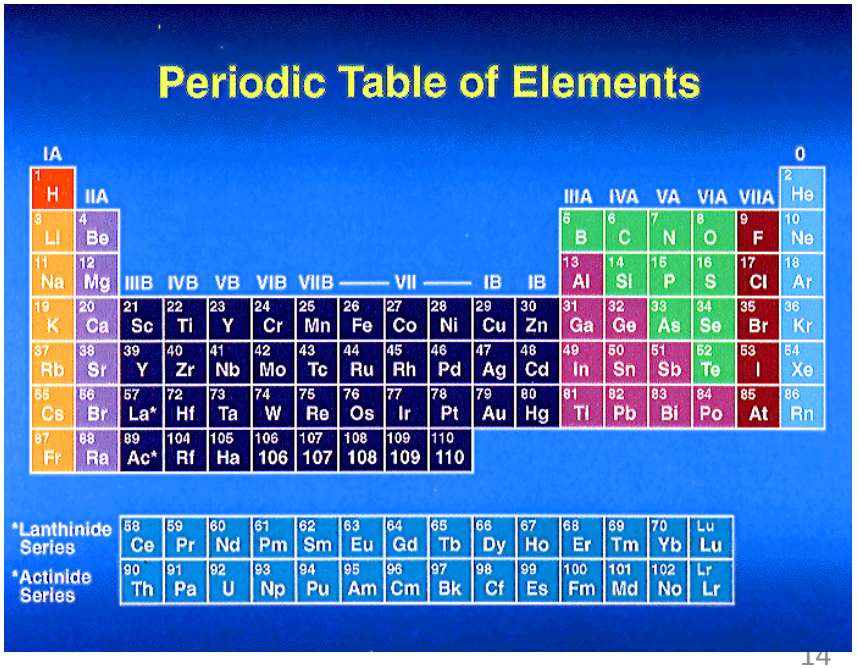

Atomic compositions of some biological tissues

	H	C	N	O	Na	Mg	P	S	Cl	K	Ca
Atomic number Z	1	6	7	8	11	12	15	16	17	19	20
Tissue: percent content by mass											
Fat	11.4	59.8	0.7	27.8	0.1			0.1	0.1		
(Water)	11.2			88.8							
Blood	10.2	11.0	3.3	74.5	0.1		0.1	0.2	0.3	0.2	
Liver	10.2	13.9	3.0	71.6	0.3		0.2	0.3	0.2	0.3	
Brain	10.7	14.5	2.2	71.2	0.2		0.4	0.2	0.3	0.3	
Bone	3.4	15.5	4.2	43.5	0.1		10.3	0.3			22.5

Four biological tissues can be resolved by x-ray micro-CT due to natural absorption contrast

- Bone
- Lean tissue
- Fat
- Lung

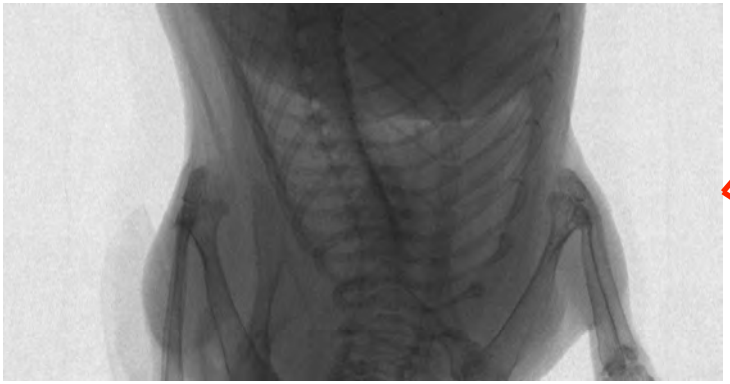

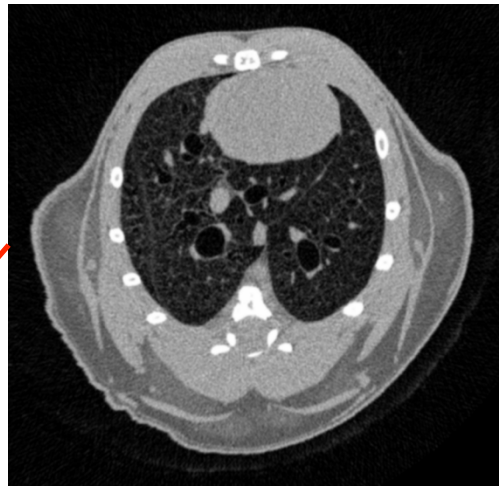

However contrast can be added by the use of contrast agents, such as resins containing heavy elements (e.g. Microfil™)

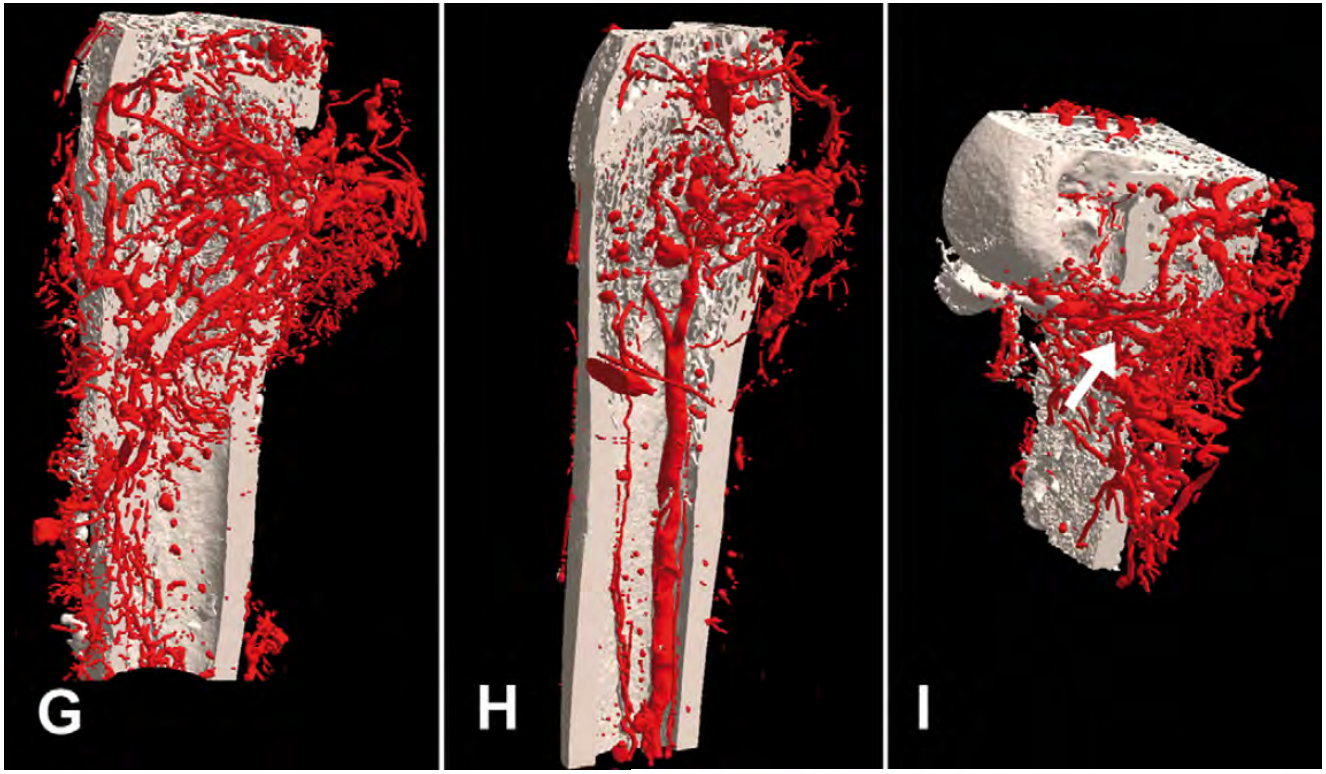

OPEN ACCESS Freely available online

PLoS one

Three-Dimensional Characterization of the Vascular Bed in Bone Metastasis of the Rat by Microcomputed Tomography (MicroCT)

Hervé Nyangoga, Philippe Mercier, Hélène Libouban, Michel Félix Baslé, Daniel Chappard*

INSERM, U922 – LHEA, IRIS-IBS Institut de Biologie en Santé, CHU d'Angers, Angers, France

2D histomorphometry requires **indirect model assumptions** to make 3D parameter estimates

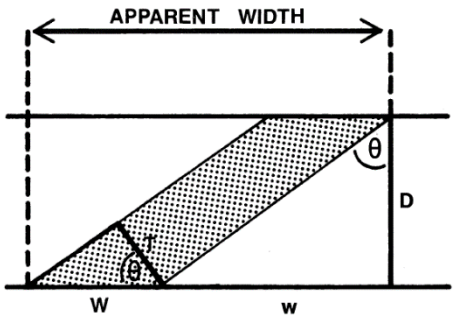

1. $w/D = Tan\theta$, so $w = D\,Tan\theta$

2. $T/W = Cos\theta$, so $W = T/Cos\theta$

3. $w/W = \frac{D}{T} Tan\theta\, Cos\theta = \frac{D}{T} Sin\theta$

The mean value of $Sin\theta$ is given by:

4. $\overline{Sin\theta} = \int \frac{Sin\theta\, d\theta}{\theta} = \frac{-Cos\theta}{\theta}$

Assuming all values of θ between 0 and 90 ($\pi/2$ radians) to be equally likely, the mean value of w/W ($\overline{w}/\overline{W}$) is given by:

$$\overline{w/W} = \frac{2}{\pi} \cdot \frac{D}{T} (-Cos\, \pi/2 + Cos\theta)$$

$$= \frac{2}{\pi} \cdot \frac{D}{T} = \frac{2}{\pi} R, \text{ where } R = \frac{D}{T}$$

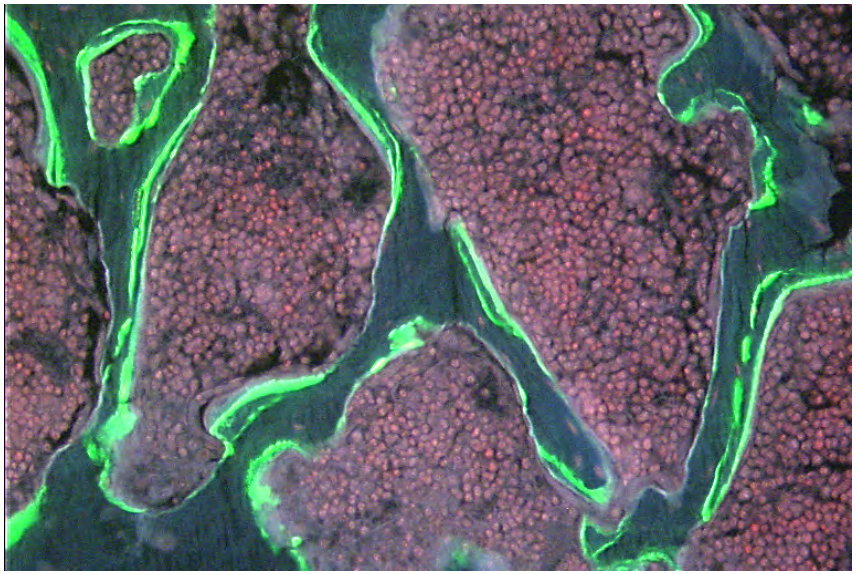

TABLE 4. DERIVED INDICES IN BONE HISTOMORPHOMETRY

Type of index	*Name of index*[a]	*Abbreviation*[a]	*Formula*[b]
I. *Structural*	Trabecular number	Tb.N	(BV/TV)/Tb.Th[c]
	Trabecular separation	Tb.Sp	(1/Tb.N) − Tb.Th[c]
II. *Kinetic*	Mineralizing surface[d]	MS	(dLS + sLS/2)/BS[e]
	Mineral apposition rate	MAR	Ir.L.Th/Ir.L.t
	Adjusted apposition rate[f]	Aj.AR	MAR*(MS/OS)
	Osteoid apposition rate	OAR	same[g]
	Mineral formation rate[d]	MFR	MAR*(MS/BS)
	Bone formation rate[d]	BFR	same[g]
	Bone resorption rate[d]	BRs.R	see text
	Mineralization lag time	Mlt	O.Th/Aj. AR
	Osteoid maturation time	Omt	O.Th/MAR[h]
	Formation period	FP	W.Th/Aj.AR
	Resorption period	Rs.P	FP*(Oc.S/OS)[h]
	Reversal period	Rv.P	FP*(ES − Oc.S)/OS
	Remodeling period[i]	Rm.P	FP*(ES + OS)/OS
	BMU lifespan (sigma)	Sg (or σ)	see text
	Quiescent period	QP	FP*(QS/OS)
	Total period[j]	Tt.P	FP*(BS/OS)
	Activation frequency[k]	Ac.f[l]	(1/Tt.P)

By contrast, micro-CT morphometry of bone makes DIRECT MEASUREMENTS in 3D, no model assumptions

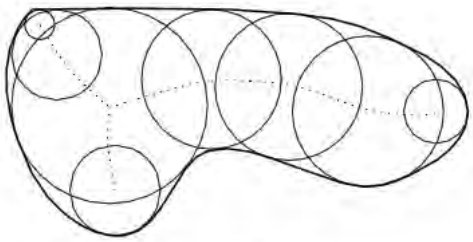

Fig. 1. Medial axis with circles.

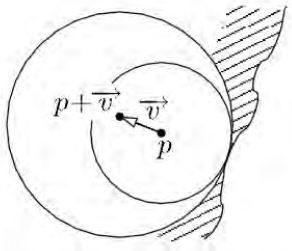

Fig. 4. Balls inside the shape.

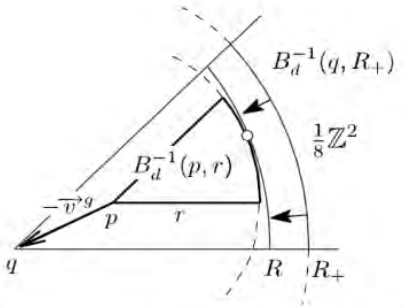

Fig. 7. Covering test on two balls restricted to $\frac{1}{8}\mathbb{Z}^2$.

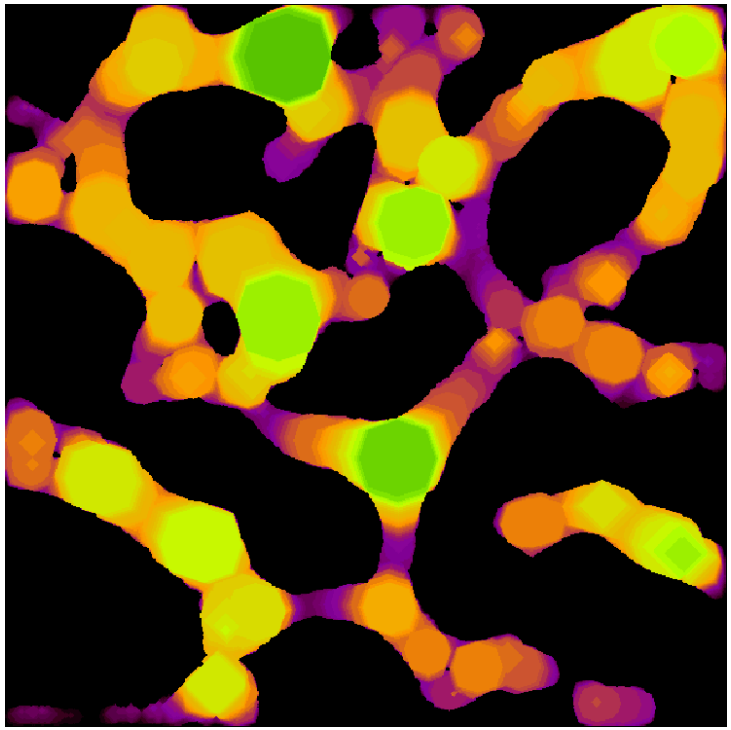

Color-coded thickness map in cortical bone
Haversian canals (SkyScan1172 scan)

Overview

1. Principles of micro-computed x-ray tomography (“micro-CT”)
2. SkyScan 1172
   - Specifications
   - Adaptive Geometry
   - Thermal Correction
   - In Situ Stages
3. Solutions for Life Science Applications
4. New Features in DataViewer, CTVox, CTAN

The SkyScan 1172 High Resolution Micro-CT

SkyScan 1172	
Min. voxel size	0.6 µm
Max.sample FOV*	50 x 70 mm
Max. X-ray voltage	100 kV
X-ray camera mega-pixels	11 Mp (4000 x 2670)
Key advantages	Resolution, speed (adaptive geometry), high throughput, versatility – wide range of applications

Adaptive Geometry

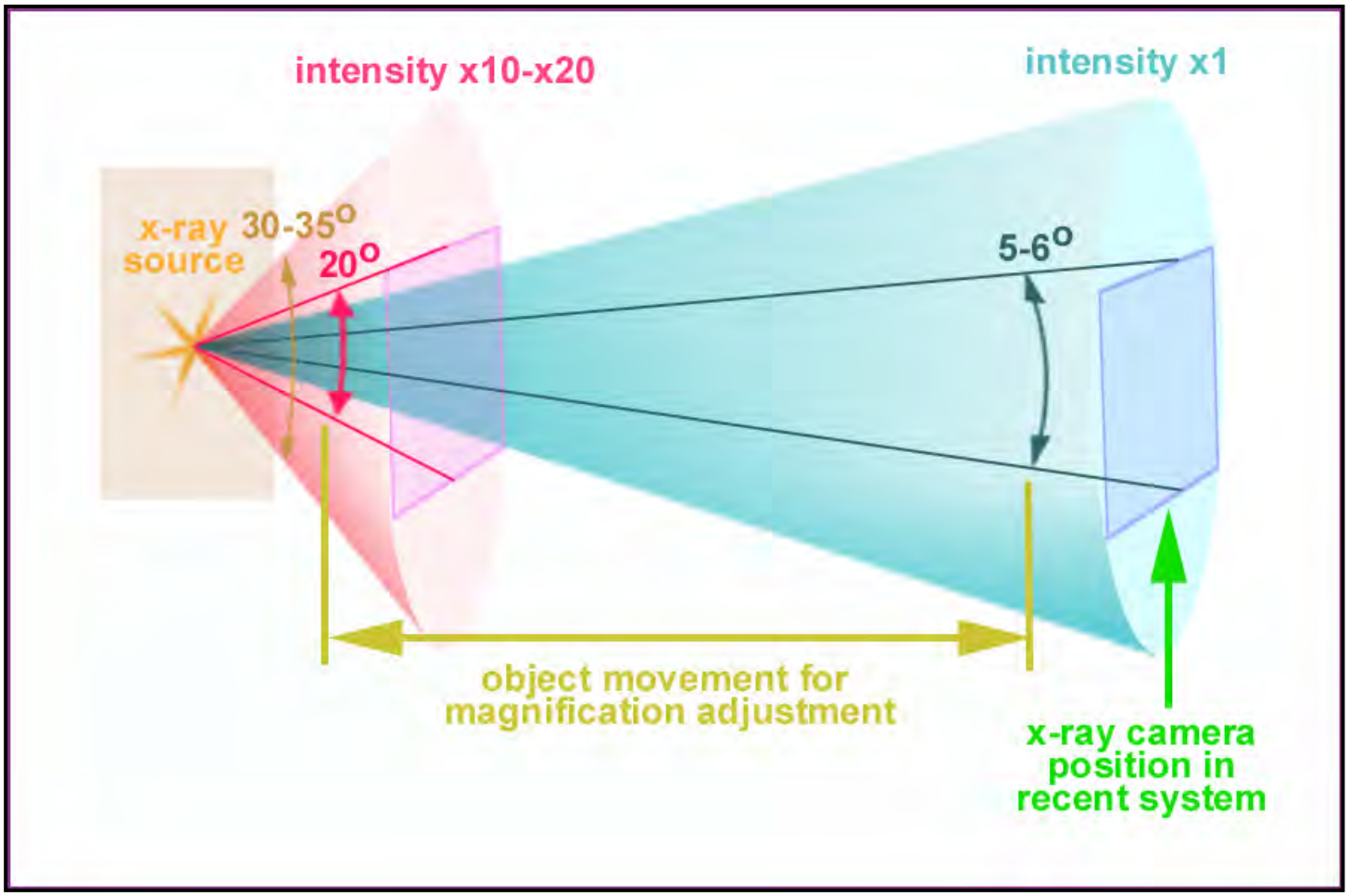

The SkyScan 1172 High Resolution Micro-CT

Adaptive Geometry

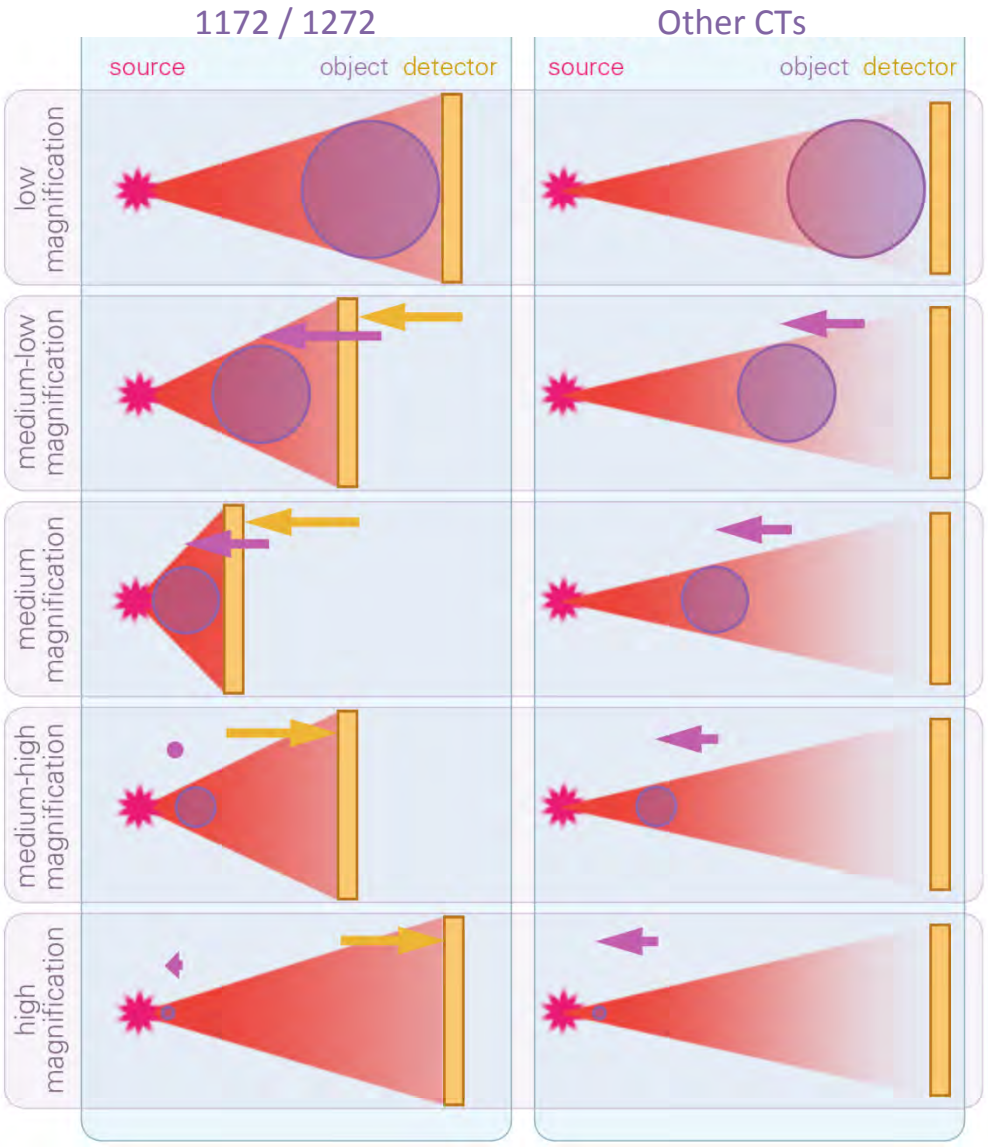

SkyScan 1172 / 1272 are the only scanner with Adaptive Geometry

Projection Pixel Shift Correction

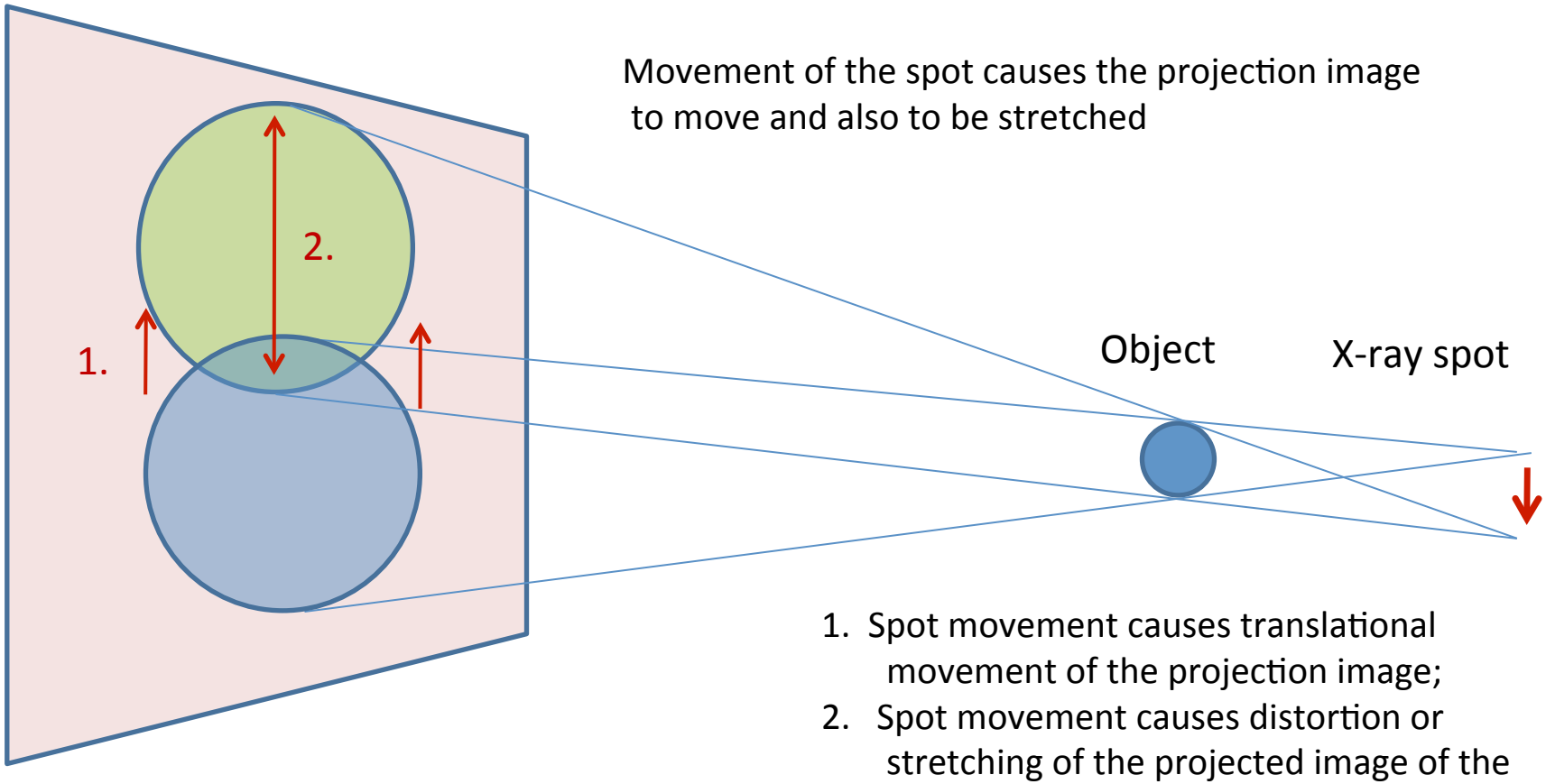

1. Spot movement causes translational movement of the projection image;
2. Spot movement causes distortion or stretching of the projected image of the object

In Situ Stages

Materials Testing Stage

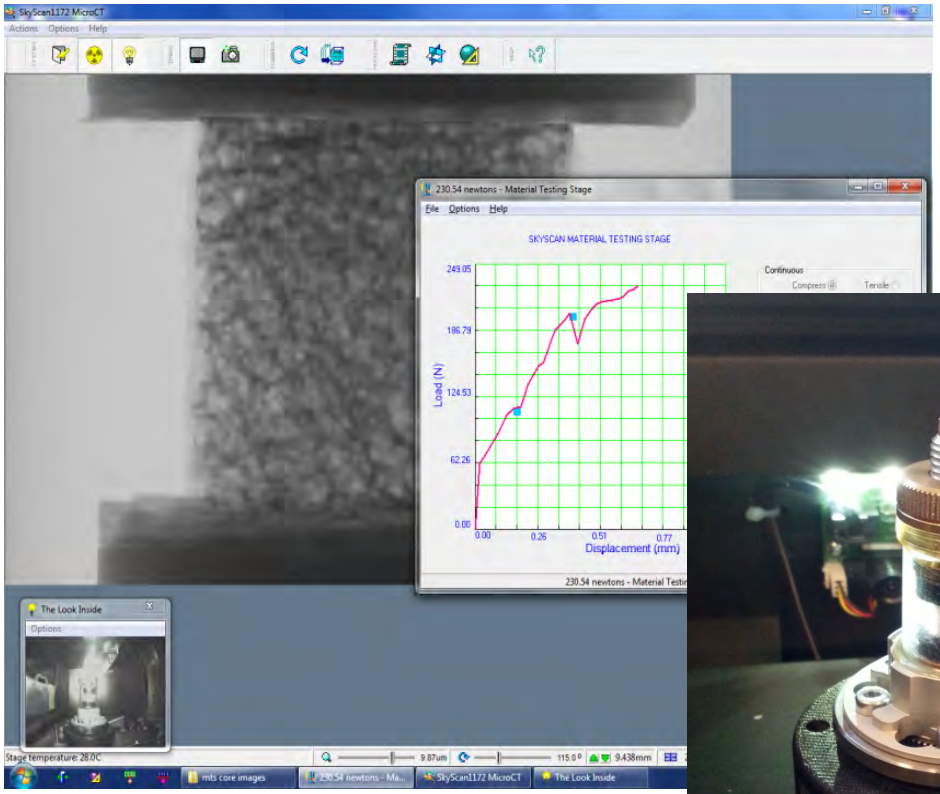

Overview

1. Principles of micro-computed x-ray tomography (“micro-CT”)
2. SkyScan 1172
3. Solutions for Life Science Applications
   - Dental (Teeth)
   - Dental (Scaffolds)
   - Bone
   - Bone (Biomechanics / Implants)
   - Soft Tissue
4. New Features in DataViewer, CTVox, CTAN

Orthodontic analysis of the mouse mandible

- The molars can be automatically separated from the rest of the mandible by the image processing tools

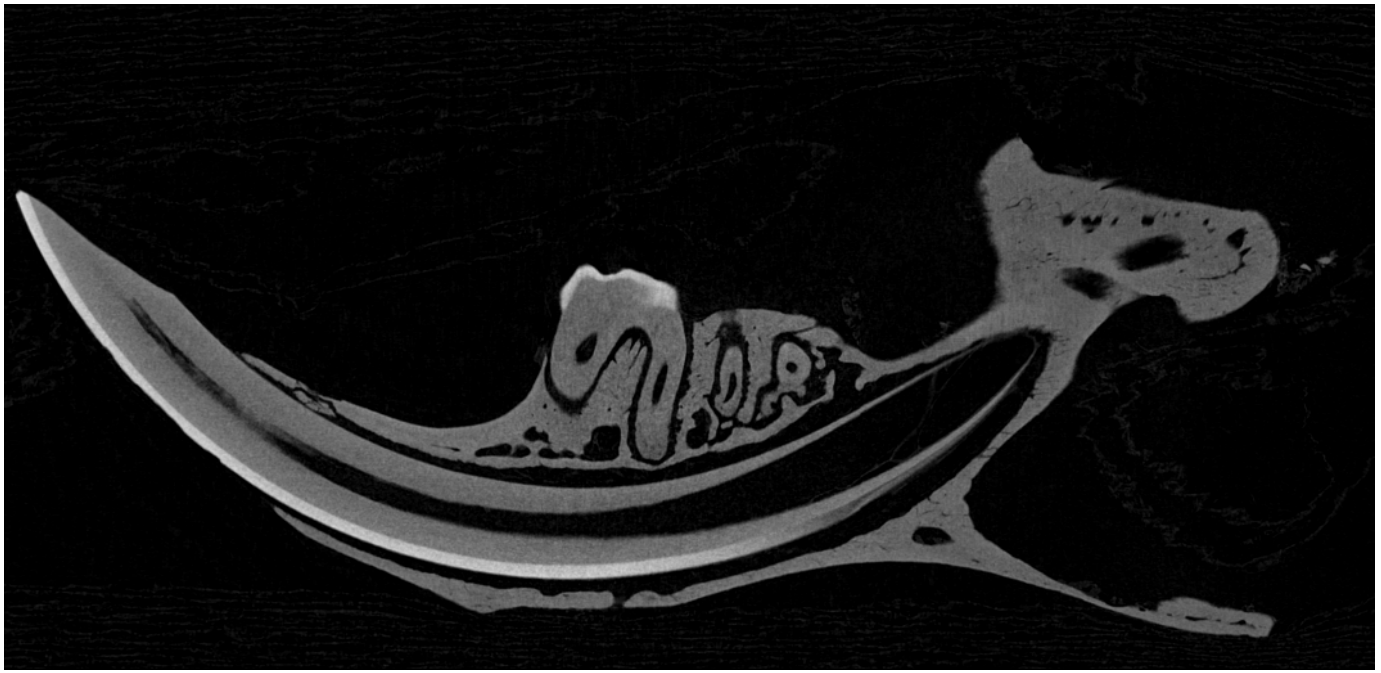

SkyScan 1172, 6 micron voxel

Separation of molars from the mandible by size criteria. *Note: periodontal ligament separates the molars from mandibular bone*

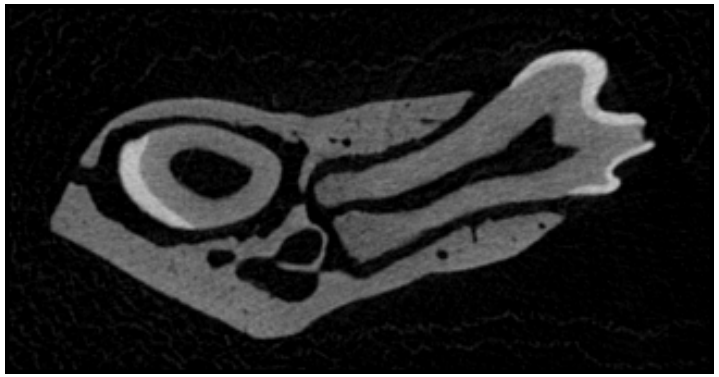

1. Crossection

2. Binarised whole image

3. Mandible > molars: remove smaller part

4. Molars < mandible: remove larger part

- 3D animation of separated mandible and molars

Imaging of human tooth samples

- Preliminary micro-CT results from analysis of MIH (molar incisor hypomineralisation) tooth samples

MIH tooth sample 1

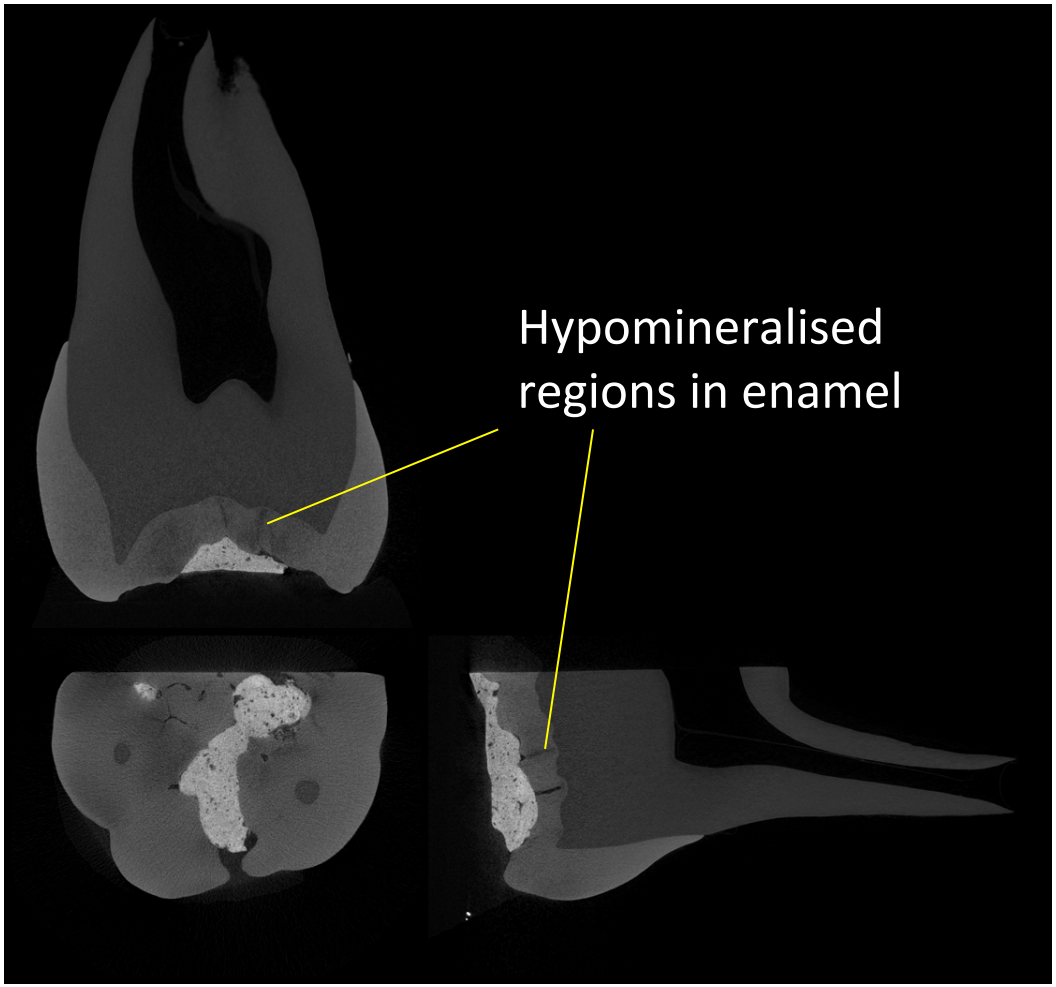

MIH tooth sample 2

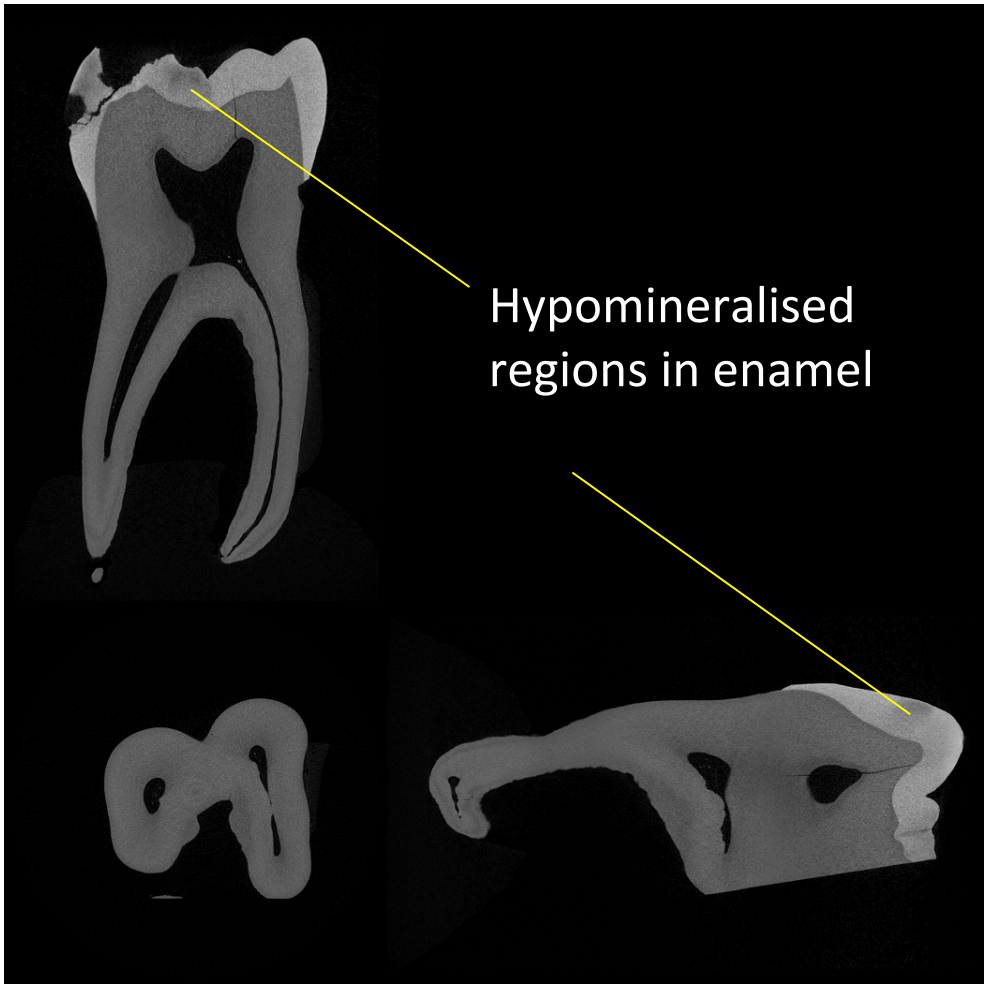

Surface modeling of an MIH tooth (CTVol)

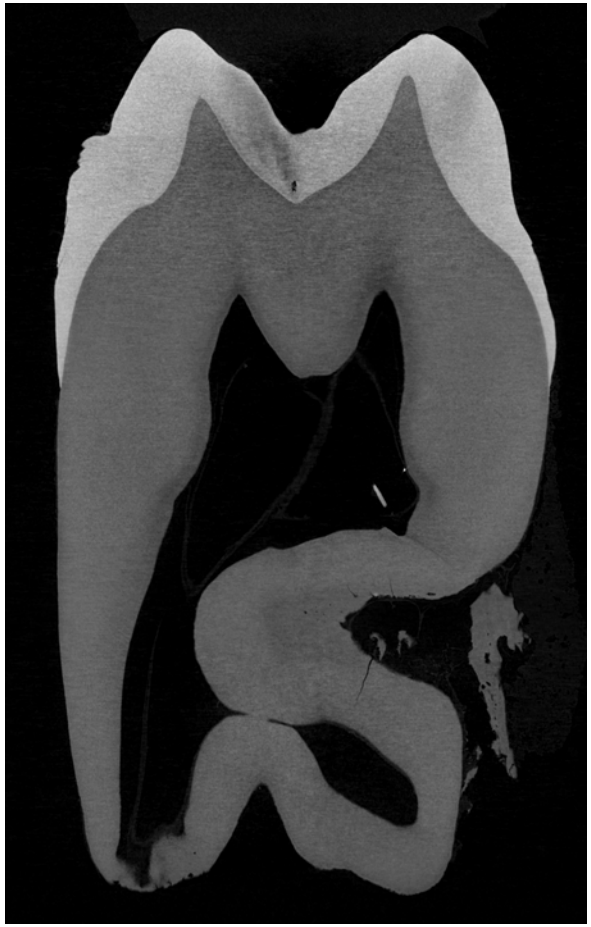

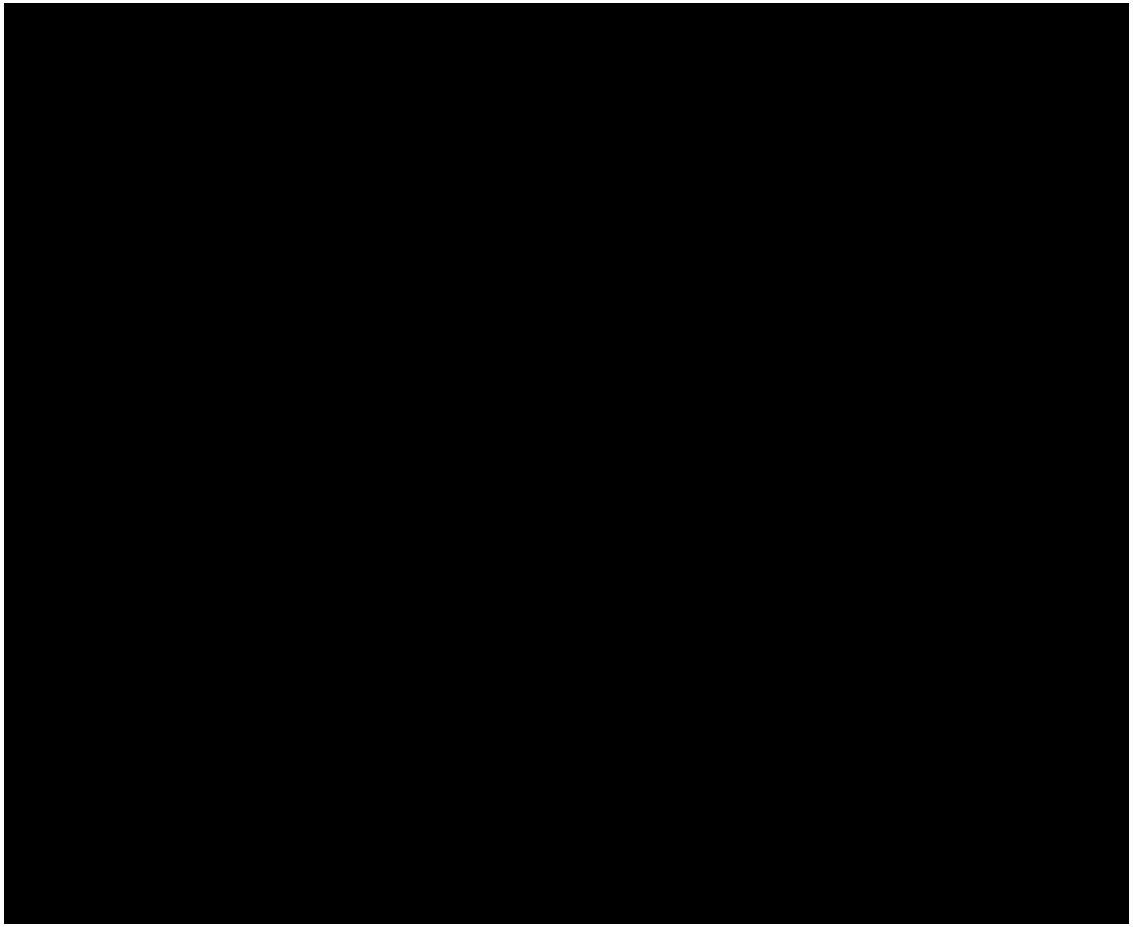

Enamel crown with treatment applied

Surface rendering

Volume rendering

Tooth with implant material lining the pulp cavity

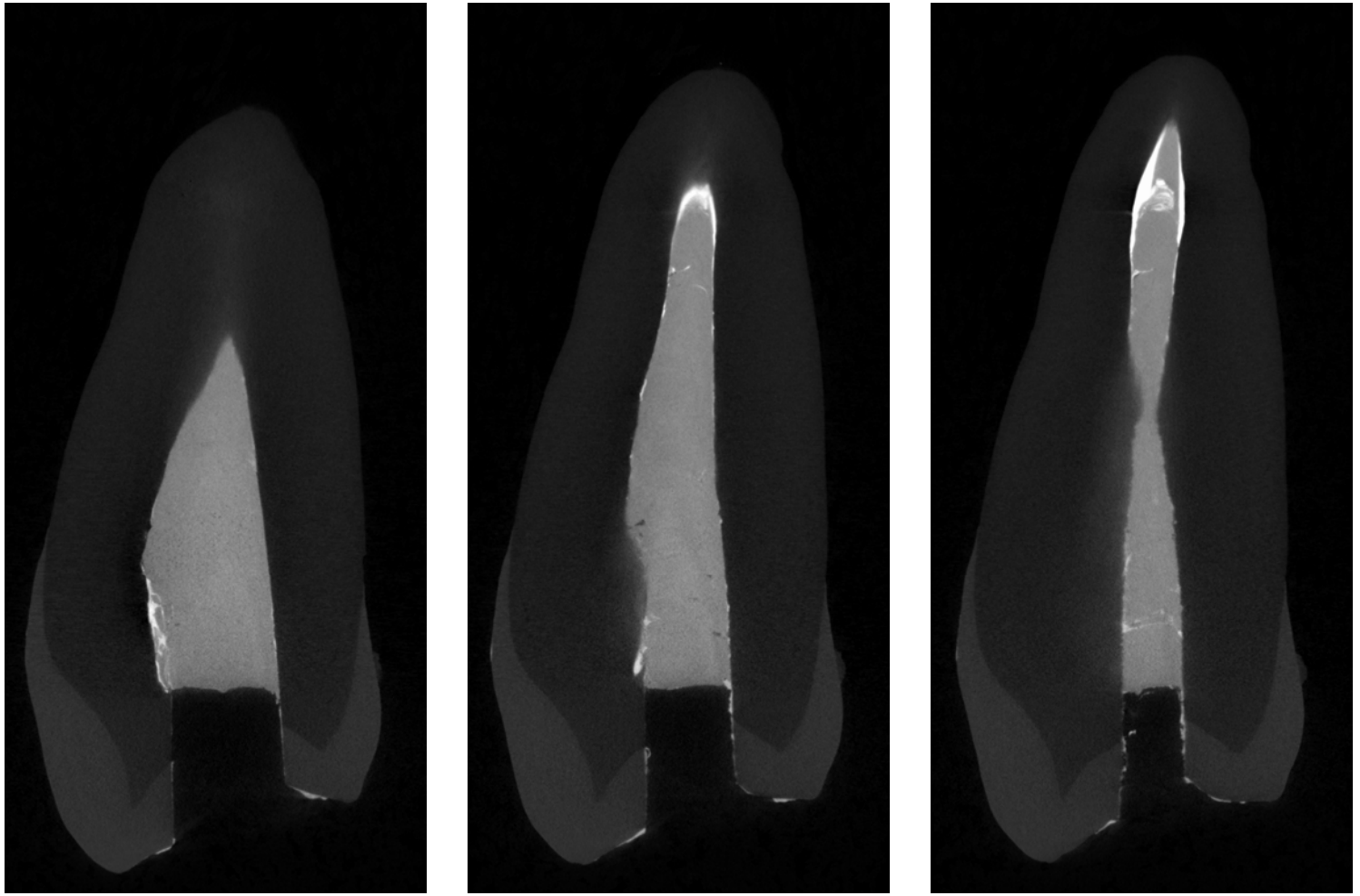

Three-dimensional Evaluation of Effectiveness of Hand and Rotary Instrumentation for Retreatment of Canals Filled with Different Materials

Mohammad Hammad, MSc, Alison Qualtrough, PhD, and Nick Silikas, PhD

(J Endod 2008;34:1370–1373)

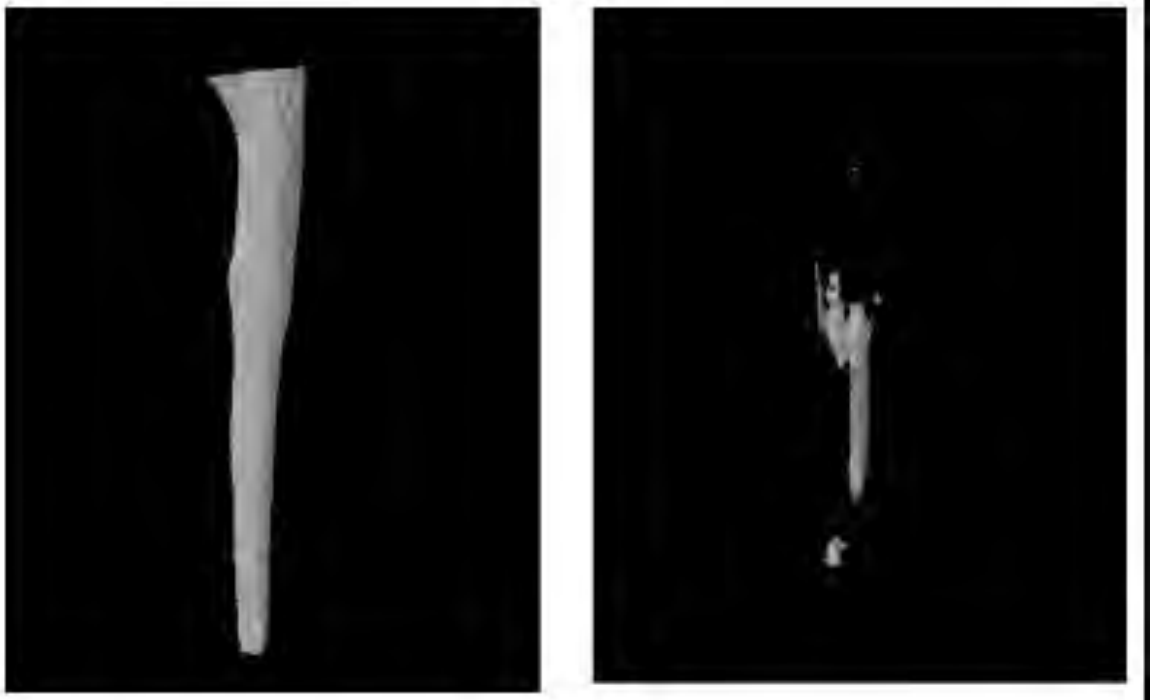

Figure 1. (*A*) Micro-CT 3-D reconstructed image of a root canal filling. (*B*) Micro-CT 3-D reconstructed image of remaining root canal filling.

Endodontic fillings and treatments in pulp cavity

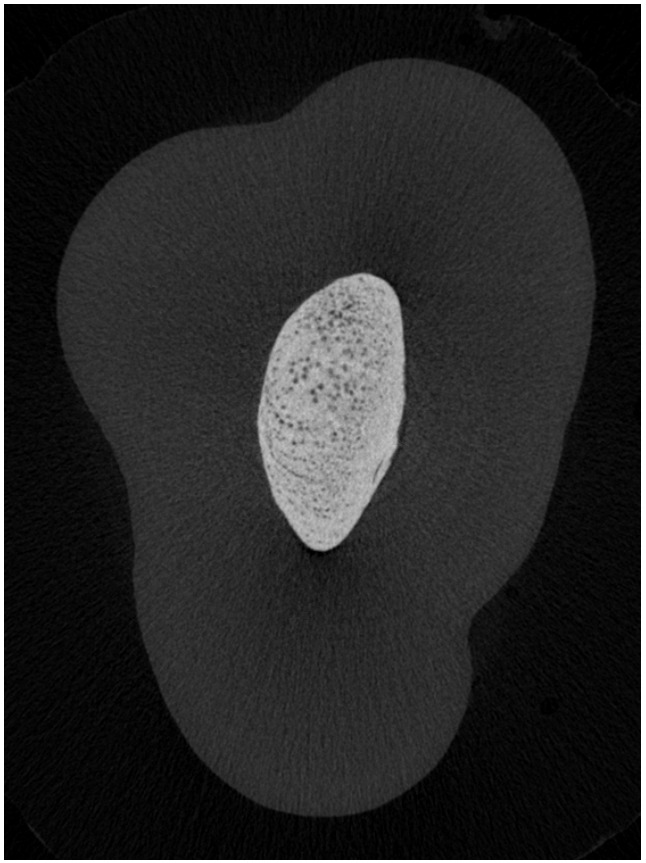

Within the pulp cavity

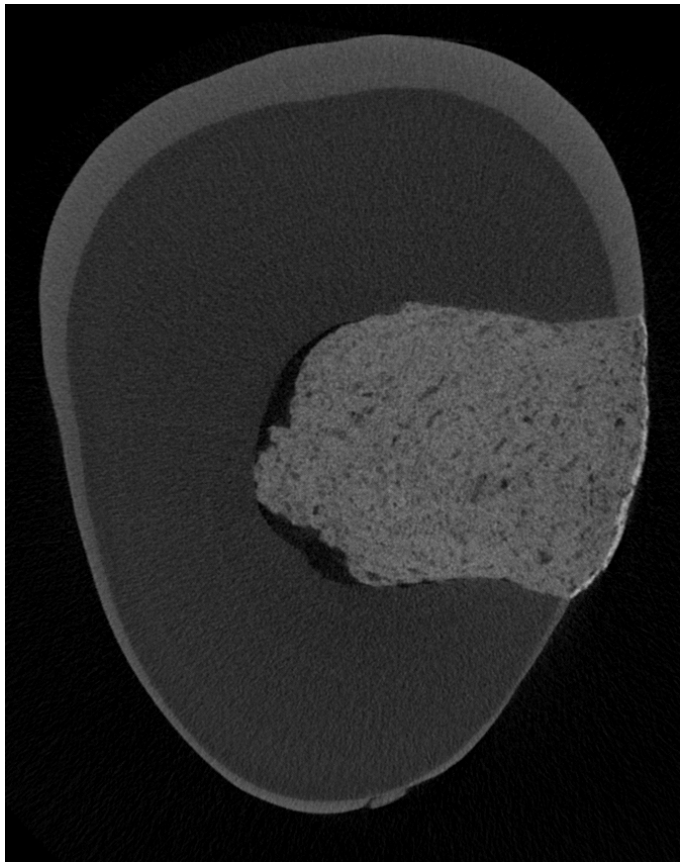

Connecting the pulp cavity with the outside

Tooth fragment showing severe caries with some endodontic treatments

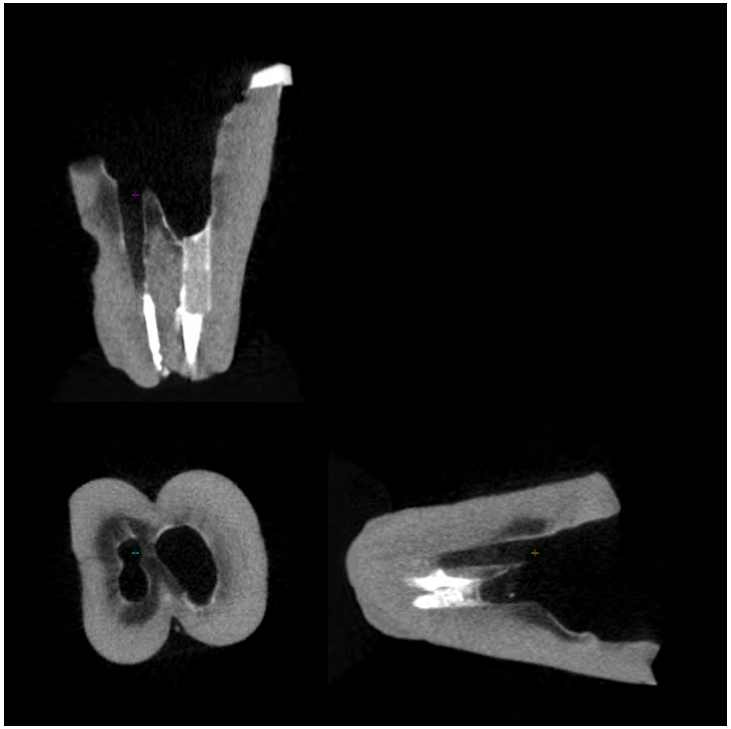

Binarisation and surface rendering of the caries region

In research from Jeddah, Saudi Arabia, SkyScan CT-Analyser software tools allow demineralisation to be quantified in selected dentine bands around the pulp canal:

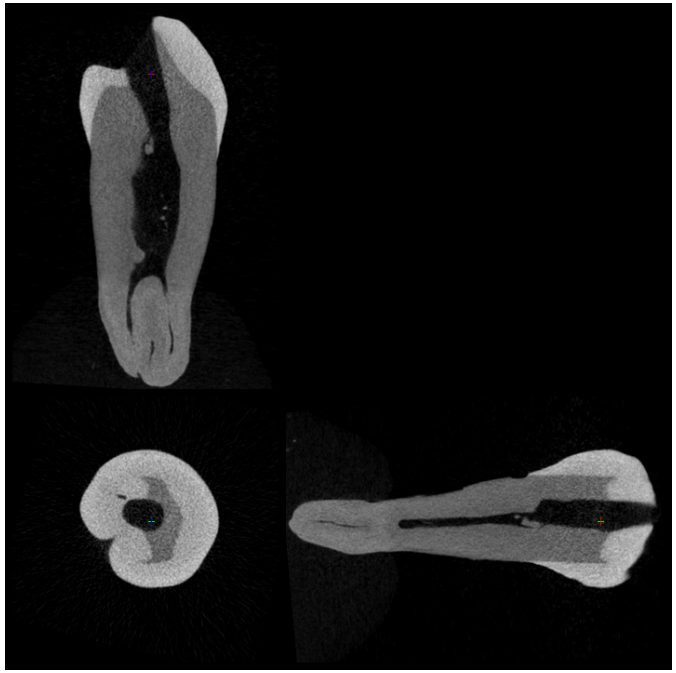

Endodontic procedures: before and after

Endodontic research requires COMPARISON of a root canal before (gold) and after (blue) a treatment procedure

SkyScan CTAn allows comparison of before and after datasets, using custom processing functions

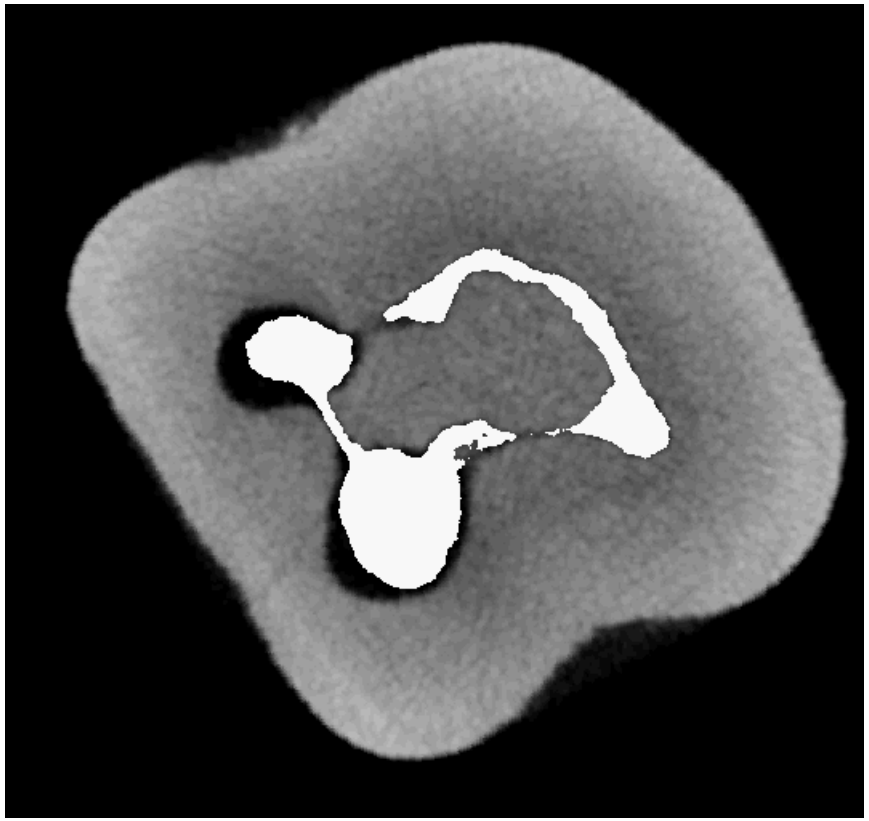

Here the white mask is the root BEFORE the procedure

Overview

1. Principles of micro-computed x-ray tomography (“micro-CT”)
2. SkyScan 1172
3. Solutions for Life Science Applications
   - Dental (Teeth)
   - Dental (Scaffolds)
   - Bone
   - Bone (Biomechanics / Implants)
   - Soft Tissue
4. New Features in DataViewer, CTVox, CTAN

Dental related and periodontal reconstruction involves the development of osteoconductive **scaffold materials**

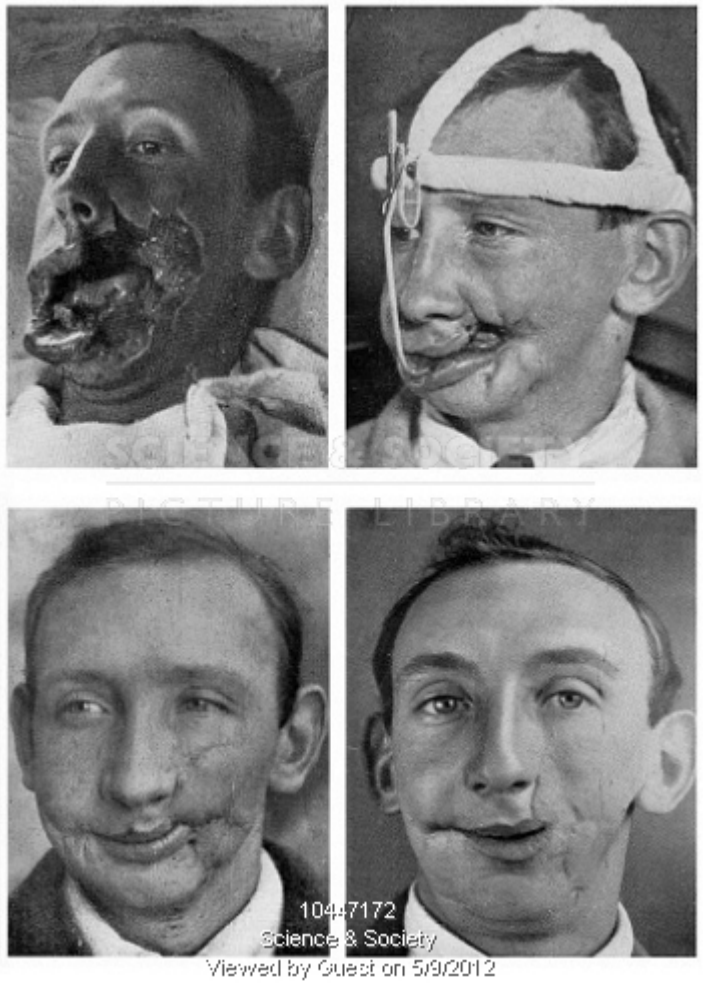

Scaffold materials can be scanned ex vivo, such as PLA polymer type scaffolds

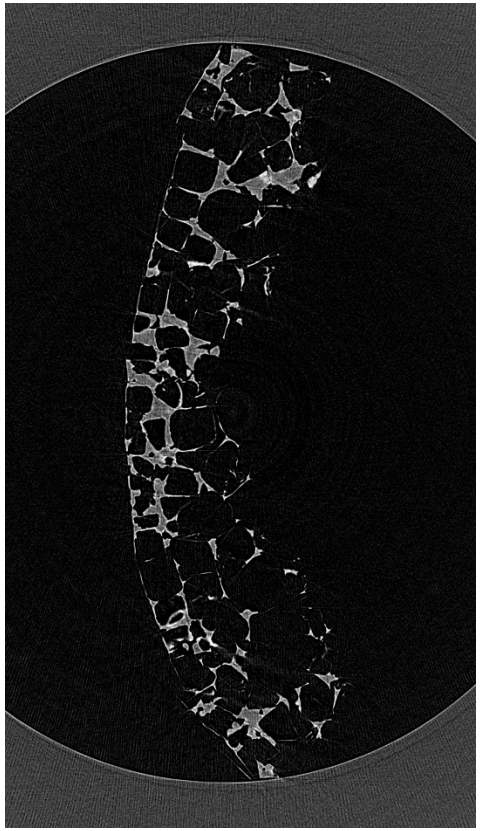

Poly LLA

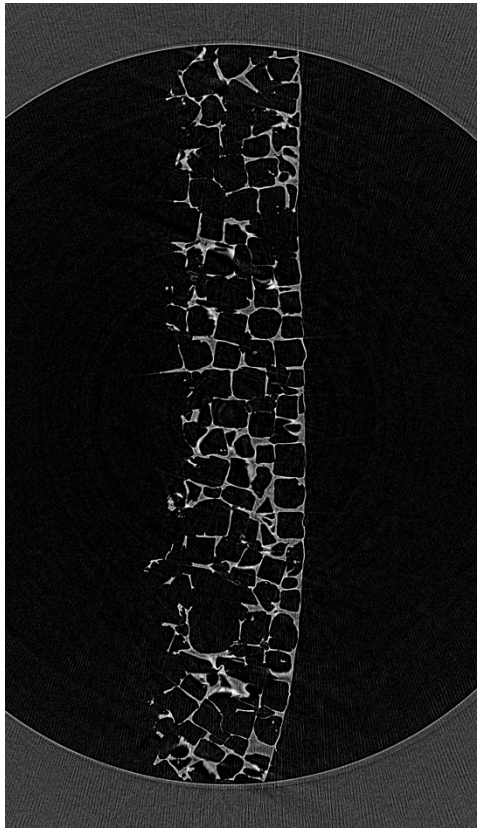

Poly LLA CO CL

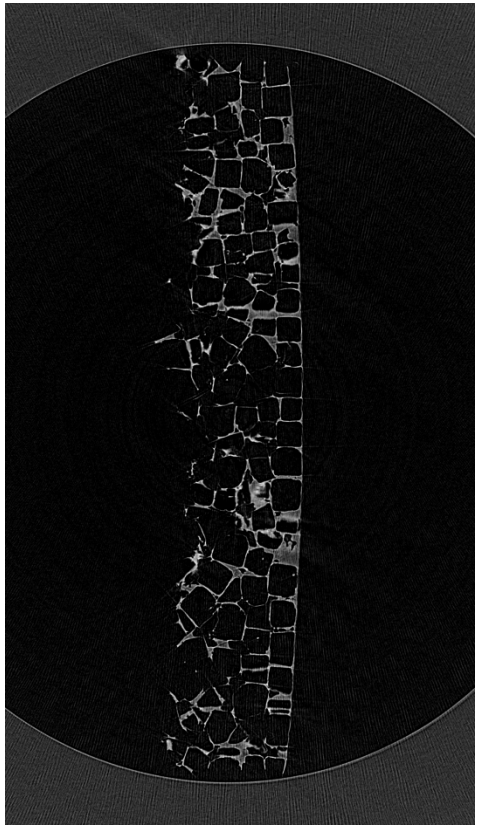

Poly LLA CO DXO

Analysis of scaffolds involves – as always – the definition and delineation of the **VOI** (volume of interest) for measurement

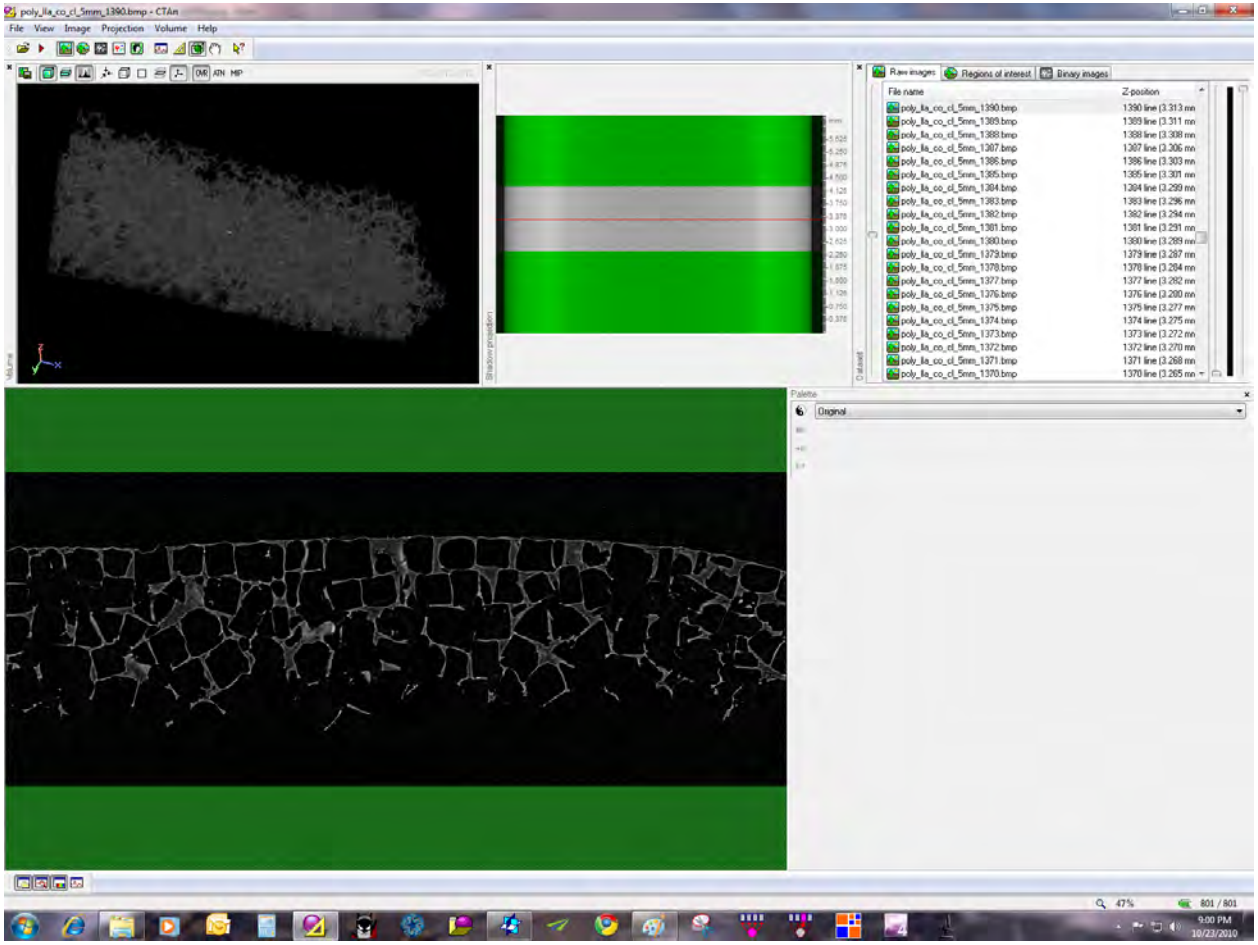

Auto-wrapping or "shrink-wrap" of the VOI around an irregular object boundary (SkyScan CT-Analyser)

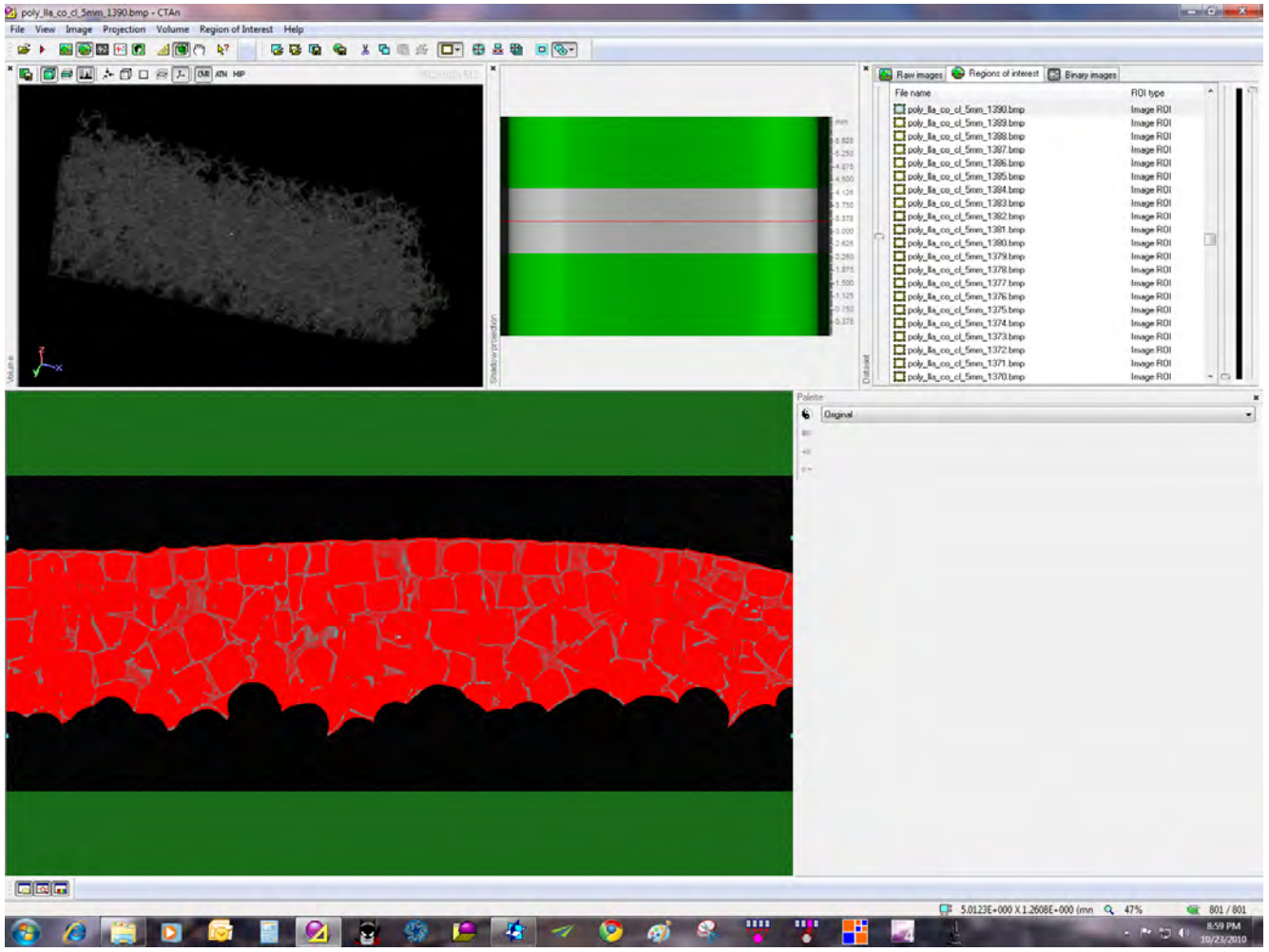

A PLA CO CL type scaffold – imaged by the SkyScan 1172

A woven type scaffold – imaged by the SkyScan 1172

In other, calcified scaffolds, detailed analysis of the porosity is required, to assess accessibility to bone cells

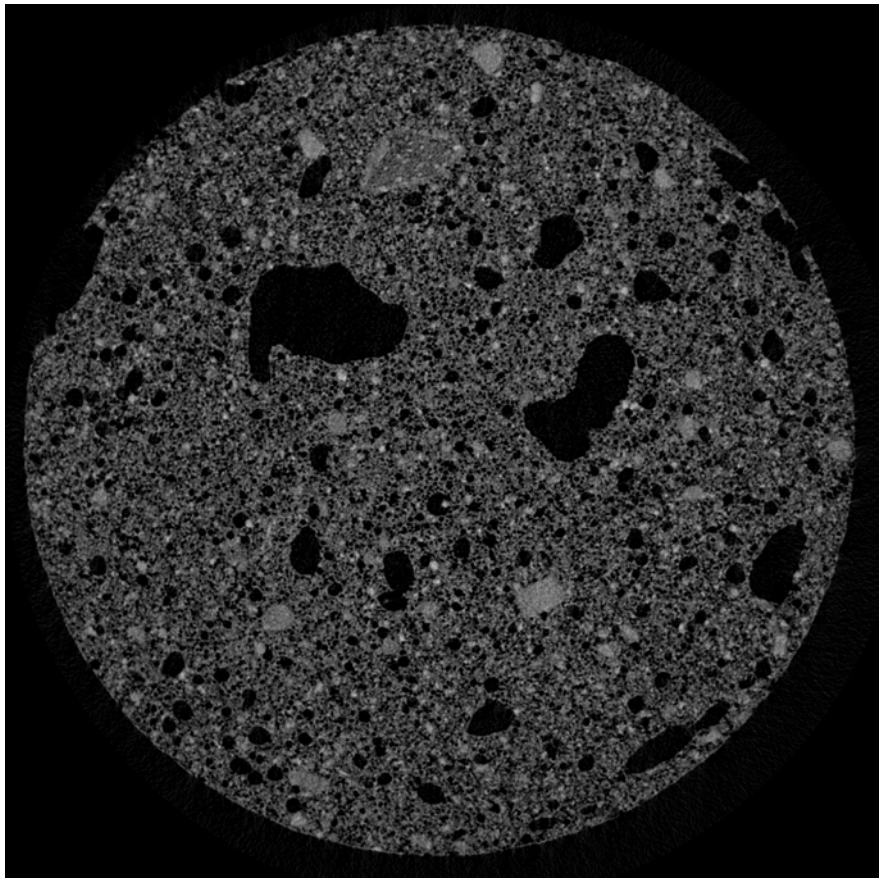

Acta Biomaterialia xxx (2011) xxx–xxx

Contents lists available at SciVerse ScienceDirect

Acta Biomaterialia

journal homepage: www.elsevier.com/locate/actabiomat

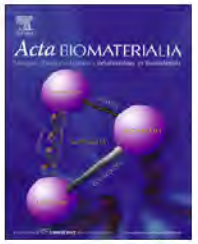

Influence of the pore generator on the evolution of the mechanical properties and the porosity and interconnectivity of a calcium phosphate cement

M.A. Lopez-Heredia [a], K. Sariibrahimoglu [a,1], W. Yang [a,1], M. Bohner [b], D. Yamashita [c], A. Kunstar [d], A.A. van Apeldoorn [d], E.M. Bronkhorst [a], R.P. Félix Lanao [a], S.C.G. Leeuwenburgh [a], K. Itatani [c], F. Yang [a], P. Salmon [e], J.G.C. Wolke [a], J.A. Jansen [a,*]

[a] *Department of Biomaterials, College of Dental Science, Radboud University Nijmegen, Medical Centre, Nijmegen, The Netherlands*
[b] *RMS Foundation, Bettlach, Switzerland*
[c] *Department of Materials and Life Sciences, Faculty of Science and Engineering, Sophia University, Tokyo, Japan*
[d] *Department of Tissue Regeneration, Faculty of Technological Sciences, MIRA—Institute for Biomedical Technology and Technical Medicine, University of Twente, Enschede, The Netherlands*
[e] *SkyScan NV, Kontich, Belgium*

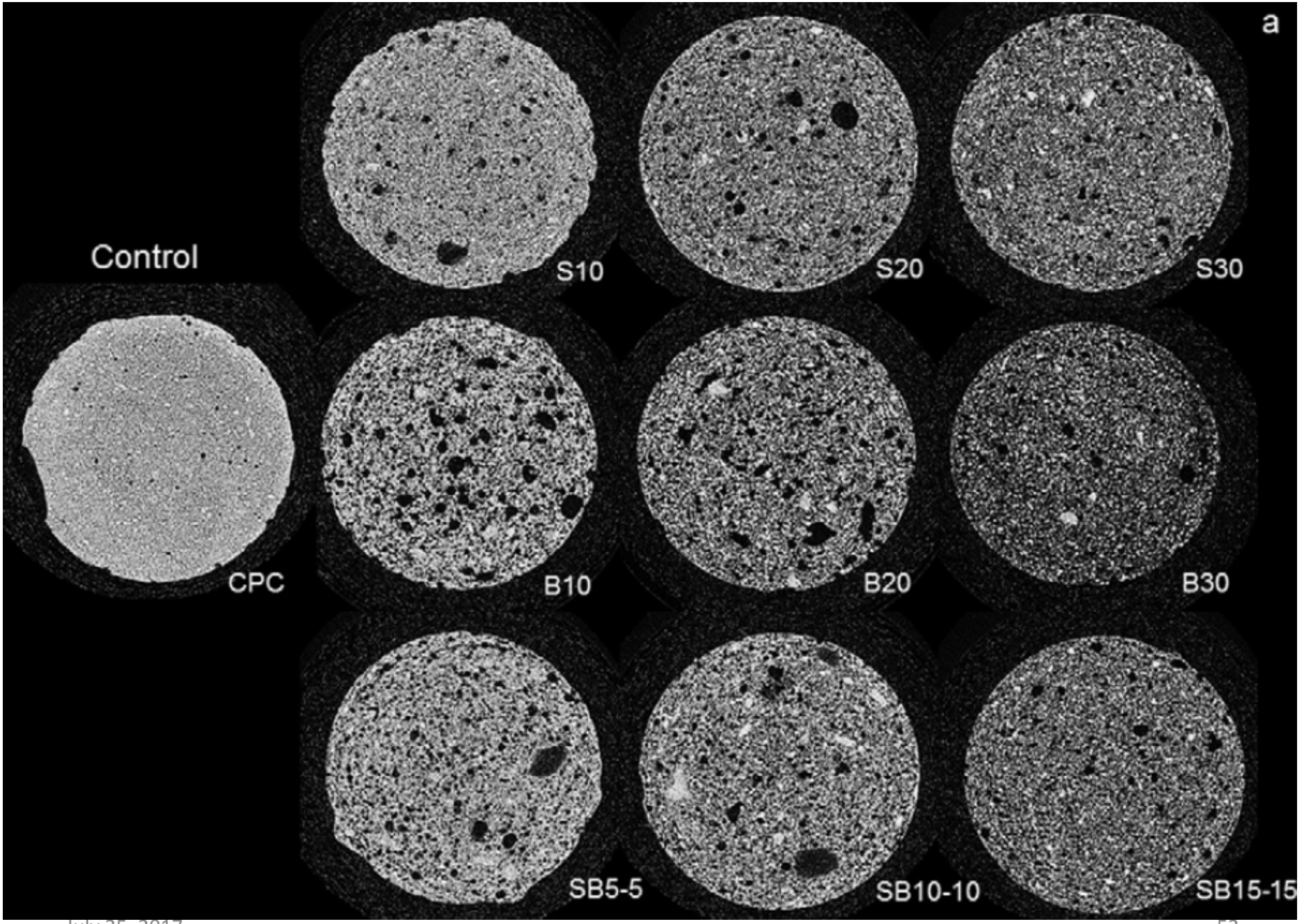
a
Control
S10
S20
S30
CPC
B10
B20
B30
SB5-5
SB10-10
SB15-15

Pore size distribution

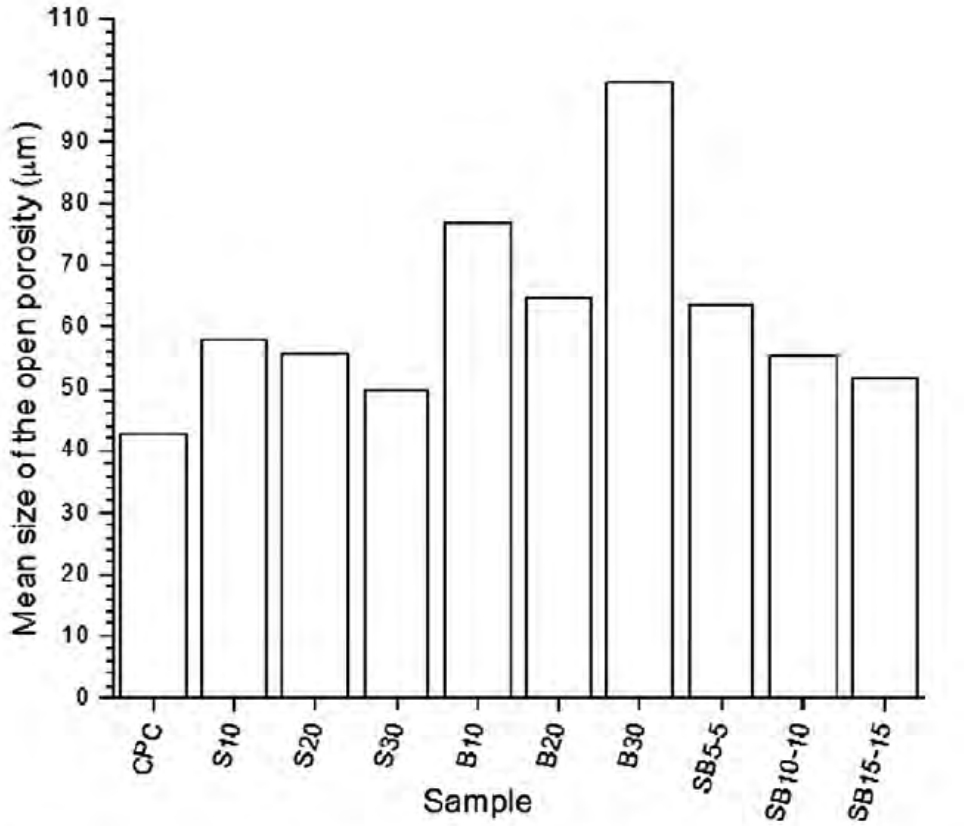

Fig. 6. Mean size of the open porosity for the different CPC–PLGA basic samples. S, small particles (~20 μm); B, big particles (~40 μm); SB, mixture of small and big particles. Numbers next to prefixes are the weight percentages of PLGA loaded into the CPC.

The analysis used here, developed by SkyScan, assesses how far a **virtual sphere** can penetrate a scaffold

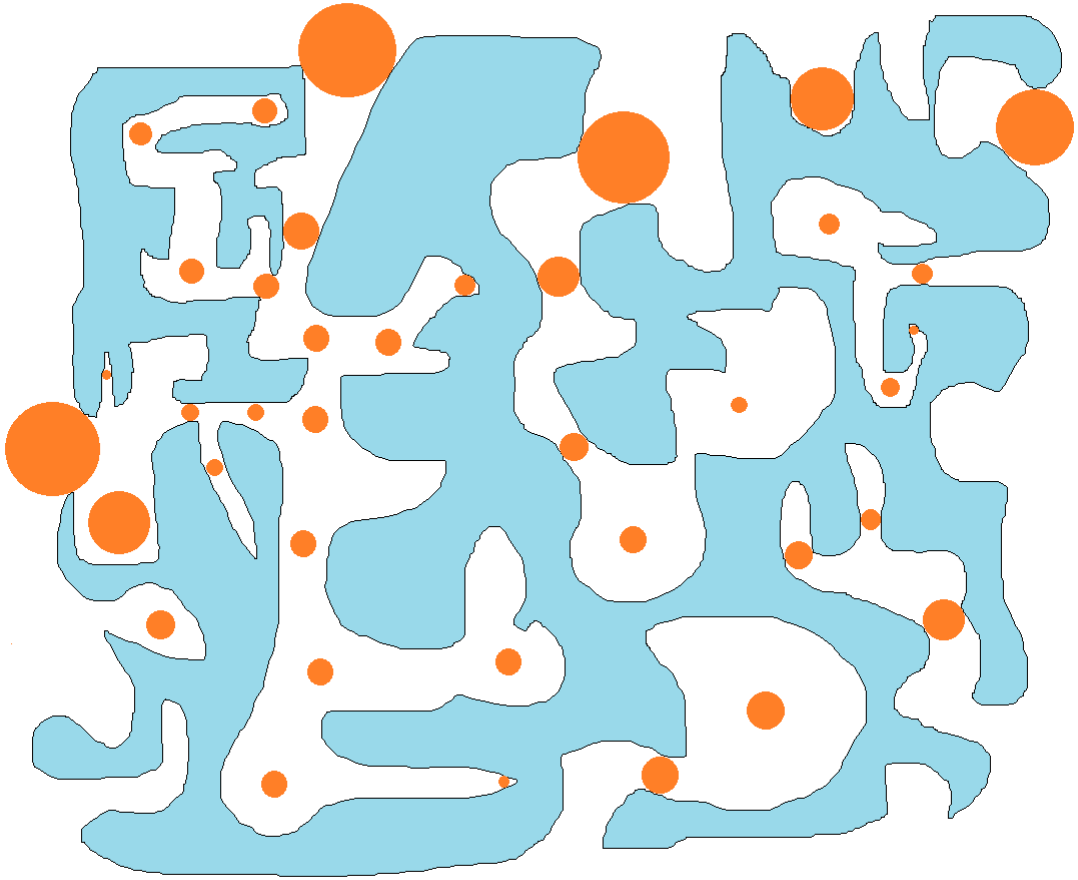

…to simulate **cell** ingrowth

The sphere analysis: curve displacement to right means the furthest access into scaffold

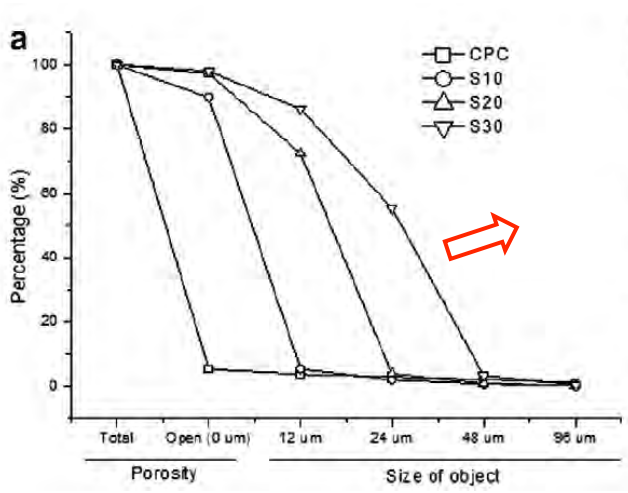

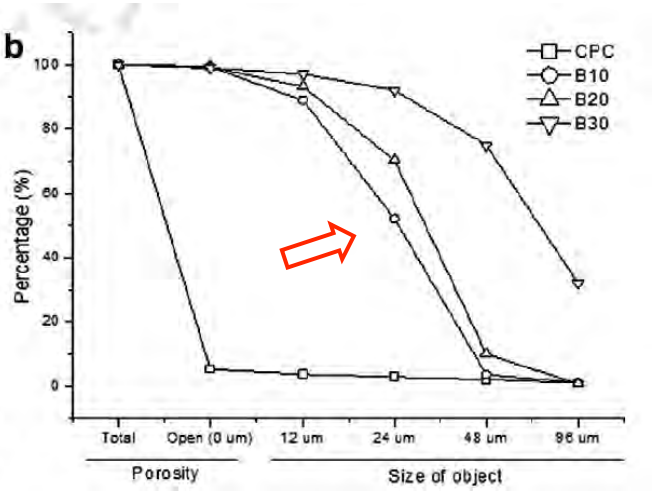

More access

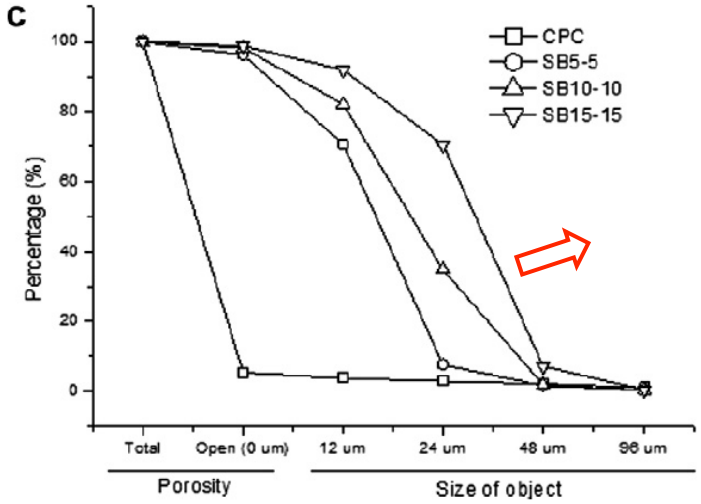

Porosity analysis applied to starch fiber mesh scaffold research

TISSUE ENGINEERING: Part A
Volume 14, Number 00, 2008

DOI: 10.1089/ten.tea.2008.0025

The Role of Lipase and α-Amylase in the Degradation of Starch/Poly(ε-Caprolactone) Fiber Meshes and the Osteogenic Differentiation of Cultured Marrow Stromal Cells

Ana M. Martins, B.S.,[1–3] Quynh P. Pham, Ph.D.,[3] Patrícia B. Malafaya, Ph.D.,[1,2] Rui A. Sousa, Ph.D.,[1,2] Manuela E. Gomes, Ph.D.,[1,2] Robert M. Raphael, Ph.D.,[3] F. Kurtis Kasper, Ph.D.,[3] Rui L. Reis, Ph.D., D.Sc.,[1,2] and Antonios G. Mikos, Ph.D.[3]

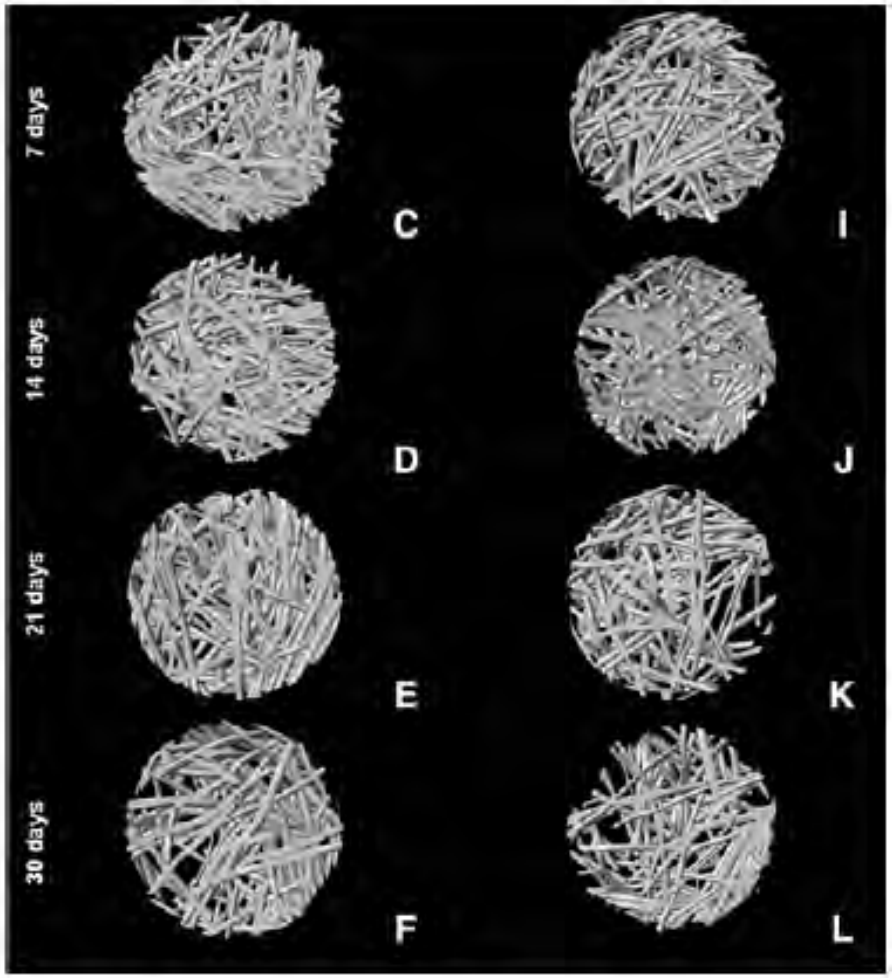

FIG. 2. Starch and poly(ε-caprolactone) fiber mesh images obtained using micro-computed tomography before (**A, G**) and after degradation with α-amylase (150 U/L) under static (**B–F**) and dynamic (**H–L**) conditions up to 30 days. The scale bar is 2 mm and applies to all images.

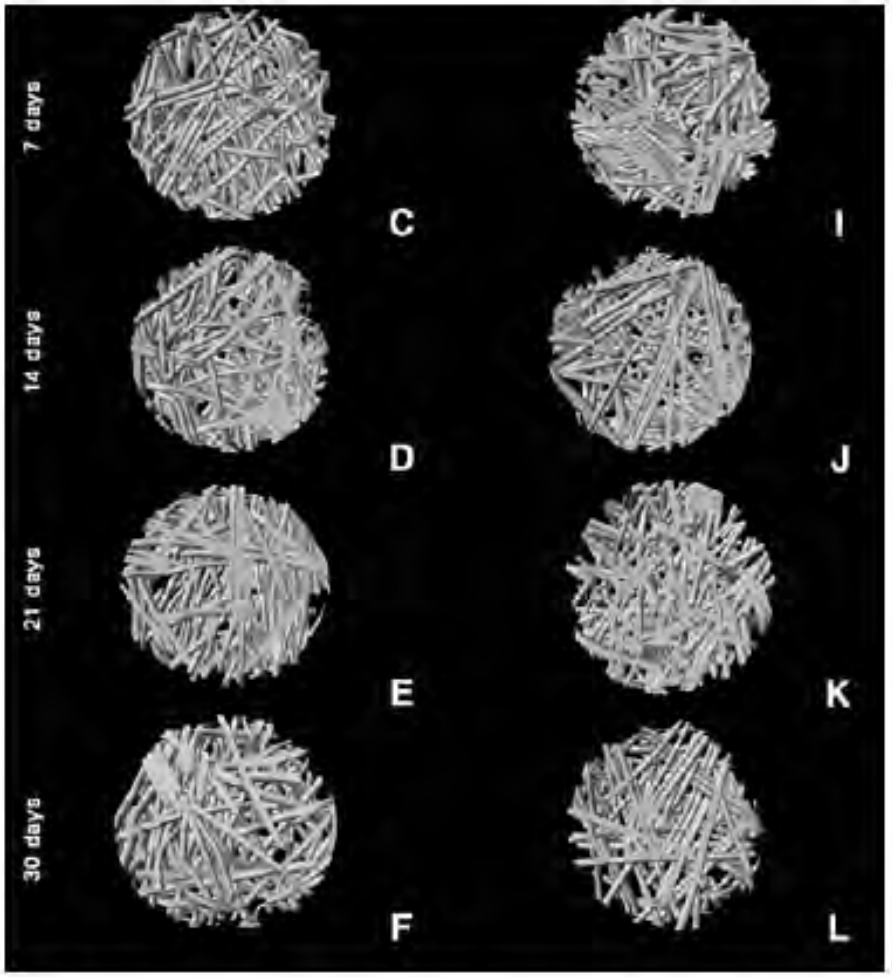

FIG. 3. Starch and poly(ε-caprolactone) fiber mesh images obtained using micro-computed tomography before (**A, G**) and after degradation with lipase (110 U/L) under static (**B–F**) and dynamic (**H–L**) conditions up to 30 days. The scale bar is 2 mm and applies to all images.

Overview

1. Principles of micro-computed x-ray tomography (“micro-CT”)
2. SkyScan 1172
3. Solutions for Life Science Applications
   - Dental (Teeth)
   - Dental (Scaffolds)
   - Bone
   - Bone (Biomechanics / Implants)
   - Soft Tissue
4. New Features in DataViewer, CTVox, CTAN

PNAS

Differential effects on bone of estrogen receptor α and androgen receptor activation in orchidectomized adult male mice

Sofia Movérare*, Katrien Venken†, Anna-Lena Eriksson*, Niklas Andersson*, Stanko Skrtic*, Jon Wergedal‡, Subburaman Mohan‡, Phil Salmon§, Roger Bouillon†, Jan-Åke Gustafsson¶, Dirk Vanderschueren†, and Claes Ohlsson*‖

*Center for Bone Research, Department of Internal Medicine, The Sahlgrenska Academy, Göteborg University, S-41345 Göteborg, Sweden; †Laboratory for Experimental Medicine and Endocrinology, Katholieke Universiteit Leuven, B-3000 Leuven, Belgium; ‡Department of Medicine, Loma Linda University, Musculoskeletal Disease Center, Pettis Veterans Administration Medical Center, Loma Linda, CA 92357; §Skyscan N.V., B-2630 Aartselaar, Belgium; and ¶Departments of Biosciences and Medical Nutrition, Karolinska Institute, Novum, S-14157 Huddinge, Sweden

Edited by Elwood V. Jensen, University of Cincinnati Medical Center, Cincinnati, OH, and approved September 5, 2003 (received for review May 22, 2003)

Moverare *et al.* showed that testosterone had its own pathway, its bone protective effect was not "piggy-backing" the estrogen pathway

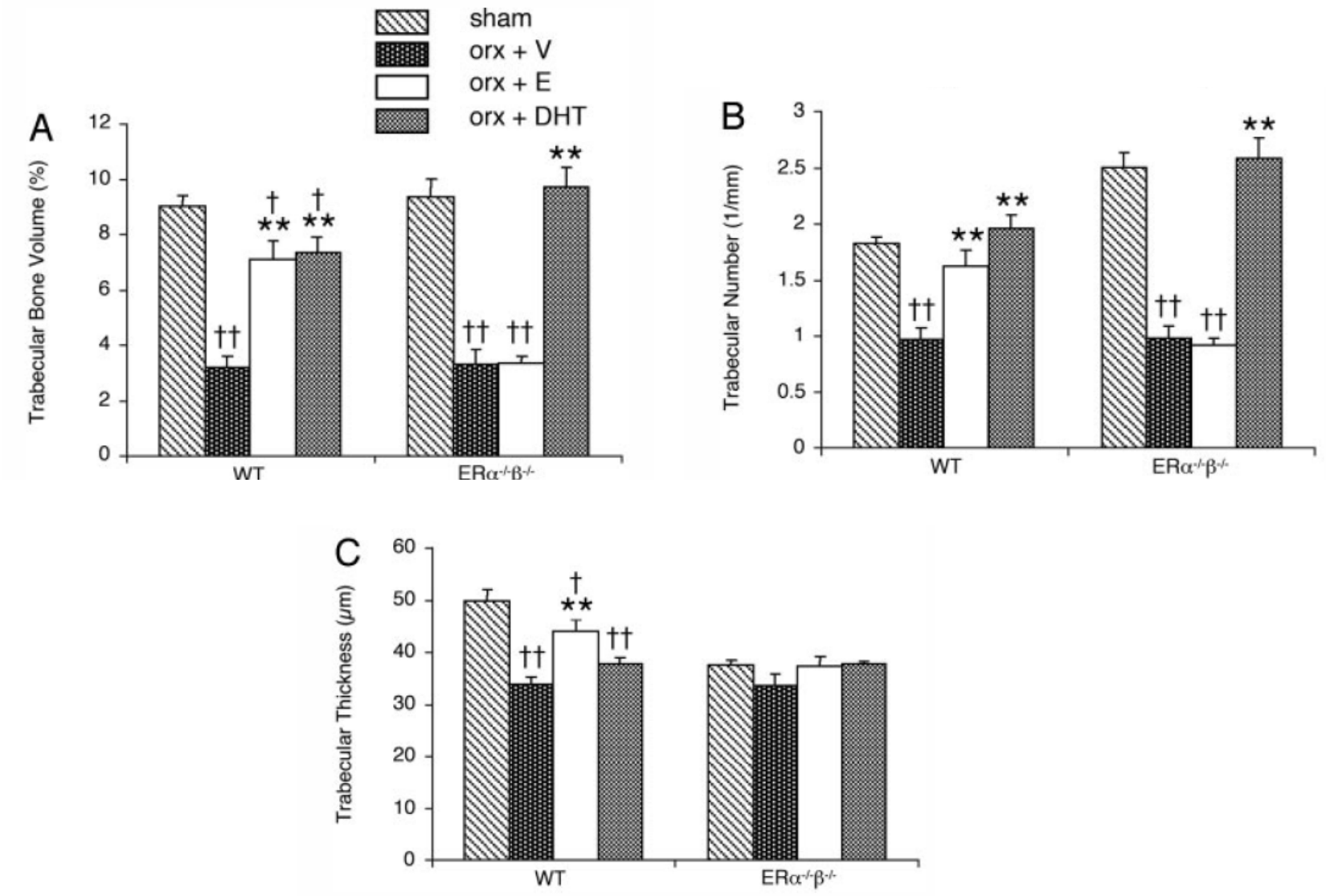

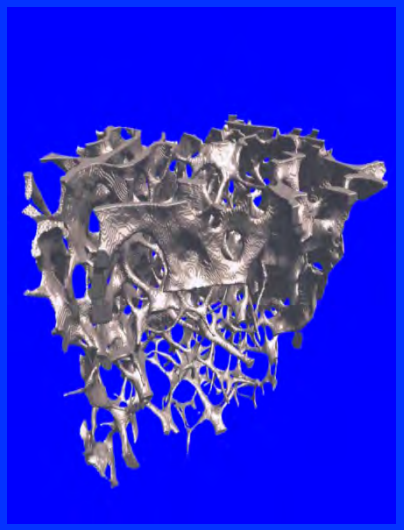

WT sham vehicle

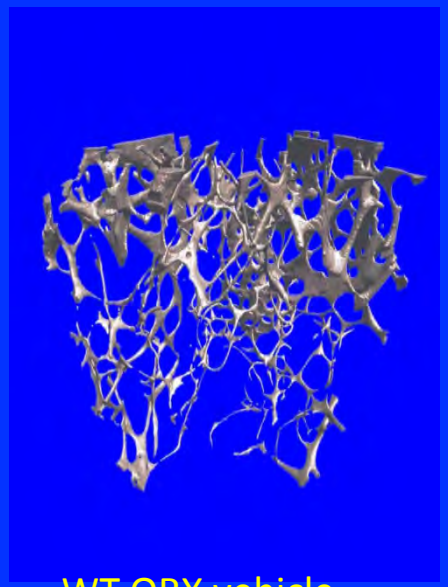

WT ORX vehicle

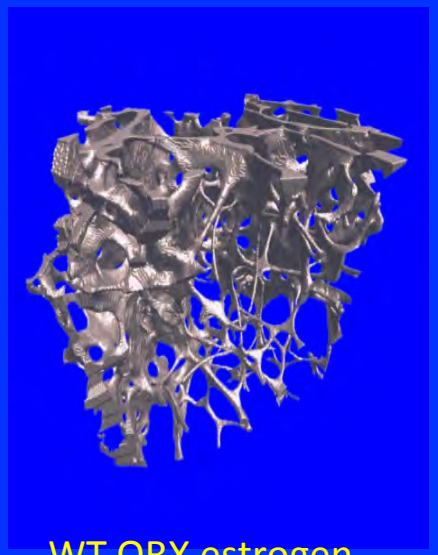

WT ORX estrogen

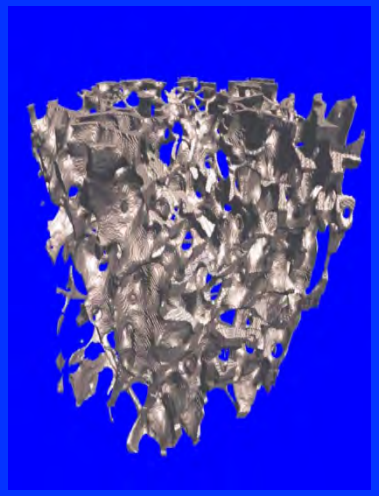

WT ORX DHT

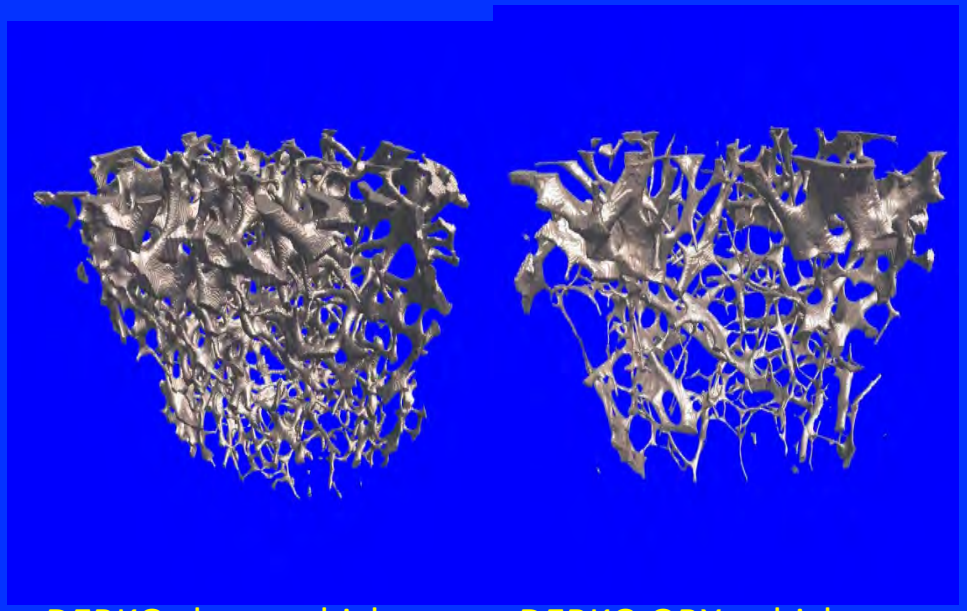

DERKO sham vehicle

DERKO ORX vehicle

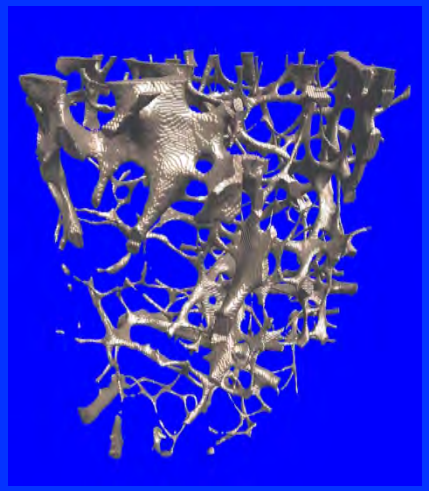

DERKO ORX estrogen

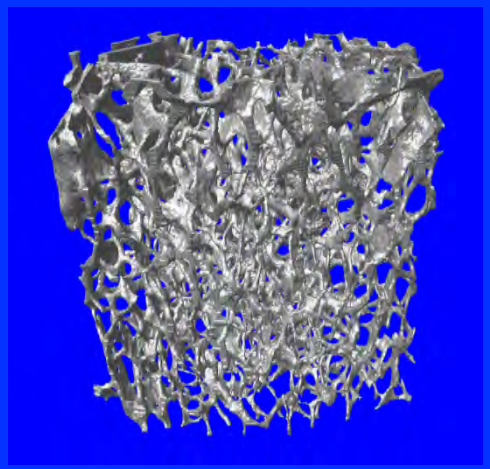

DERKO ORX DHT

JOURNAL OF BONE AND MINERAL RESEARCH
Volume 19, Number 11, 2004
Published online on August 23, 2004; doi: 10.1359/JBMR.040819

Additive Protective Effects of Estrogen and Androgen Treatment on Trabecular Bone in Ovariectomized Rats

Åsa Tivesten,[1] Sofia Movérare-Skrtic,[2] Andrei Chagin,[3] Katrien Venken,[4] Phil Salmon,[5] Dirk Vanderschueren,[4] Lars Sävendahl,[3] Agneta Holmäng,[1] and Claes Ohlsson[2]

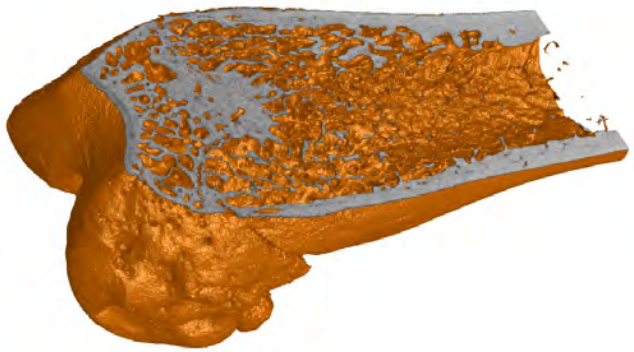

Experimental protocol:

Age at surgery: 12 weeks
Group numbers (n): 7-8
Duration of treatment: 6 weeks

- Sham operated
- Ovariectomised
- OVX, estradiol (E2)
- OVX, DH testosterone (DHT)
- OVX, E2 + DHT

Sham-op

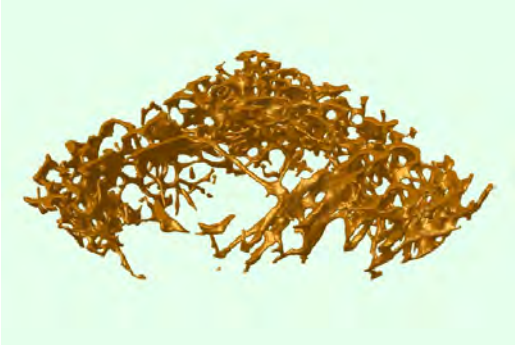

OVX

Testosterone DHT)

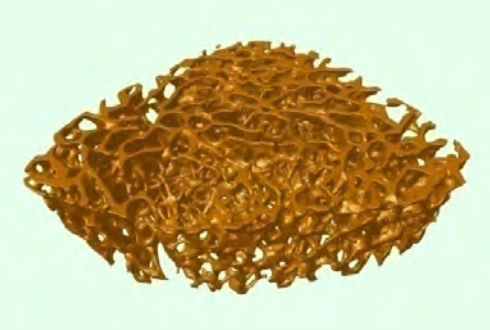

Estradiol

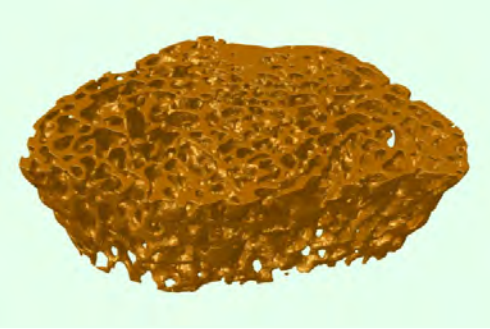

Estradiol + DHT

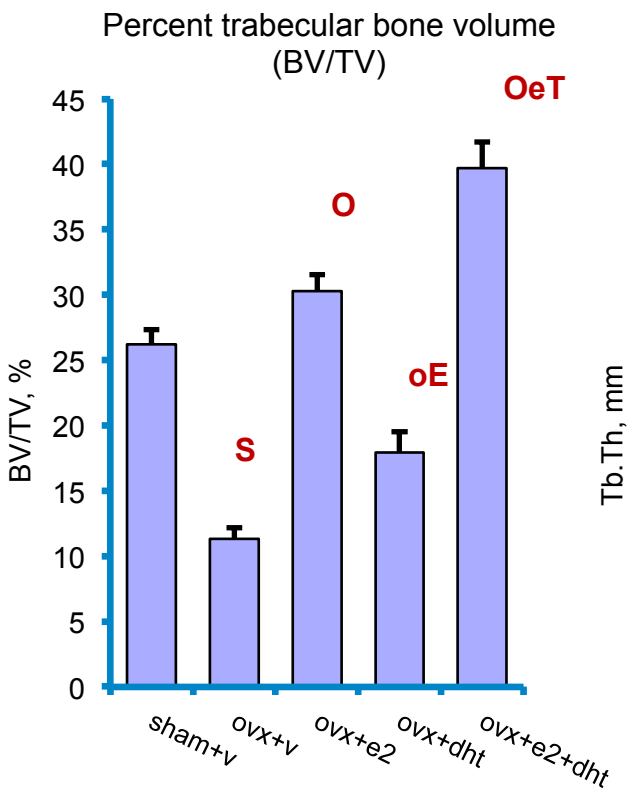
Percent trabecular bone volume (BV/TV)
BV/TV, %
45
40
35
30
25
20
15
10
5
0
OeT
O
oE
S
sham+v
ovx+v
ovx+e2
ovx+dht
ovx+e2+dht

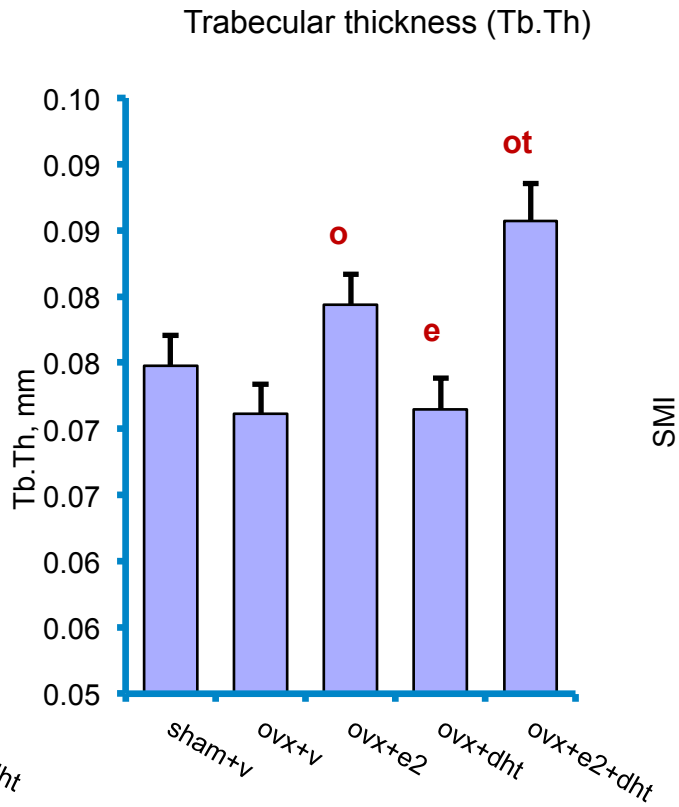
Trabecular thickness (Tb.Th)
Tb.Th, mm
0.10
0.09
0.09
0.08
0.08
0.07
0.07
0.06
0.06
0.05
ot
o
e
sham+v
ovx+v
ovx+e2
ovx+dht
ovx+e2+dht

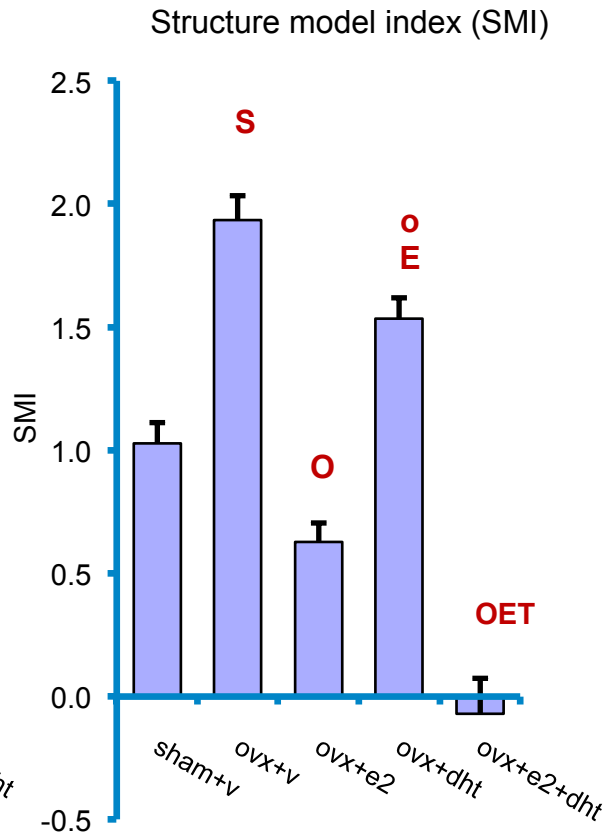
Structure model index (SMI)
SMI
2.5
2.0
1.5
1.0
0.5
0.0
-0.5
S
o
E
O
OET
sham+v
ovx+v
ovx+e2
ovx+dht
ovx+e2+dht

ELSEVIER

Contents lists available at ScienceDirect

Bone

journal homepage: www.elsevier.com/locate/bone

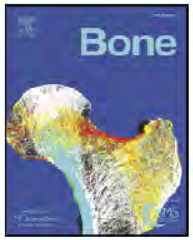

Mechanical loading enhances the anabolic effects of intermittent parathyroid hormone (1–34) on trabecular and cortical bone in mice

Toshihiro Sugiyama *, Leanne K. Saxon, Gul Zaman, Alaa Moustafa, Andrew Sunters, Joanna S. Price, Lance E. Lanyon

Department of Veterinary Basic Sciences, The Royal Veterinary College, University of London, Royal College Street, London NW1 0TU, UK

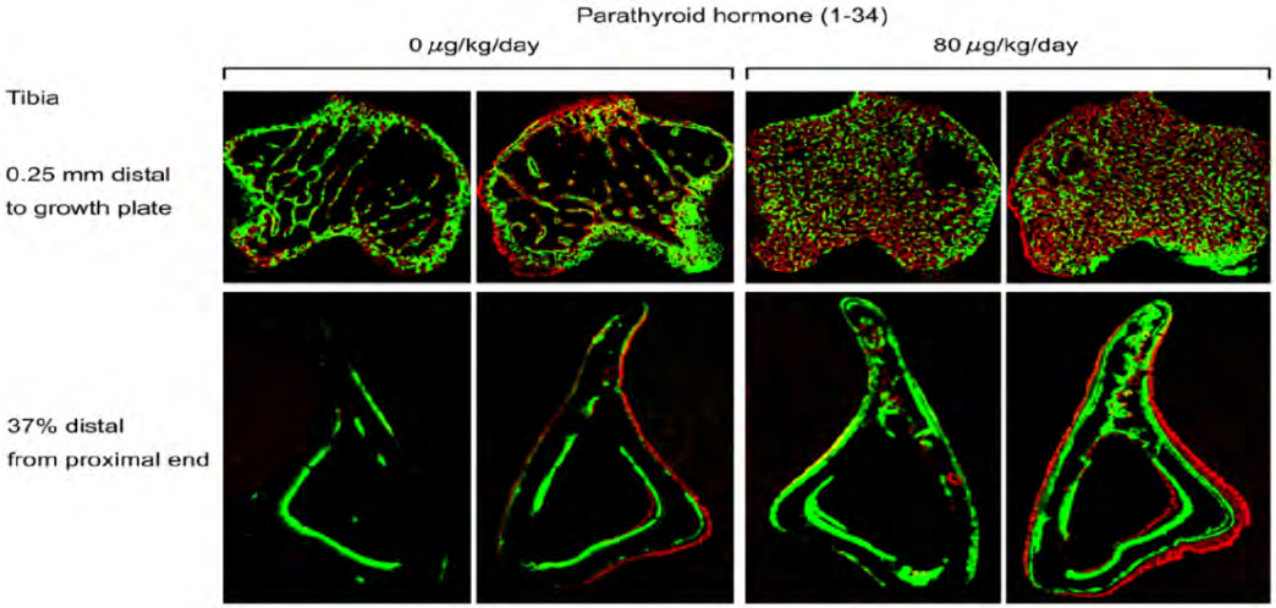

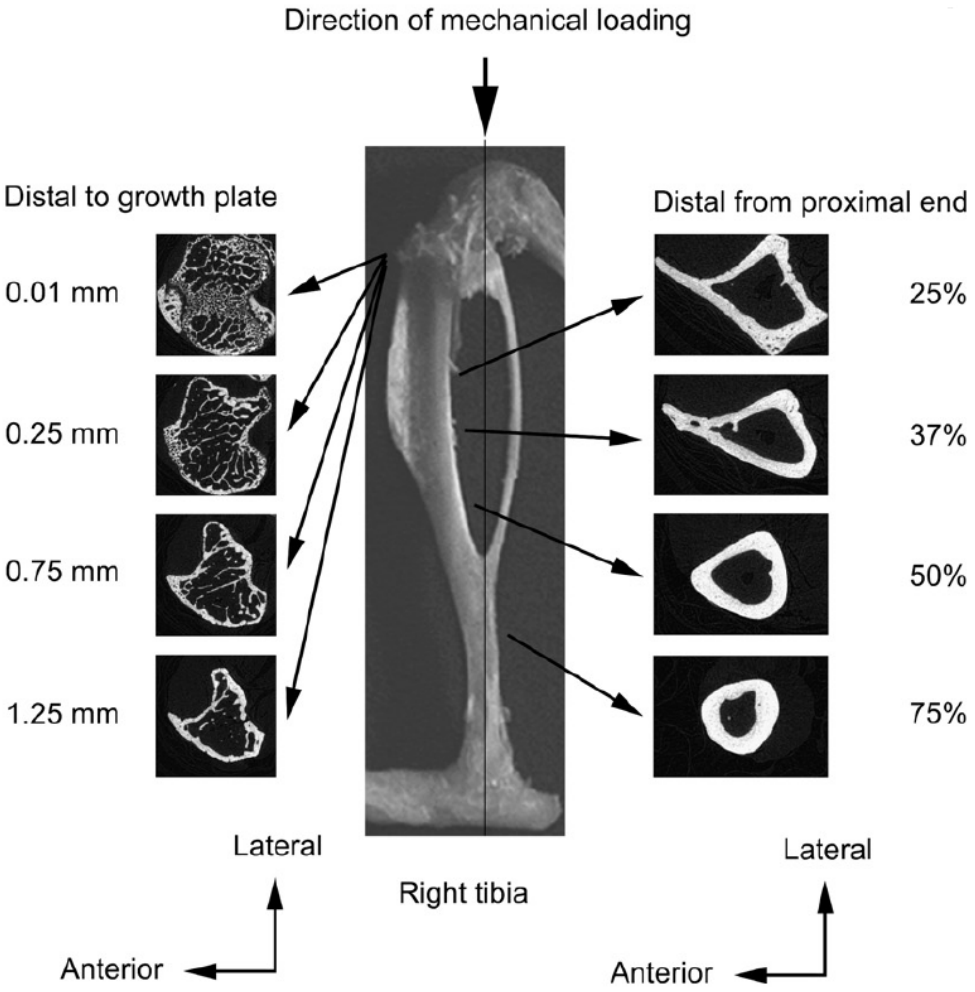
Direction of mechanical loading
Distal to growth plate
Distal from proximal end
0.01 mm
0.25 mm
0.75 mm
1.25 mm
25%
37%
50%
75%
Lateral
Anterior
Right tibia
Lateral
Anterior

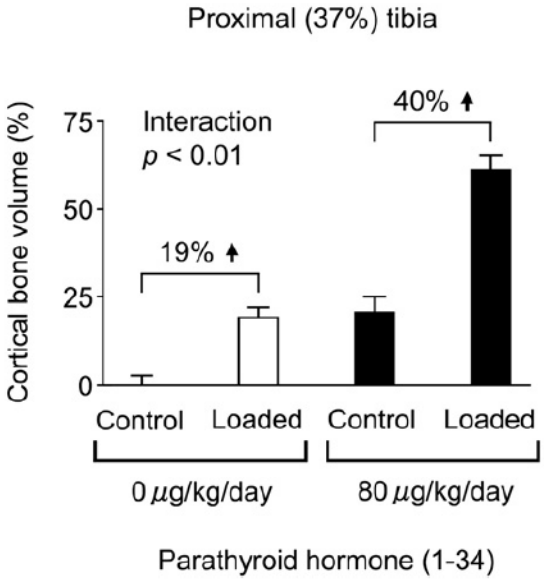
Proximal (37%) tibia
Cortical bone volume (%)
75
50
25
0
Interaction
p < 0.01
19%
40%
Control
Loaded
Control
Loaded
0 μg/kg/day
80 μg/kg/day
Parathyroid hormone (1-34)

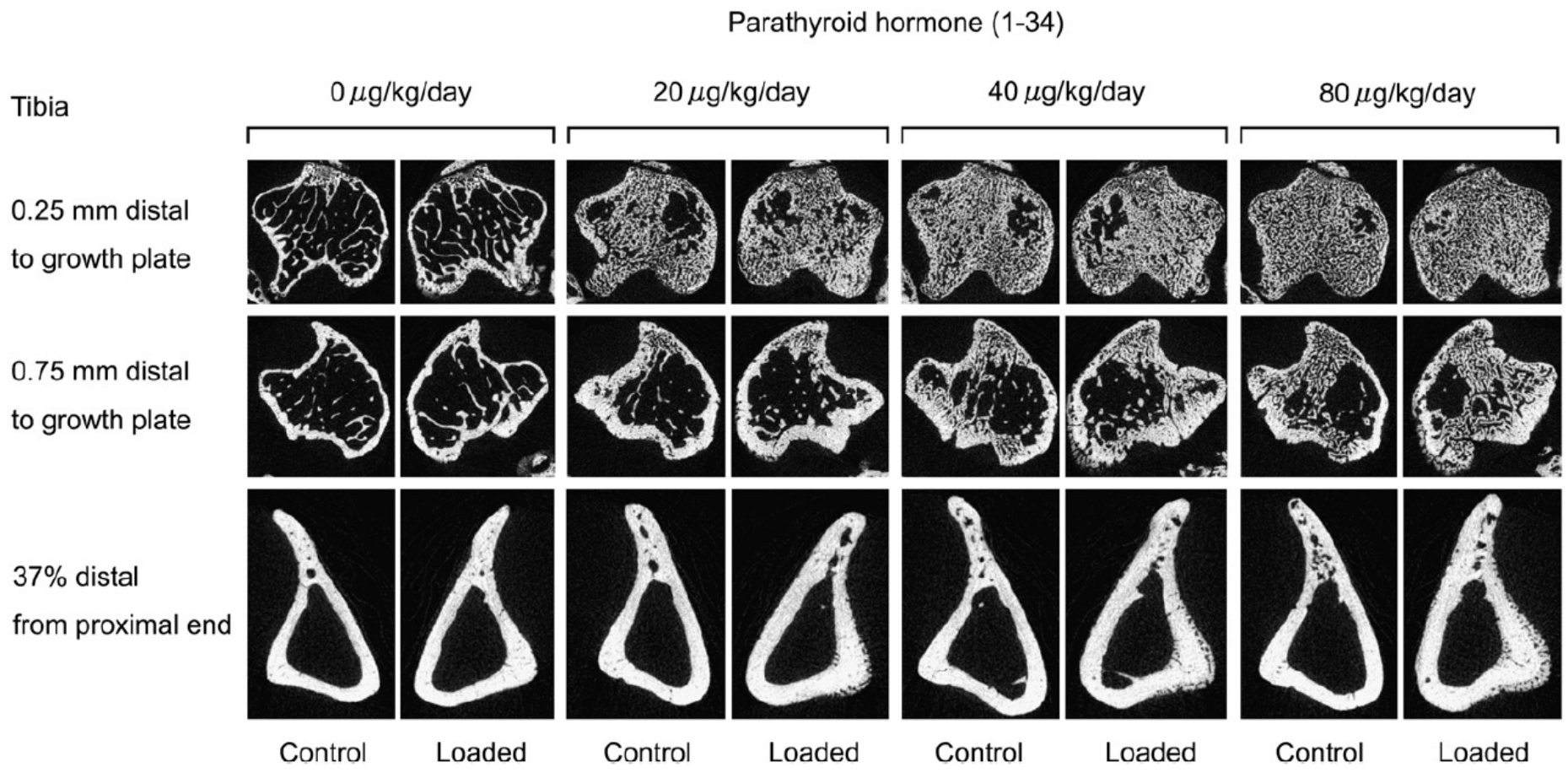
Parathyroid hormone (1-34)
Tibia
0 μg/kg/day
20 μg/kg/day
40 μg/kg/day
80 μg/kg/day
0.25 mm distal
to growth plate
0.75 mm distal
to growth plate
37% distal
from proximal end
Control
Loaded
Control
Loaded
Control
Loaded
Control
Loaded

Imaging and analysis of bone fracture healing

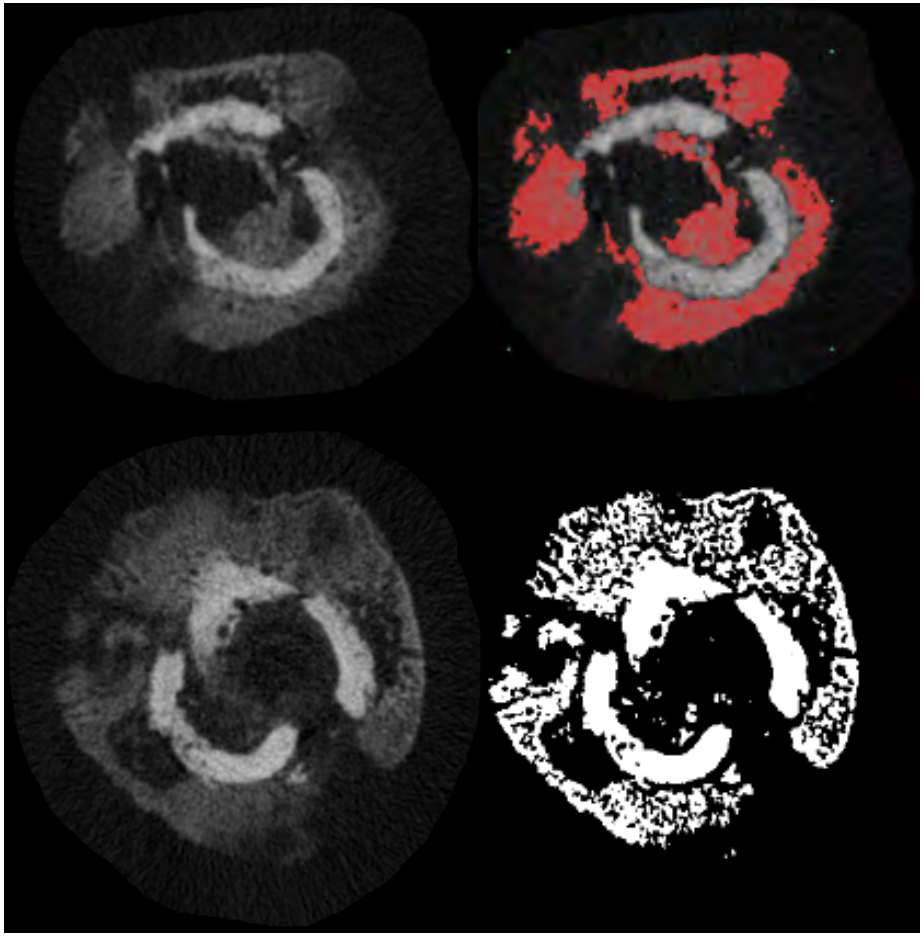

Otsu multi-level thresholding effectively delineated the mineralised callus from cortical bone. Upper images: 2 weeks post fracture; lower images, 6 weeks post fracture, showing the secondary “cortical” bone forming from the periphery of the callus.

Adaptive segmentation of the bone plus callus.

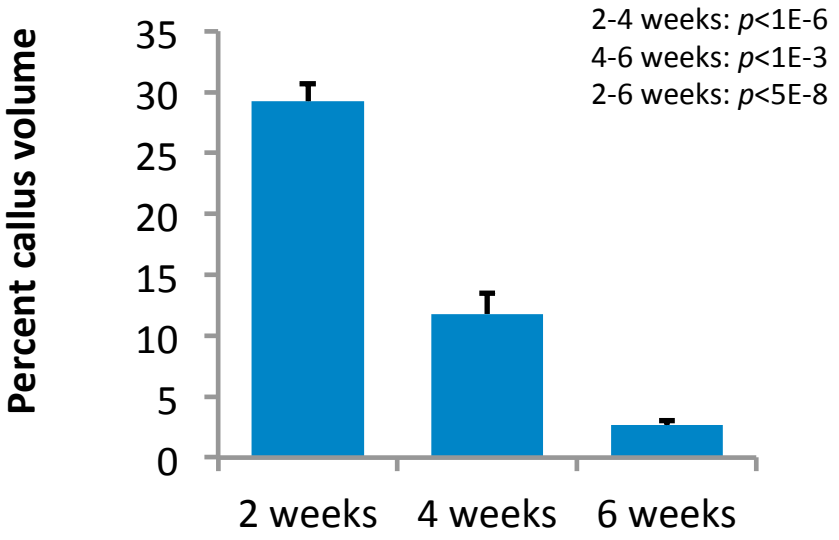

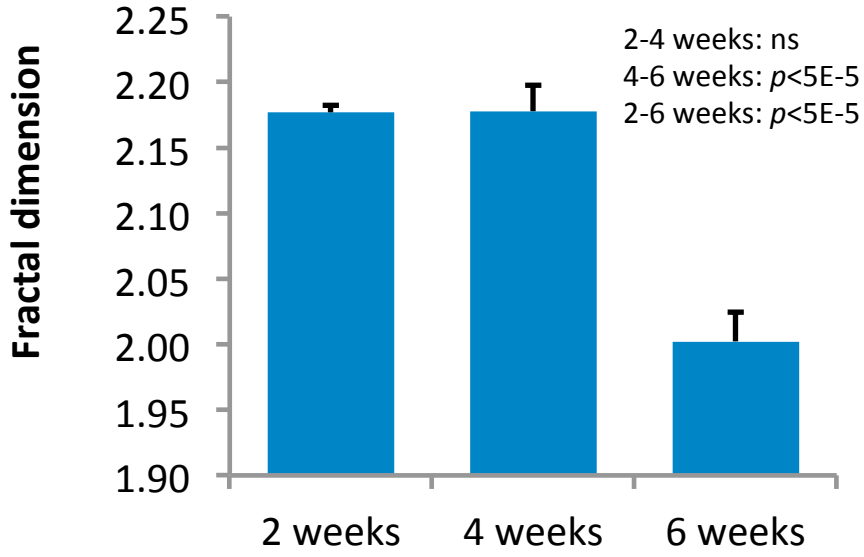

While **callus volume** and thickness decreased monotonically over the 2-6 week post-fracture period, and the nonmineralised callus (chondrocytes) likewise,

the **architectural parameters** of callus connectivity and complexity showed significant change only during 4-6 weeks post-fracture.

Thickness histogram is informative of structural change

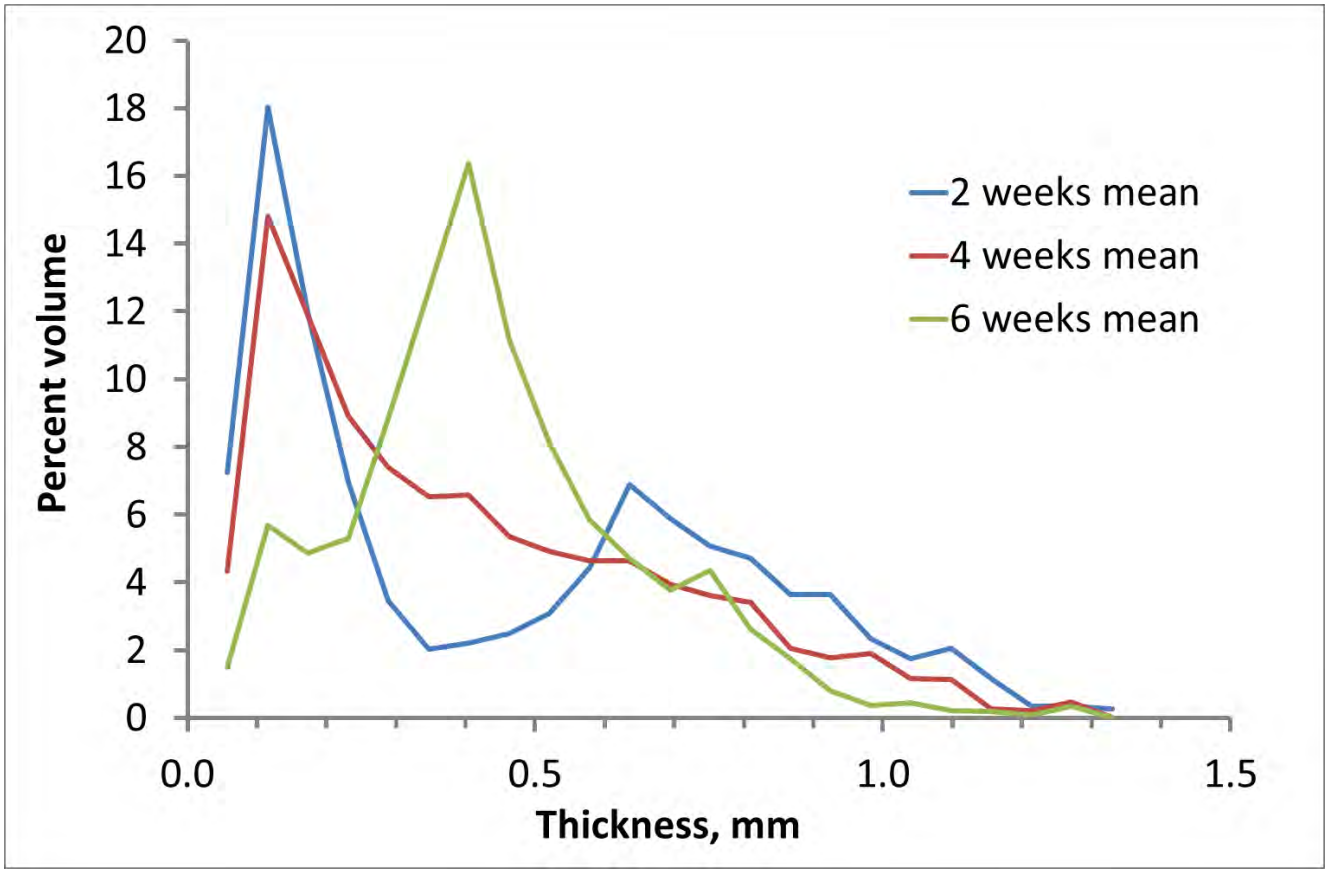

Fracture callus remodeling shows a progression toward **higher callus structure thickness**, at the expense of depletion of thinner callus structures. From 2-6 weeks post-fracture.

Triphosphate biomaterial scaffold, SkyScan1172

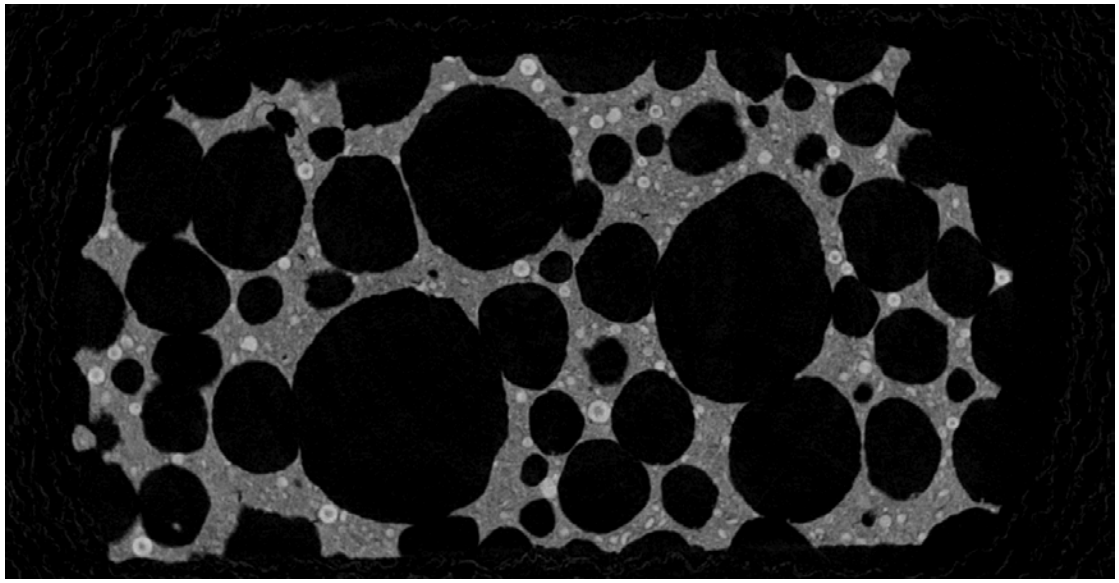

Biomaterial implants into rabbit calvarium, SkyScan1172

Arthritis models: assessment of the bone involvement

Paw with CIA

Paw with CIA, treated

Periosteal reaction around the tarsals is characteristic of CIA and quantifiable

Accurate semi-automated quantication is as important as visualising arthritis-related pathology.

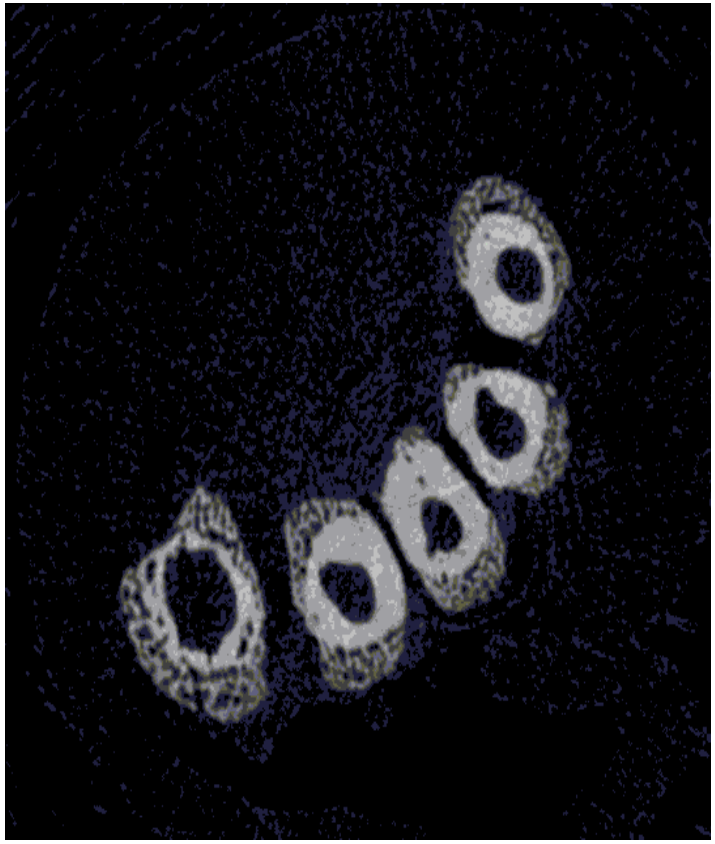

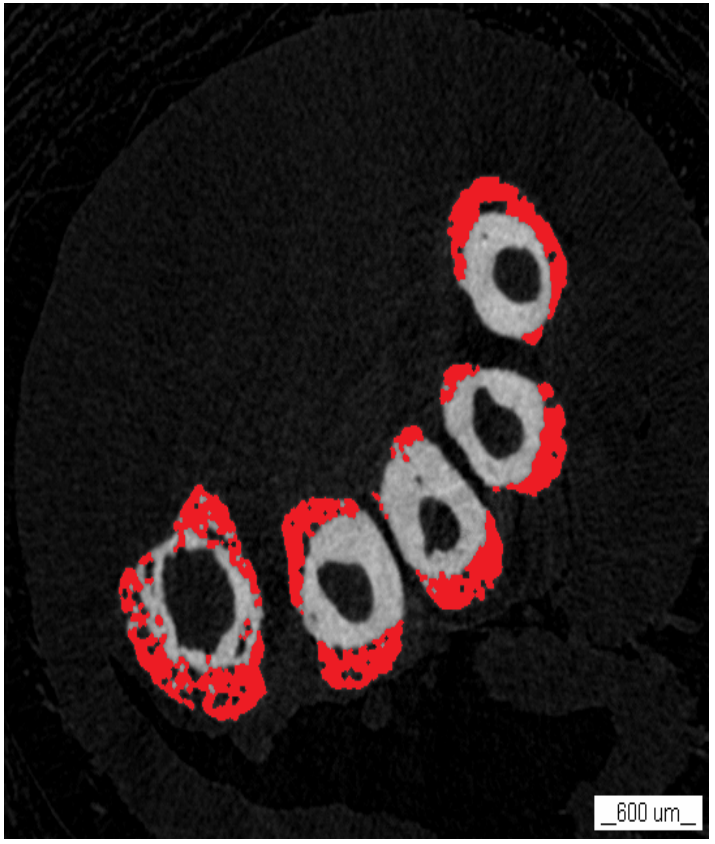

Otsu multi-threshold – morphological close + open - despeckle

Parameterization of arthritic changes

Bruker microCT

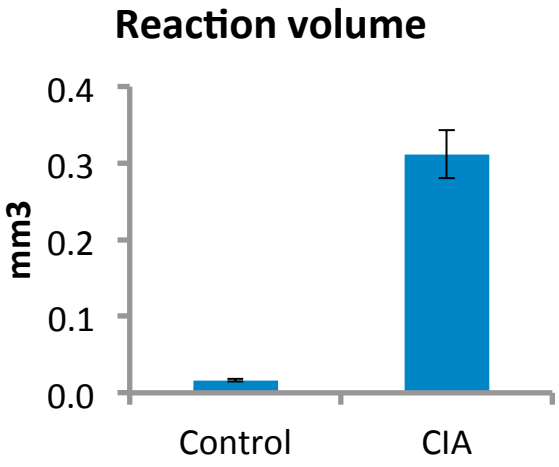

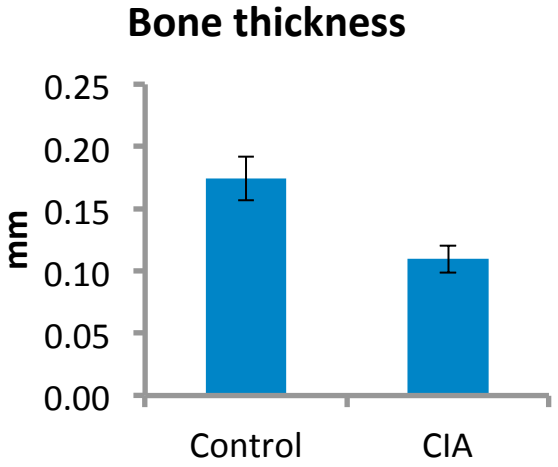

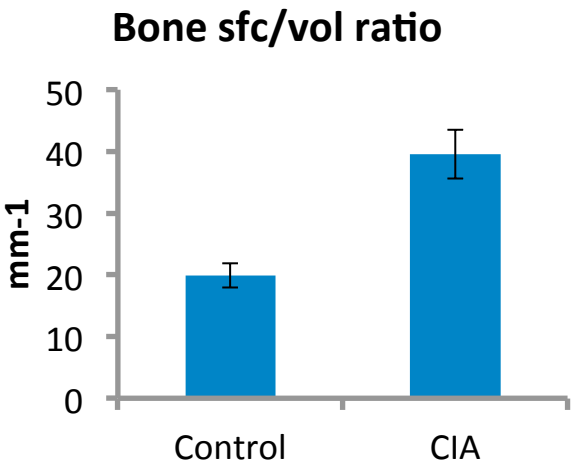

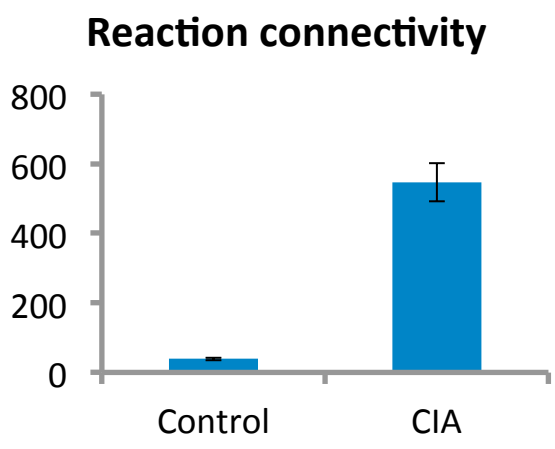

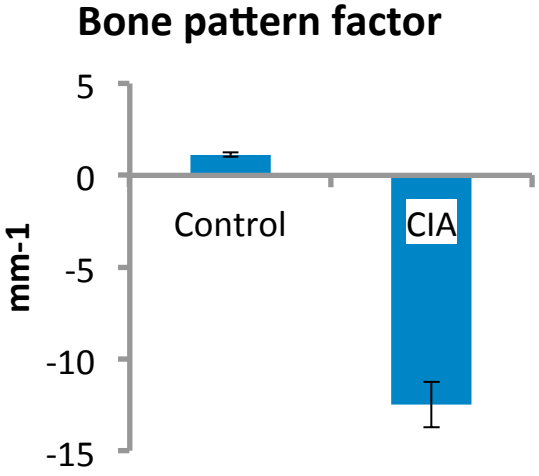

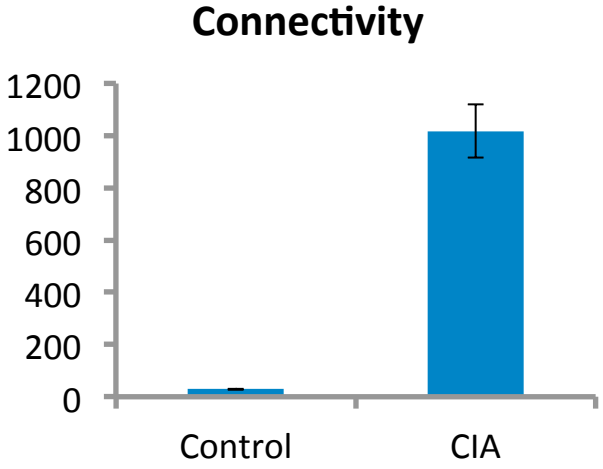

Accurate imaging and parameterisation of bone disruption in arthritis models

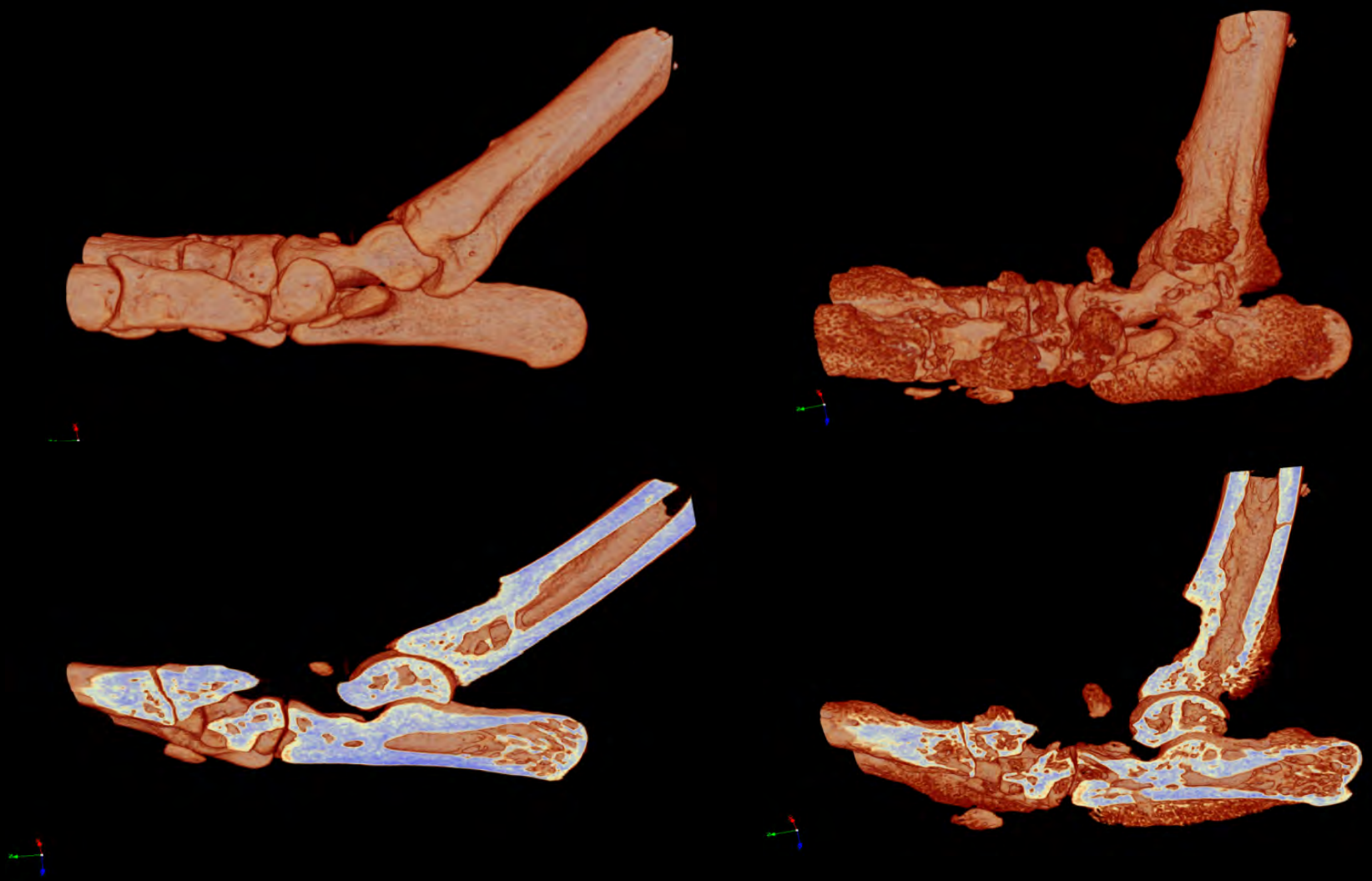

Mouse ankle, control

Mouse ankle, collagen-induced arthritis (CIA)

The rabbit subchondral bone:
osteoarthritis and osteoporosis

BRUKER
Bruker microCT

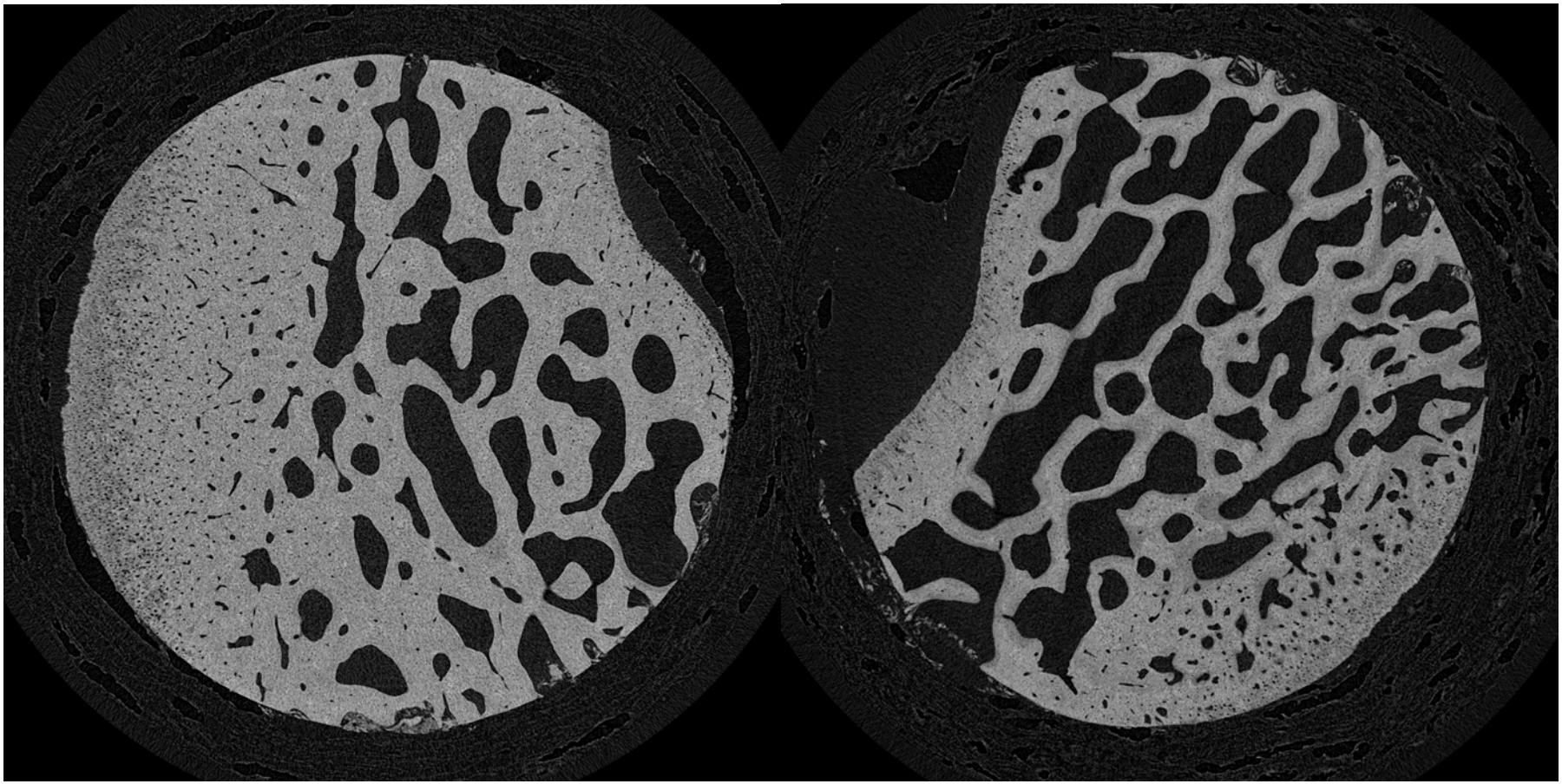

Control, left; osteoporisis + osteoarthritis, right. SkyScan1272, 3 um voxel size

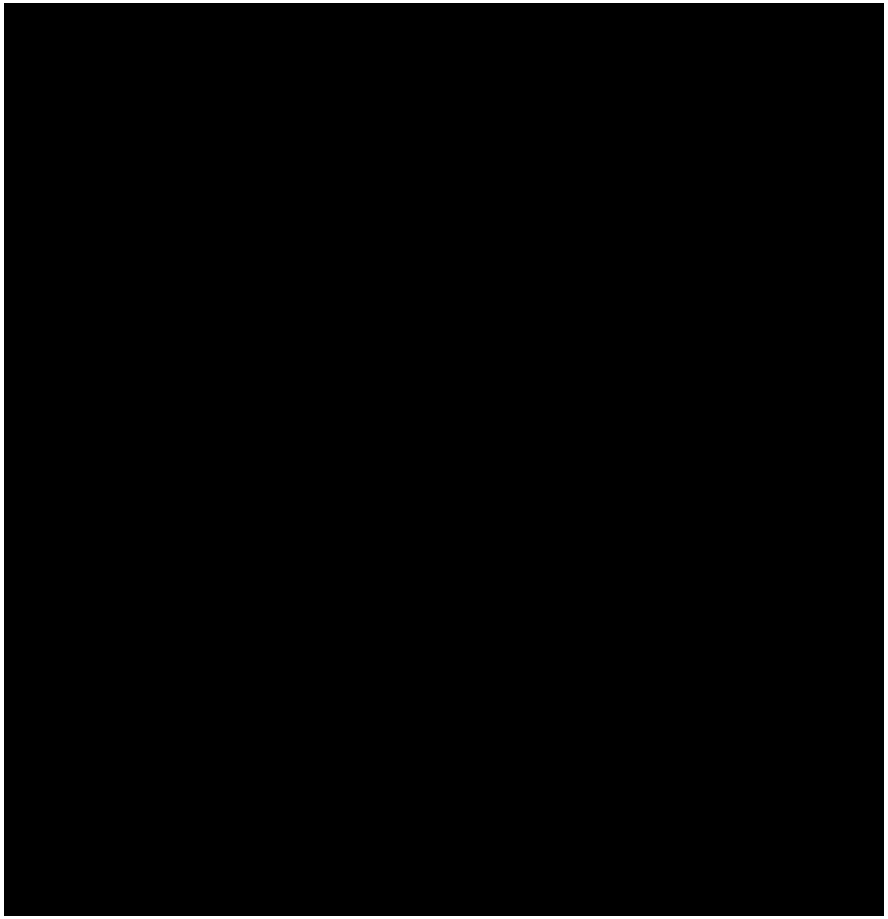

Above: osteocyte lacunae from canine cortical bone, SkyScan 1172

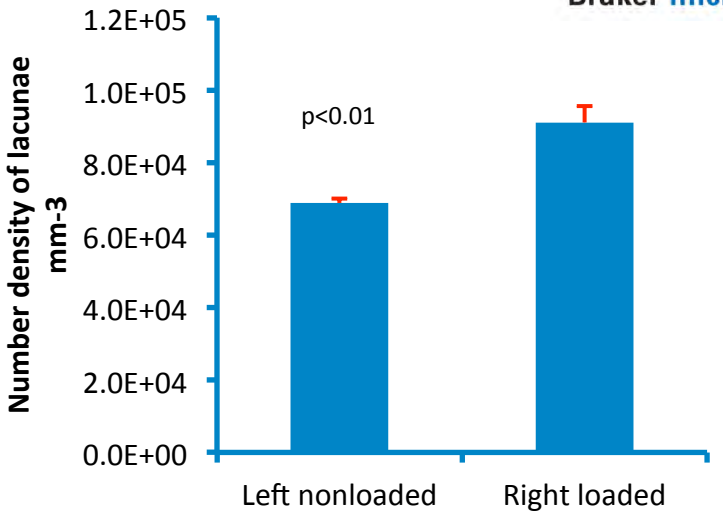

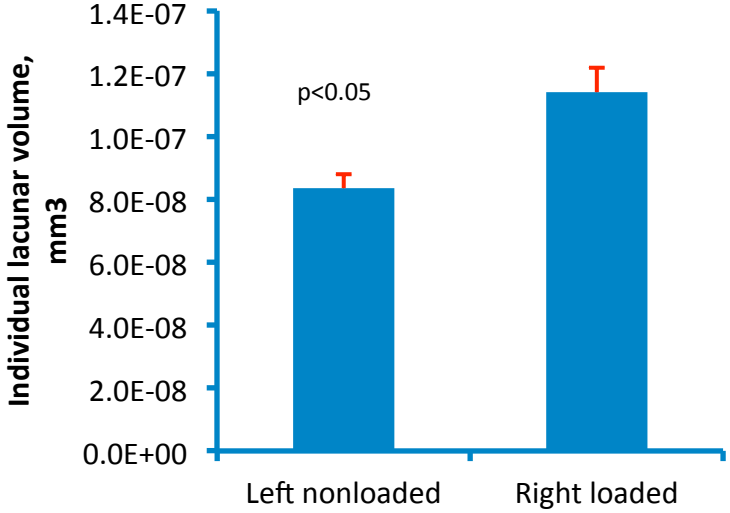

Overview

1. Principles of micro-computed x-ray tomography (“micro-CT”)
2. SkyScan 1172
3. Solutions for Life Science Applications
   - Dental (Teeth)
   - Dental (Scaffolds)
   - Bone
   - Bone (Biomechanics / Implants)
   - Soft Tissue
4. New Features in DataViewer, CTVox, CTAN

Biomechanics: head-banging woodpeckers

BRUKER
Bruker microCT

OPEN ACCESS Freely available online

PLoS one

Why Do Woodpeckers Resist Head Impact Injury: A Biomechanical Investigation

Lizhen Wang[1,2], Jason Tak-Man Cheung[3], Fang Pu[1], Deyu Li[1], Ming Zhang[2]*, Yubo Fan[1]*

1 Key Laboratory for Biomechanics and Mechanobiology of Ministry of Education, School of Biological Science and Medical Engineering, Beihang University, Beijing, People's Republic of China, **2** Department of Health Technology and Informatics, the Hong Kong Polytechnic University, Hong Kong, **3** Li Ning Sports Science Research Center, Beijing, People's Republic of China

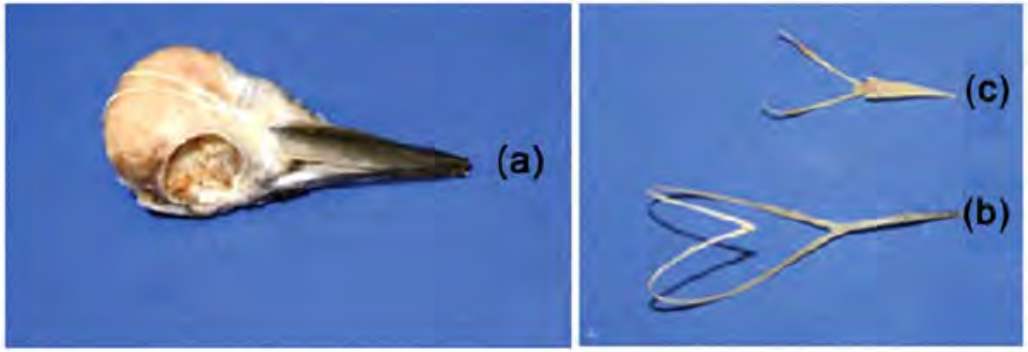

Figure 3. Anatomical structures of head and hyoid bone. (a) Great Spotted woodpecker's head; (b) Great Spotted Woodpecker's hyoid bone; (c) Eurasian hoopoe's hyoid bone.
doi:10.1371/journal.pone.0026490.g003

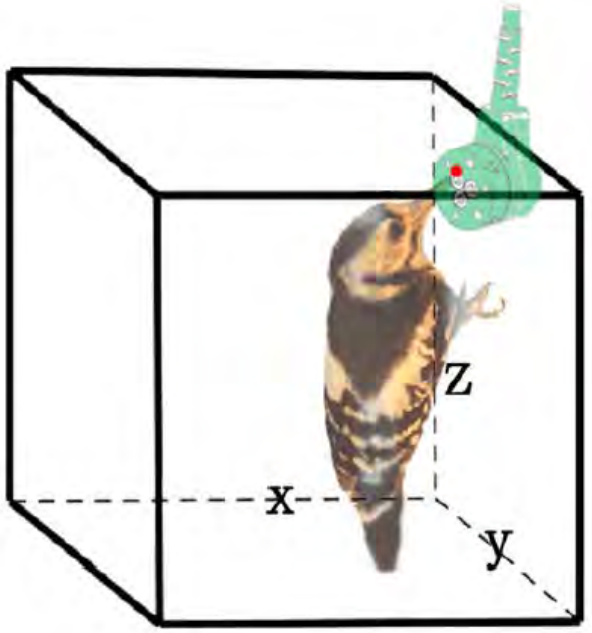

Micro-CT images (SkyScan1076) provide the input material for FEA wood-peck simulations

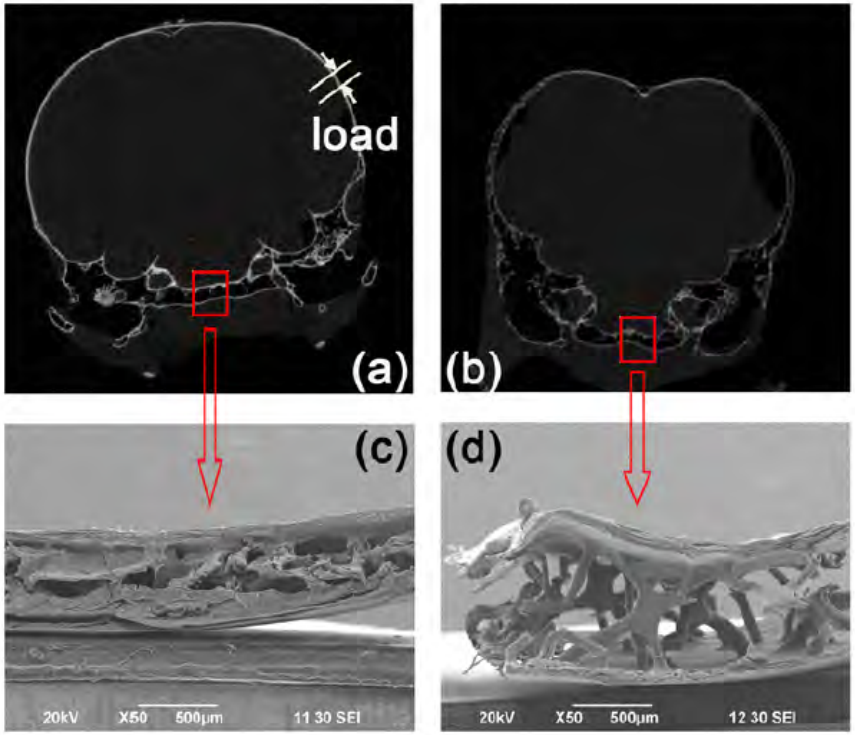

Figure 2. Micro-morphology of cranial bone. (a) The micro-CT scanning images of Great Spotted woodpecker's head on the coronal plane; (b) The micro-CT scanning images of Eurasian hoopoe's head on the coronal plane; (c) The SEM image of Great Spotted woodpecker's cranial bone; (d) The SEM image of Eurasian hoopoe's cranial bone.
doi:10.1371/journal.pone.0026490.g002

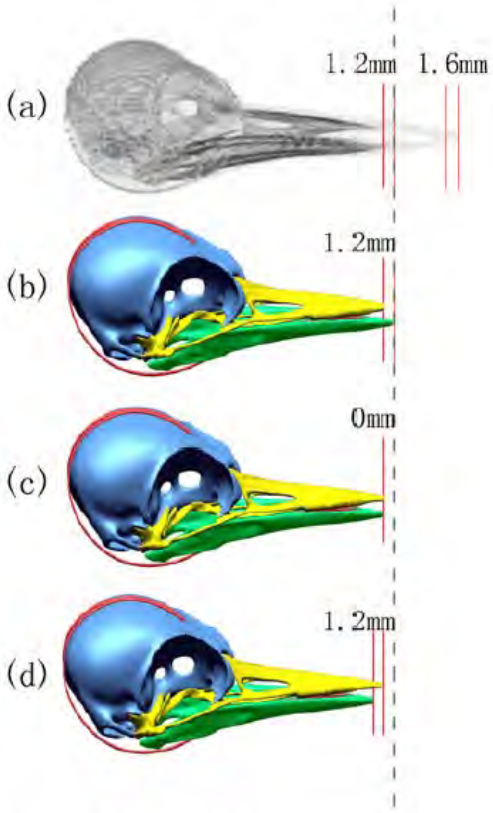

Figure 4. Micro-CT image and the FE models of Great Spotted Woodpecker' head. (a) Micro-CT image of Great Spotted Woodpecker' head; (b) $Beak_{Lower} > Beak_{Upper}$ FE model; (c) $Beak_{Lower} = Beak_{Upper}$ FE model; (d) $Beak_{Lower} < Beak_{Upper}$ FE model.
doi:10.1371/journal.pone.0026490.g004

Stress sequence of a wood-peck

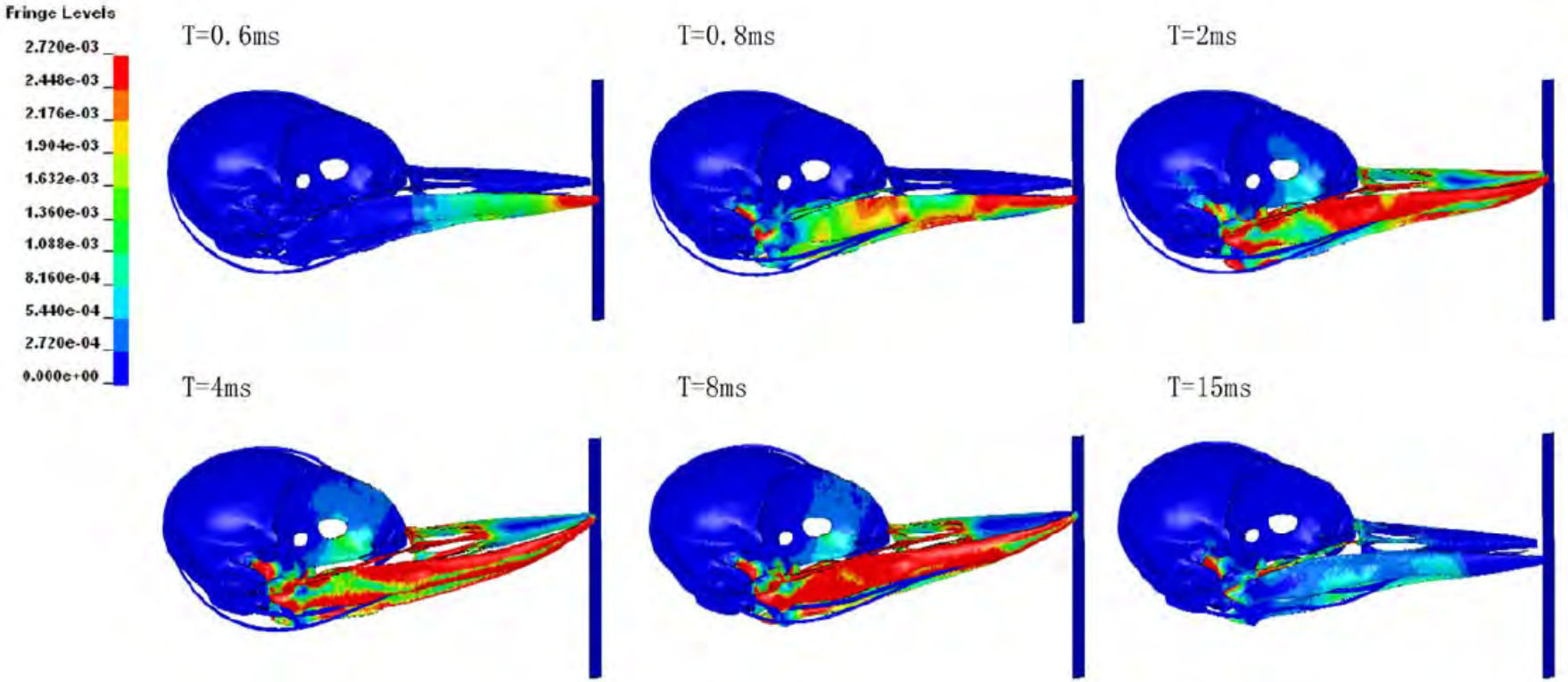

Figure 7. The effective stress distribution of woodpecker's head during pecking.
doi:10.1371/journal.pone.0026490.g007

Metallic implants play a major role in orthopedic bone reconstruction and repair

Bruker microCT

Journal of Periodontology; Copyright 2011 DOI: 10.1902/jop.2011.110569

Alveolar Bone Remodeling Around Immediate Implants Placed in Accordance With the Extraction Socket Classification — A Three-Dimensional Micro-Computed Tomography Analysis

Munirah Saleh Al-Shabeeb,[*] Mansour Al-Askar,[*] Abdulaziz Al-Rasheed,[*,†] Nadir Babay,[†] Fawad Javed,[*] Hom-Lay Wang,[‡] Khalid Al-Hezaimi,[*,†]

A series of reconstructed sagital and axial micro computed tomography images illustrating the measurements of the buccal bone thickness and volume of bone around immediate implant. a.1, b.1, and c.1) sagital sections show the buccal and lingual bone thickness around the implant placed in Group-1, -2 and -3, respectively. a.2, b.2, and c.2) Axial section at the level of the crestal bone showing the different buccal bone thickness around dental implants at the crestal bone level in each Group-1, -2, and -3, respectively. (Red line shows the border of the buccal and lingual bone).

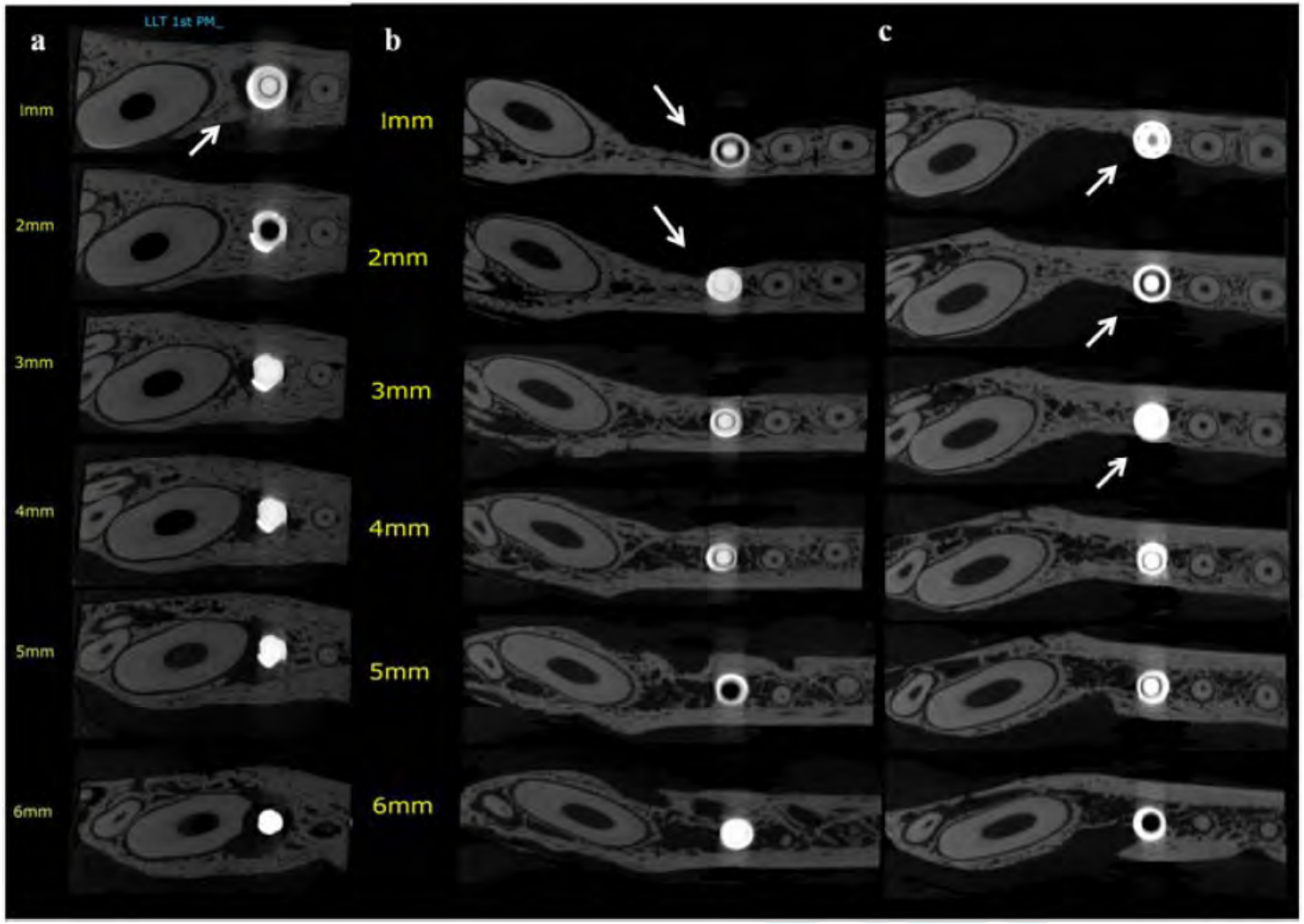

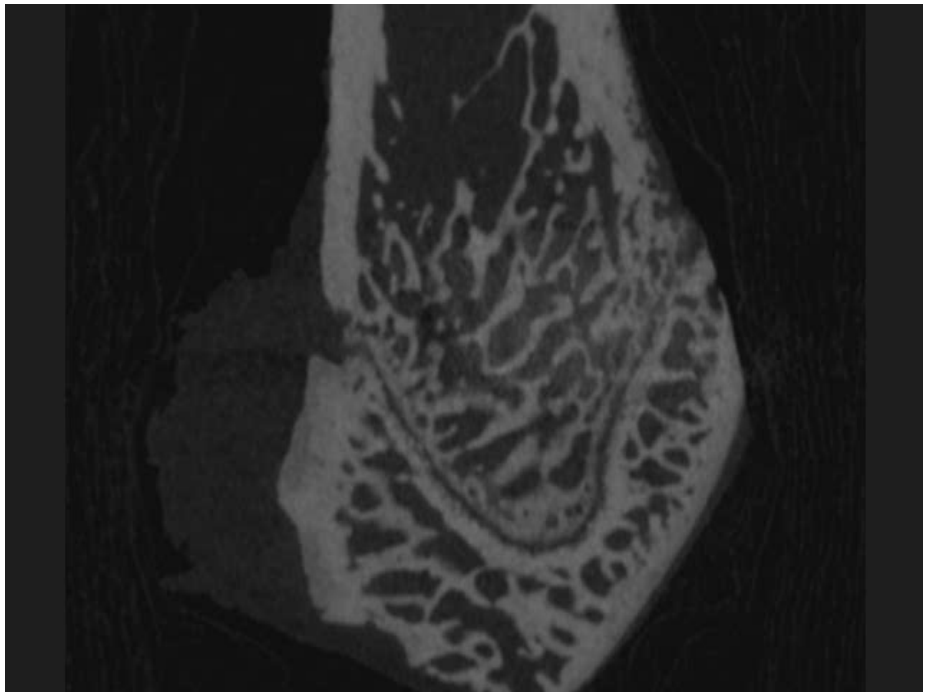

TISSUE ENGINEERING: Part A
Volume 00, Number 00, 2013

DOI: 10.1089/ten.tea.2013.0181

Original Article

Enhanced Bone Regeneration of Cortical Segmental Bone Defects Using Porous Titanium Scaffolds Incorporated with Colloidal Gelatin Gels for Time- and Dose-Controlled Delivery of Dual Growth Factors

Johan van der Stok, MD,[1,*] Huanan Wang, MSc,[2,*] Saber Amin Yavari, MSc,[3] Michiel Siebelt, MD,[1] Marjan Sandker, MD,[1] Jan H. Waarsing, PhD,[1] Jan A.N. Verhaar, MD, PhD,[1] Holger Jahr, PhD,[1] Amir A. Zadpoor, PhD,[3] Sander C.G. Leeuwenburgh, PhD,[2] and Harrie Weinans, PhD[1,3,4]

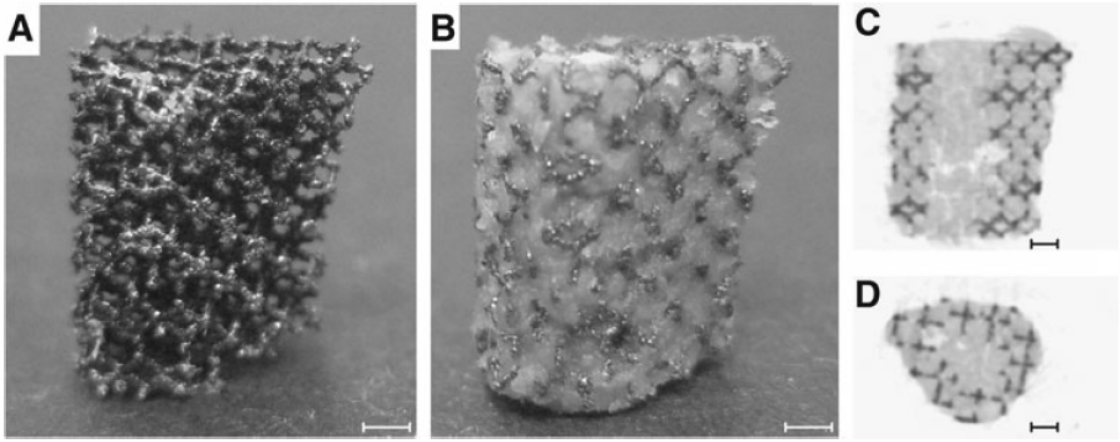

FIG. 1. Photographs of porous titanium scaffolds in the shape of the 6-mm bone segment that was replaced during the animal experiment before **(A)** and after **(B)** incorporation with colloidal gelatin gels. Micro-CT images of perpendicular **(C)** and horizontal **(D)** cross sections of porous titanium scaffold (black) incorporated with colloidal gelatin gels containing iodine-based radiographic contrast agent ioxaglate (gray). Scale bar = 1 mm. Micro-CT, micro-computed tomography.

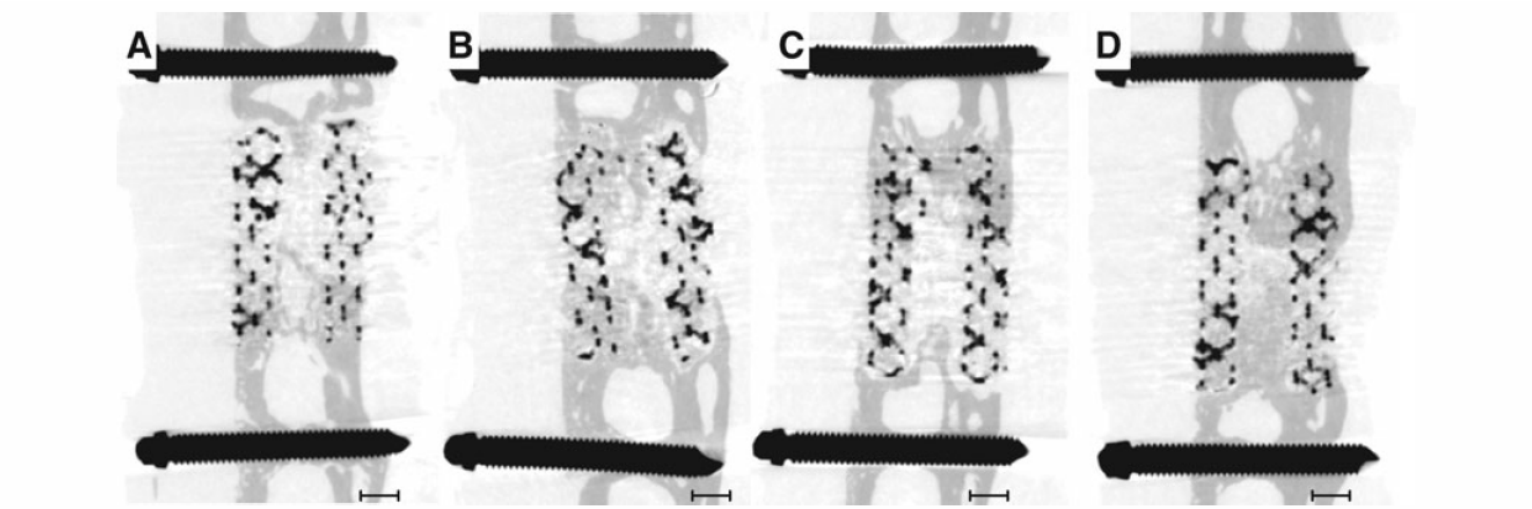

FIG. 4. Representative transversal micro-CT images of the porous titanium scaffolds containing unloaded **(A)**, fibroblast growth factor-2 (FGF-2) **(B)**, bone morphogenetic protein-2 (BMP-2) **(C)**, or BMP-2/FGF-2 **(D)** gels after 12 weeks. Porous titanium scaffolds and fixation screws appear in black, whereas bone appears in dark gray. Scale bar = 1 mm.

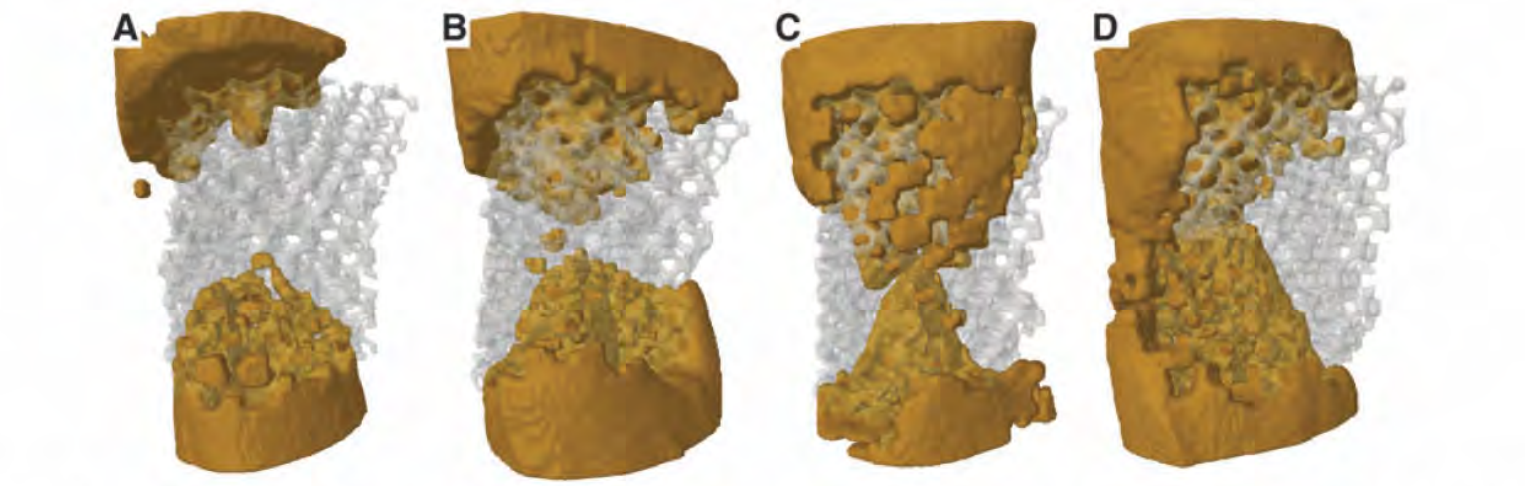

FIG. 5. Representative 3D micro-CT images of bone bridging the porous titanium scaffolds containing unloaded **(A)**, FGF-2 **(B)**, BMP-2 **(C)**, or BMP-2/FGF-2 **(D)** gels after 12 weeks. Porous titanium scaffolds are shown in transparent, whereas bone appears in dark grey. Color images available online at www.liebertpub.com/tea

SkyScan 1176 scanner, CTVol software

Overview

1. Principles of micro-computed x-ray tomography (“micro-CT”)
2. SkyScan 1172
3. Solutions for Life Science Applications
   - Dental (Teeth)
   - Dental (Scaffolds)
   - Bone
   - Bone (Biomechanics / Implants)
   - Soft Tissue
4. New Features in DataViewer, CTVox, CTAN

Contrast agents can confer contrast to soft tissue, opening the development of "micro-CT histology"

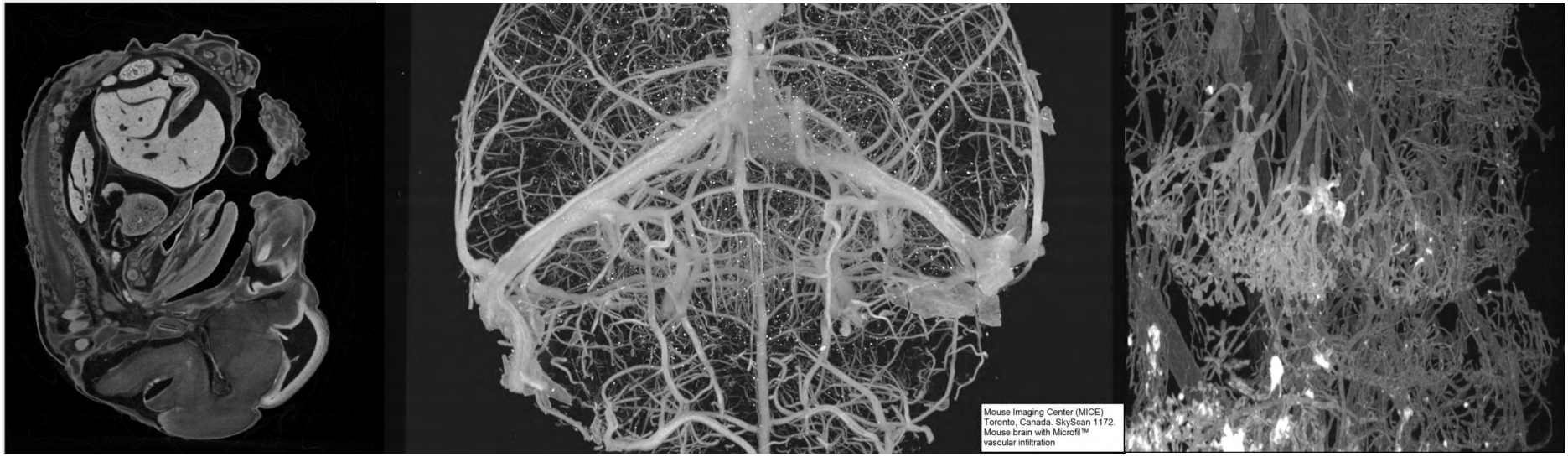

Mouse embryo 15 d, PTA

Mouse brain with Microfil infiltration of blood vessels: brain (left), femur (right)

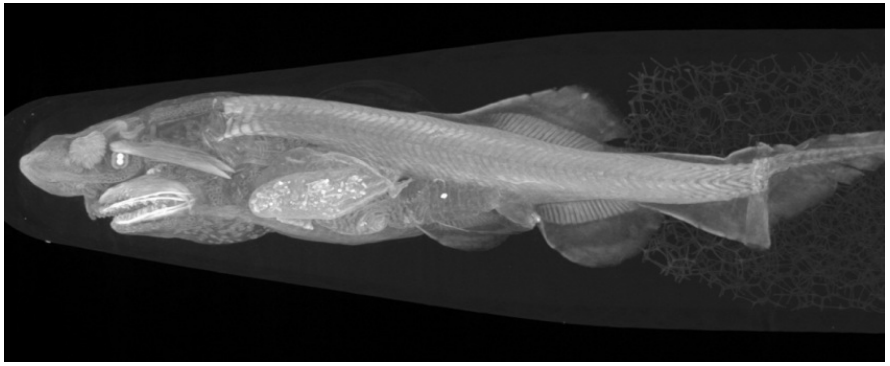

Paddlefish (tetraodon) larva, stained by phosphotungstic acid (PTA)

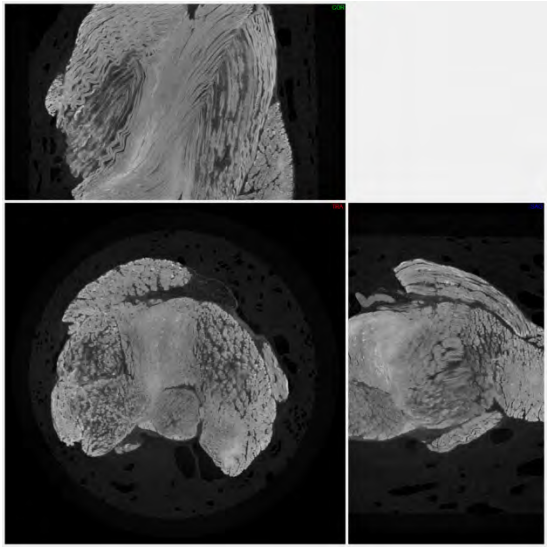

Muscle, stained by phosphotungstic acid (PTA)

Cartilage staining for microCT

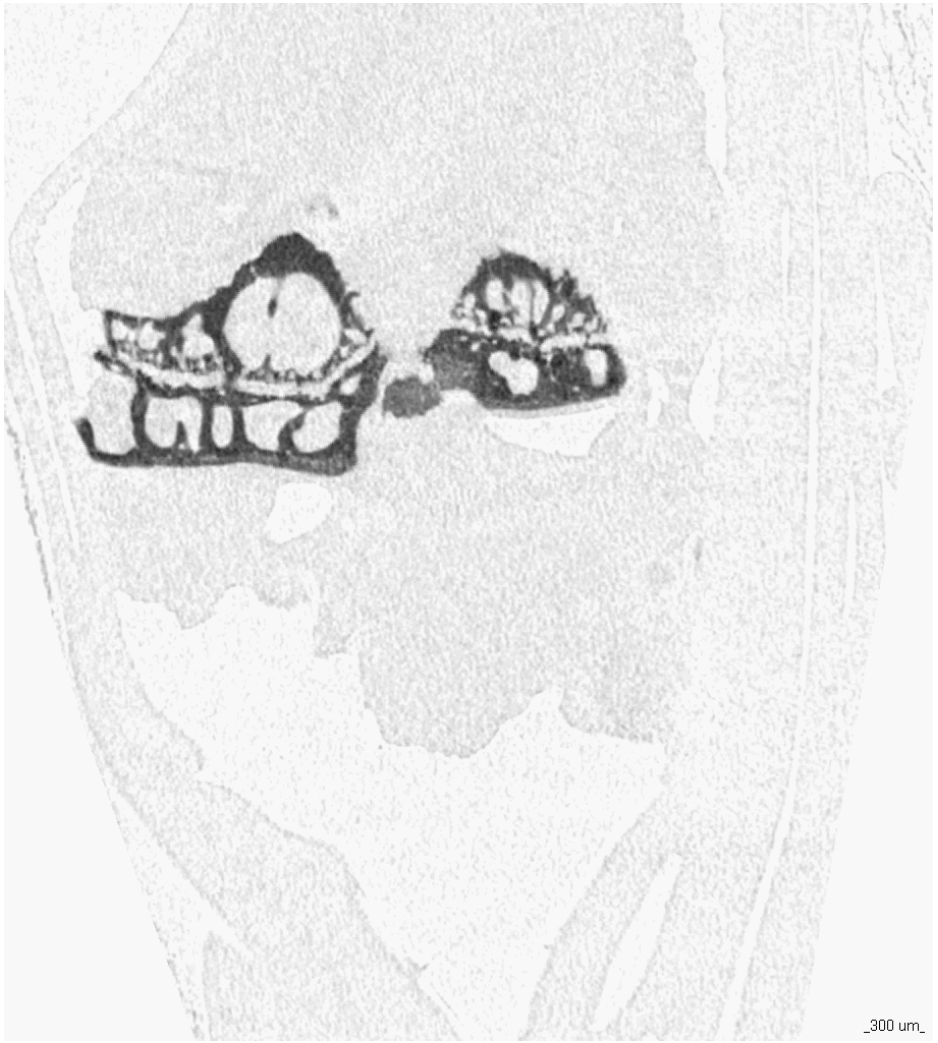

PTA – baseline: calcified cartilage is visible, but not non-mineralised cartilage

PTA – 24 hours – successful cartilage staining but bone partly demineralised.

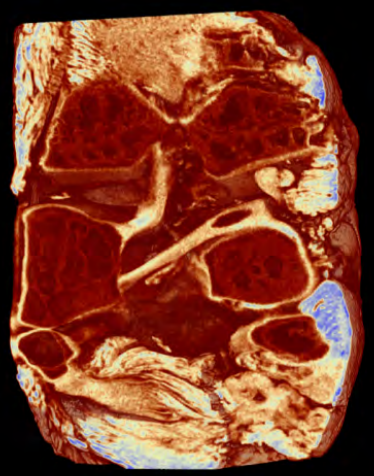

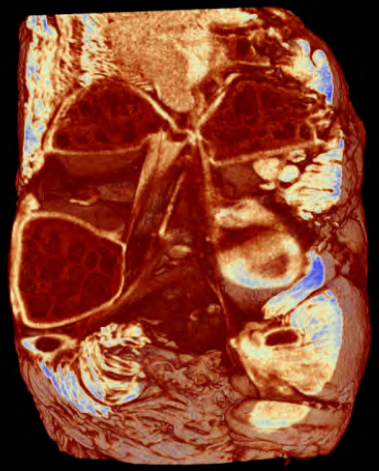

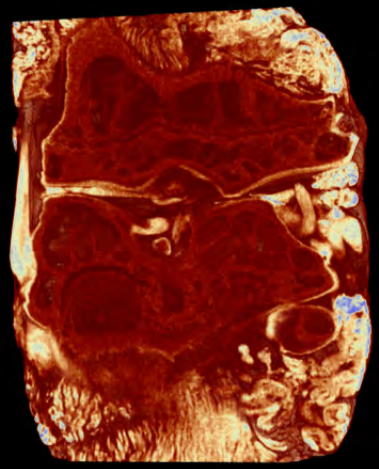

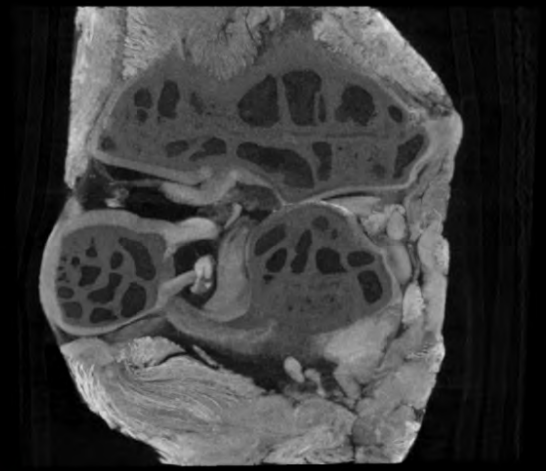

Staining of the mouse joint allows accurate imaging and quantiation of cartilage in arthritis models

Lung imaging and analysis for pulmonary research: human lung autopsy at high resolution

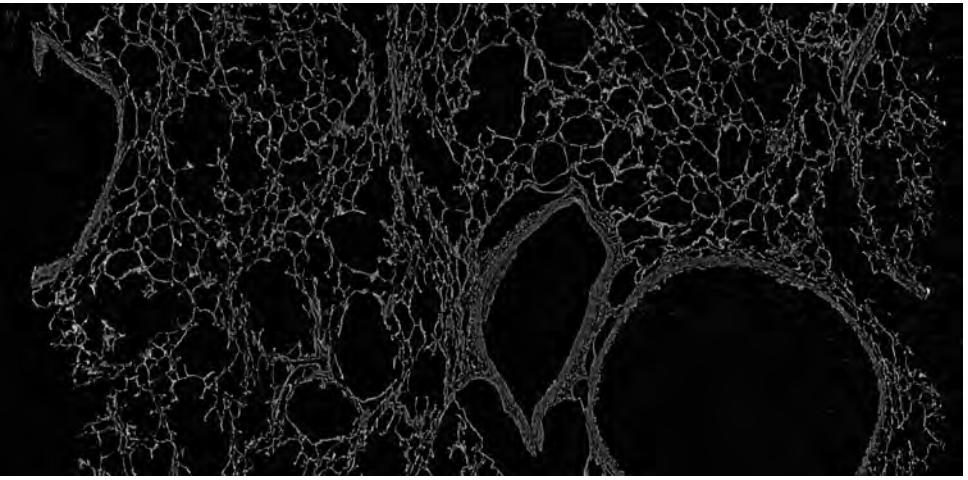

Cross-section: 2 micron pixel

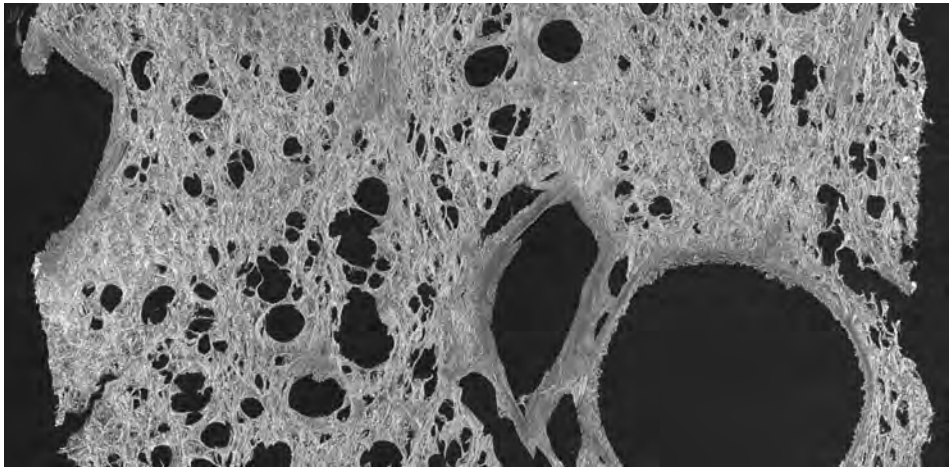

MIP (maximum intensity projection)

Lung imaging and analysis for pulmonary research: Mouse lung sample at high resolution

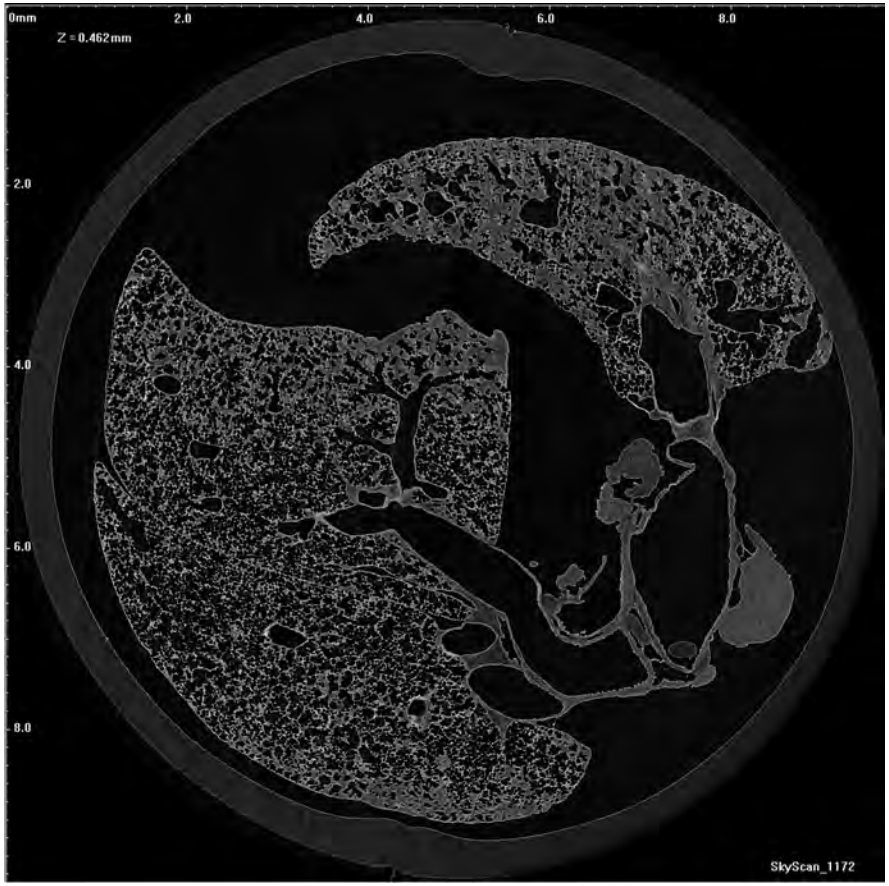

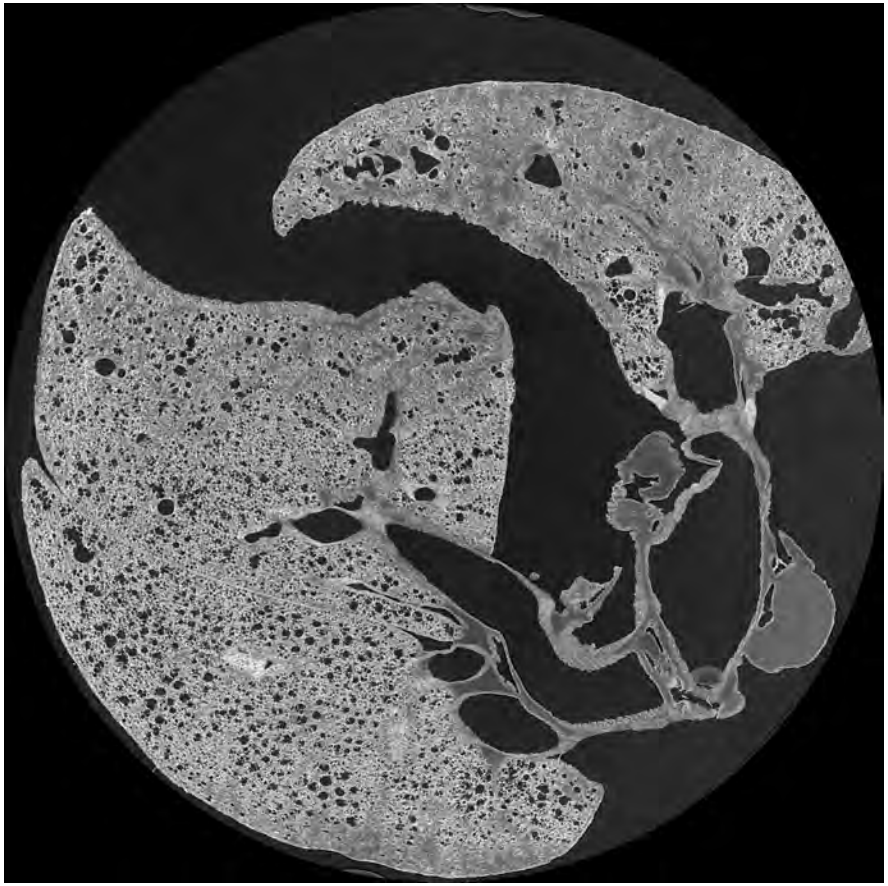

Quantification of lung tumour vasculature destruction

Mouse lung tumour (yellow) and lung vasculature (red)

no treatment

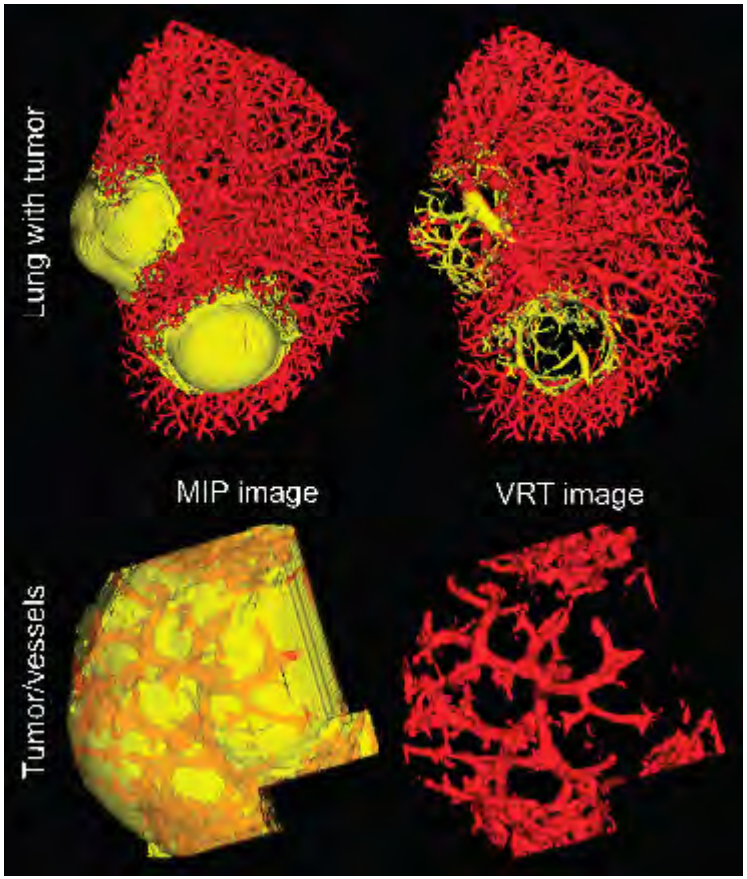

Anti-VEGF treatment

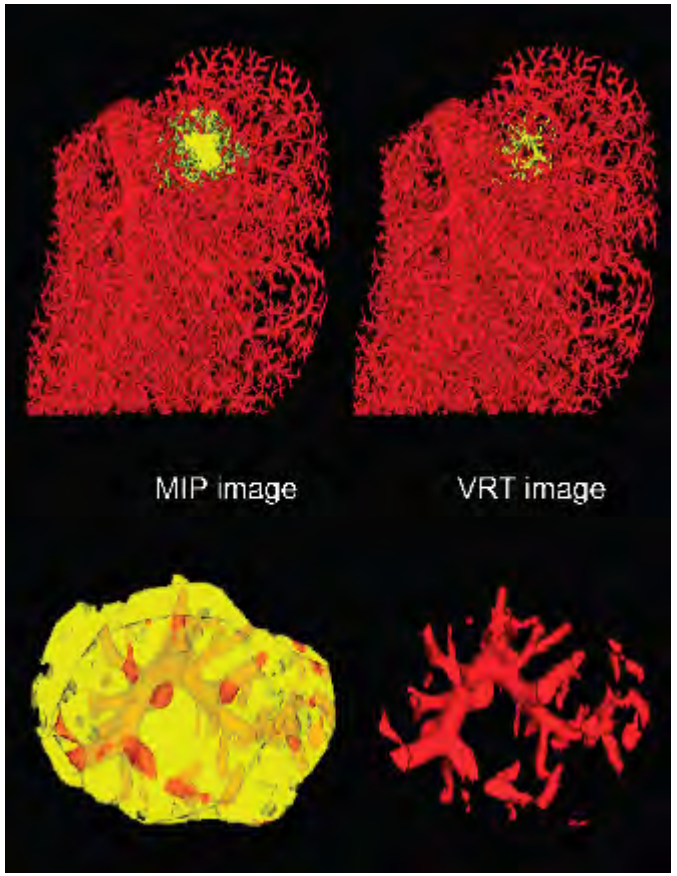

Savai R. et.al. 2009, Neoplasia, 11, 48-56

Brain vascularization imaged by blood vessel contrast agent: mouse brain with MicroFil

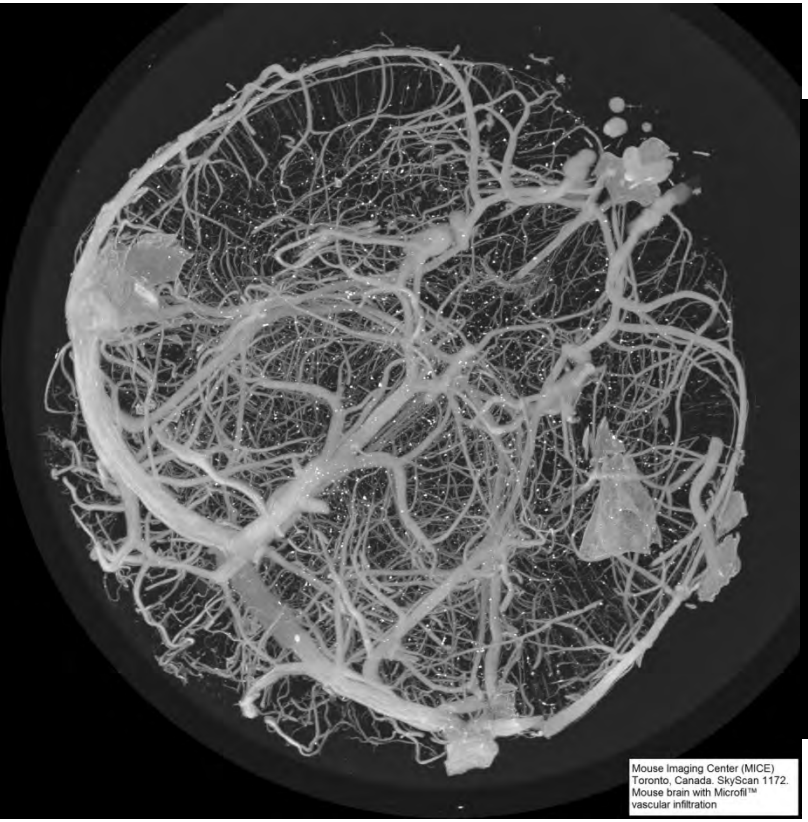

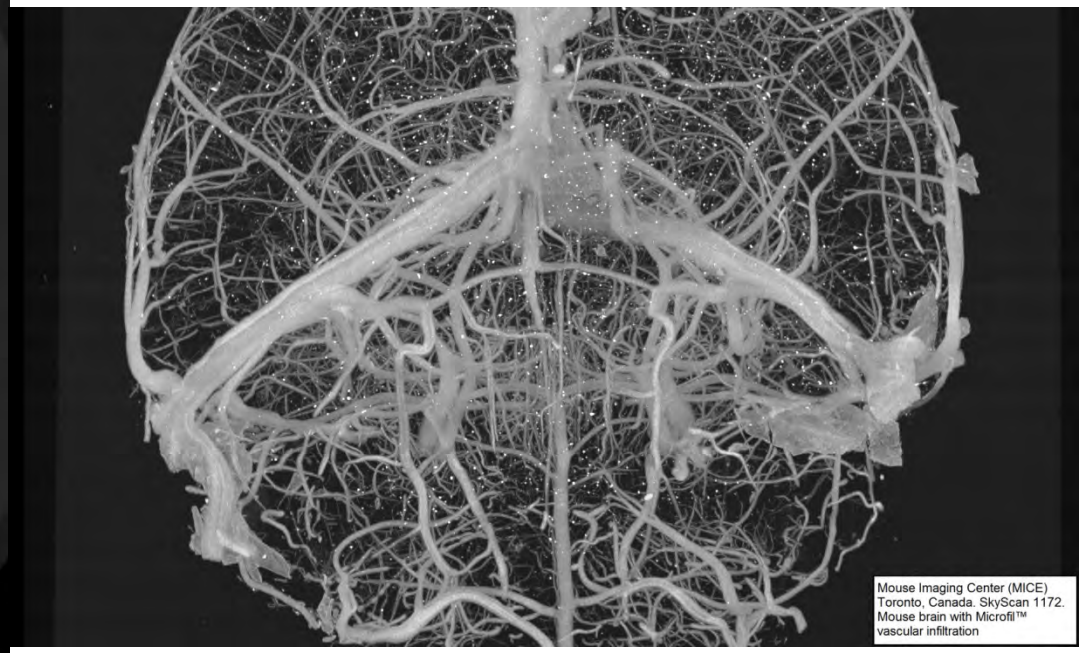

Bone vascularisation imaged by blood vessel contrast agent: mouse tibia and gastrocnemius muscle arterial structure

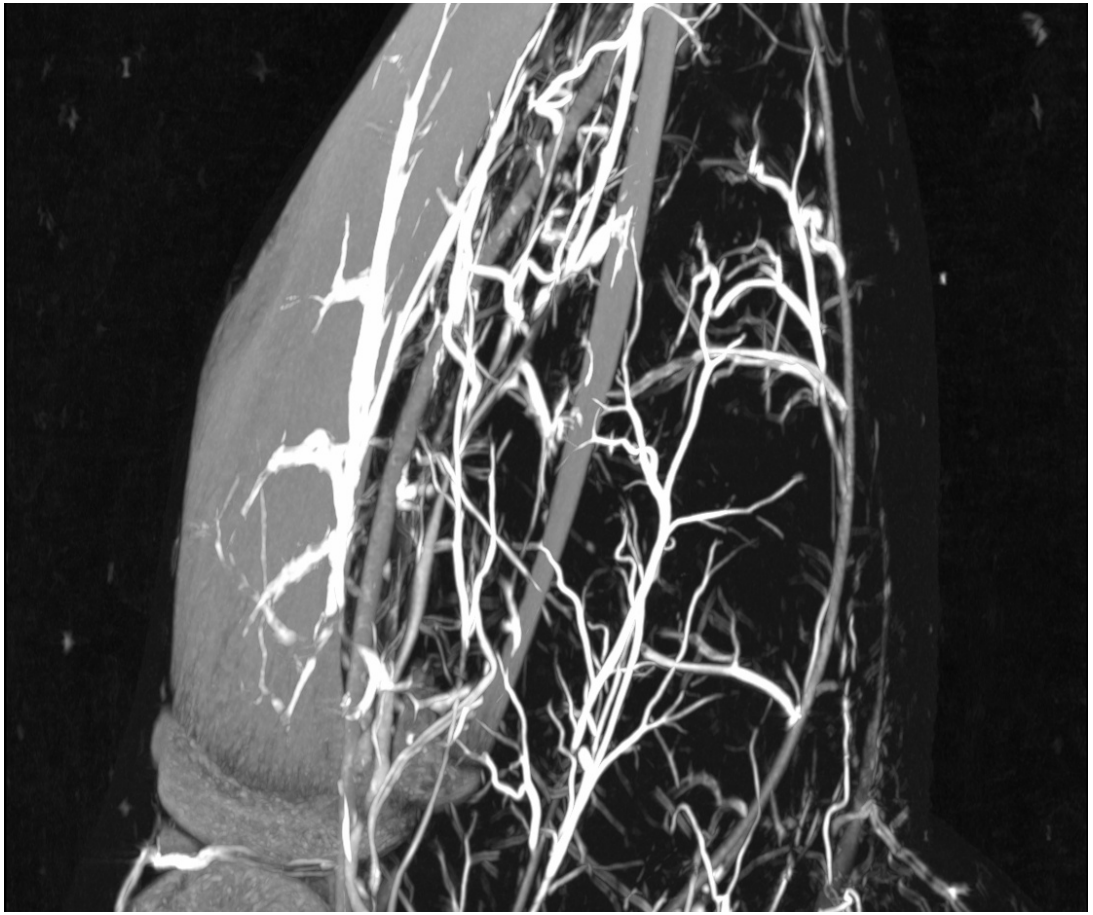

Micro-CT in animal anatomy and developmental biology: Head of embryo of Amia fish

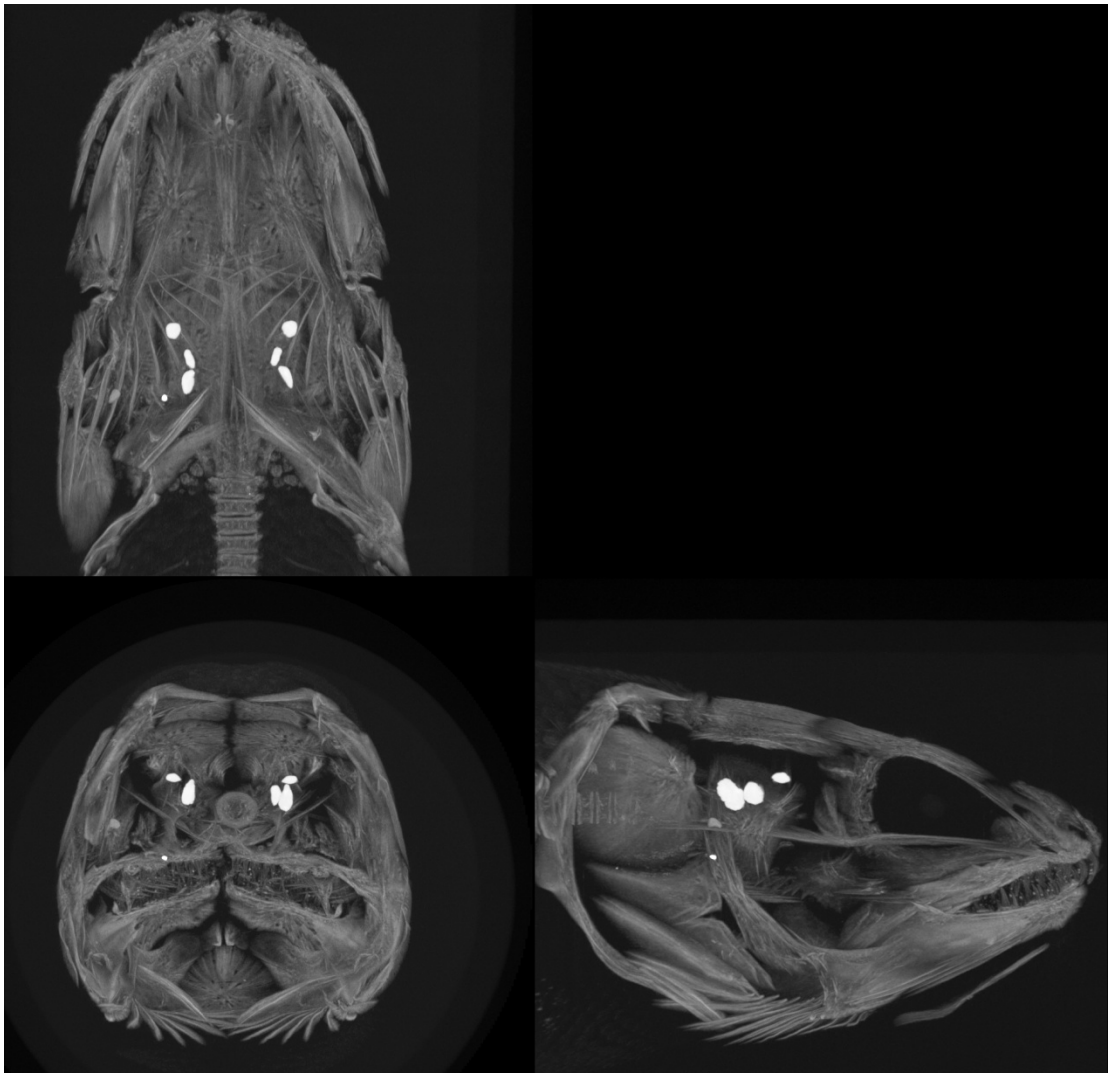

Micro-CT in animal anatomy and developmental biology: Head of embryo of paddlefish

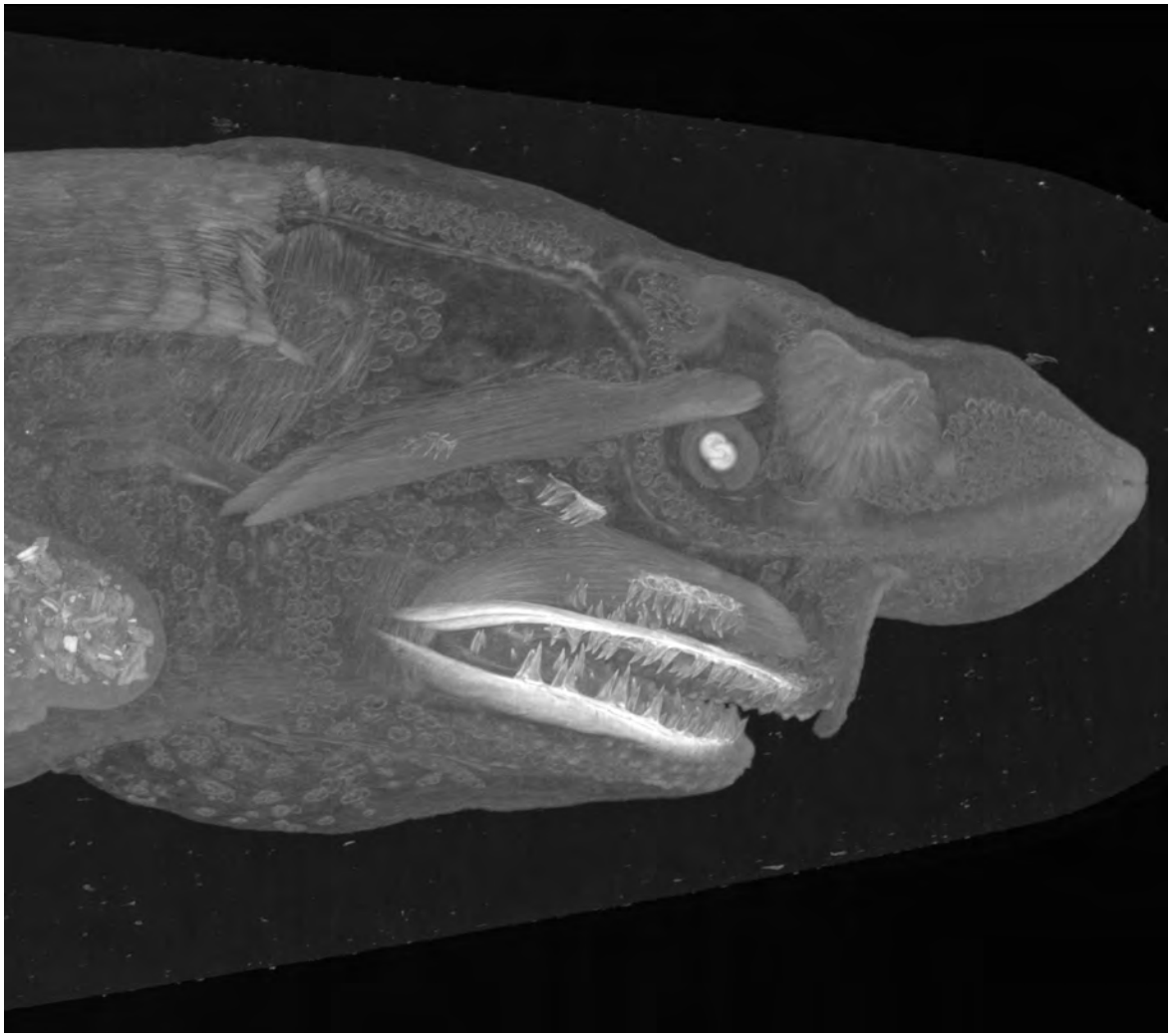

Micro-CT in animal anatomy and developmental biology: Whole embryo of paddlefish (with contrast agent for soft / neural tissues)

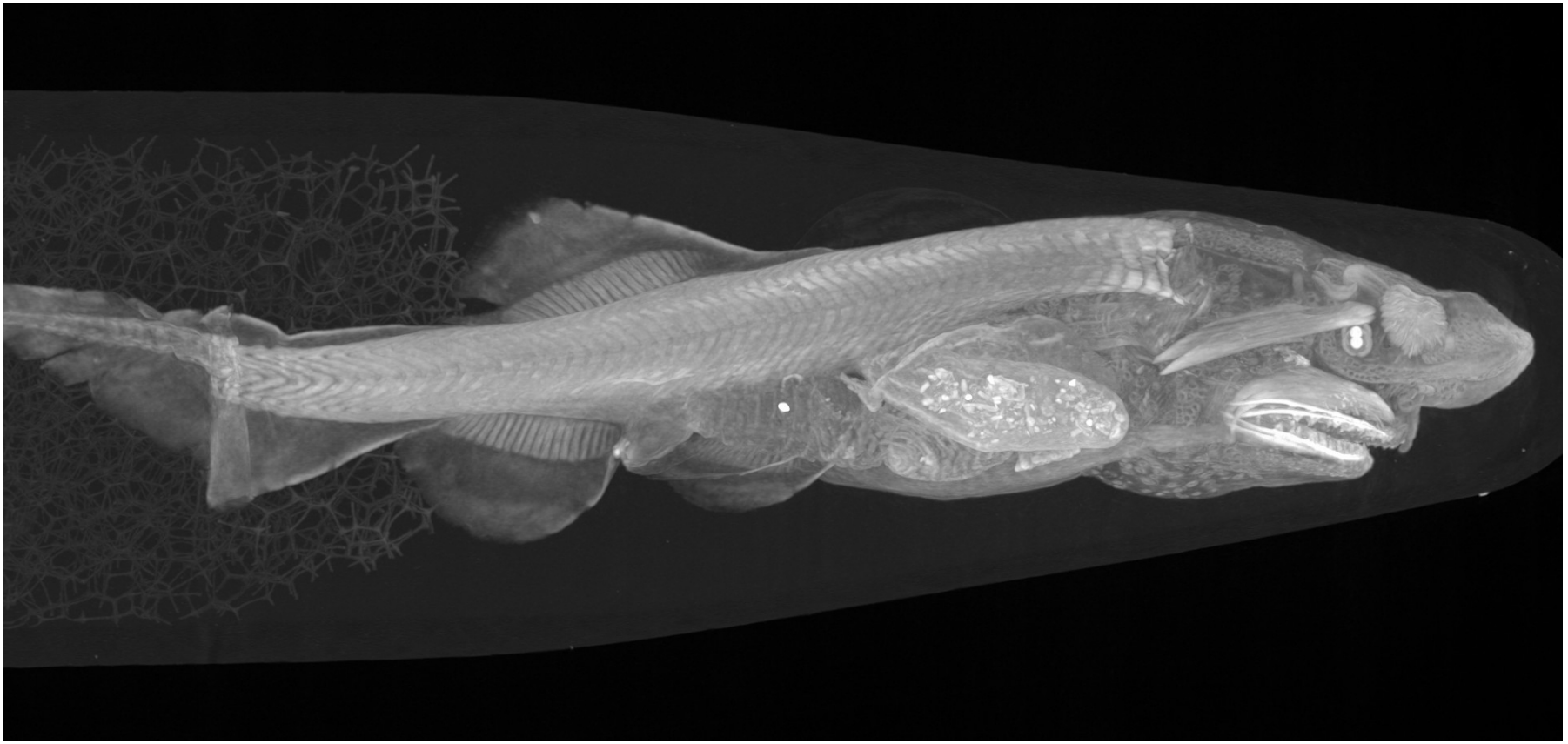

Overview

1. Principles of micro-computed x-ray tomography (“micro-CT”)
2. SkyScan 1172
3. Solutions for Life Science Applications
4. New Features in DataViewer, CTVox, CTAN
   - Image Co-Registration
   - Link Datasets
   - Multi Dataset Loading in CTVox
   - Multi-threading Structure Thickness and Separation
   - Multi ROIs and Add/Subtract ROI
   - Conditional Mean Filtering
   - Watershed Separation
   - Collections Tab
   - Reference “Upside Down”
   - Exclude Top/Bottom Surface Area

New Features in “DataViewer”

Image Co-Registration of Datasets

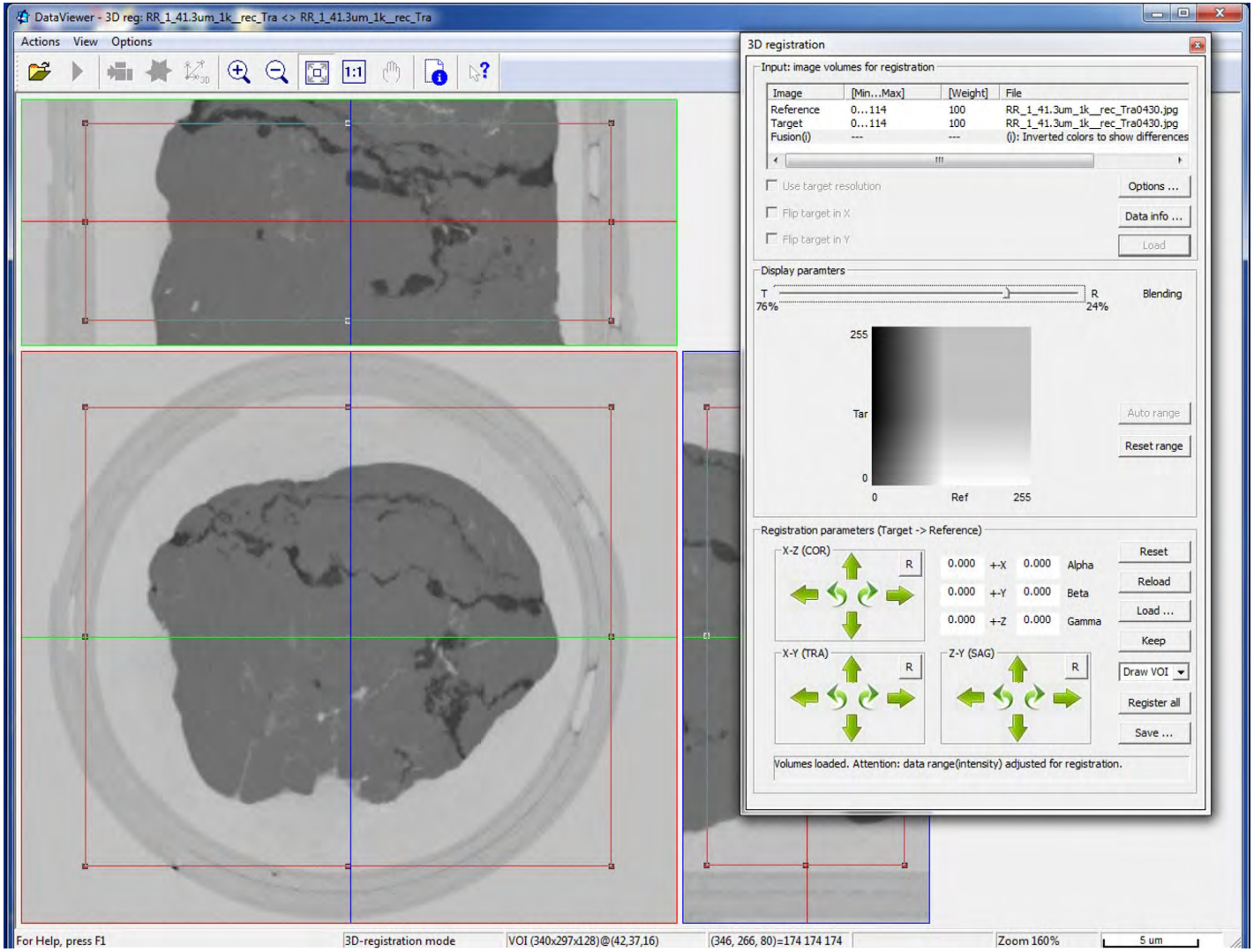

Possibility to co-register two different dataset in the 3 orthogonal directions.

Important in comparative assessments: Pre- and Post Treatments

New Features in “DataViewer”

Image Co-Registration of Datasets

Links two datasets of same size into one screen. Ideal for changing the zoom and visual comparison.

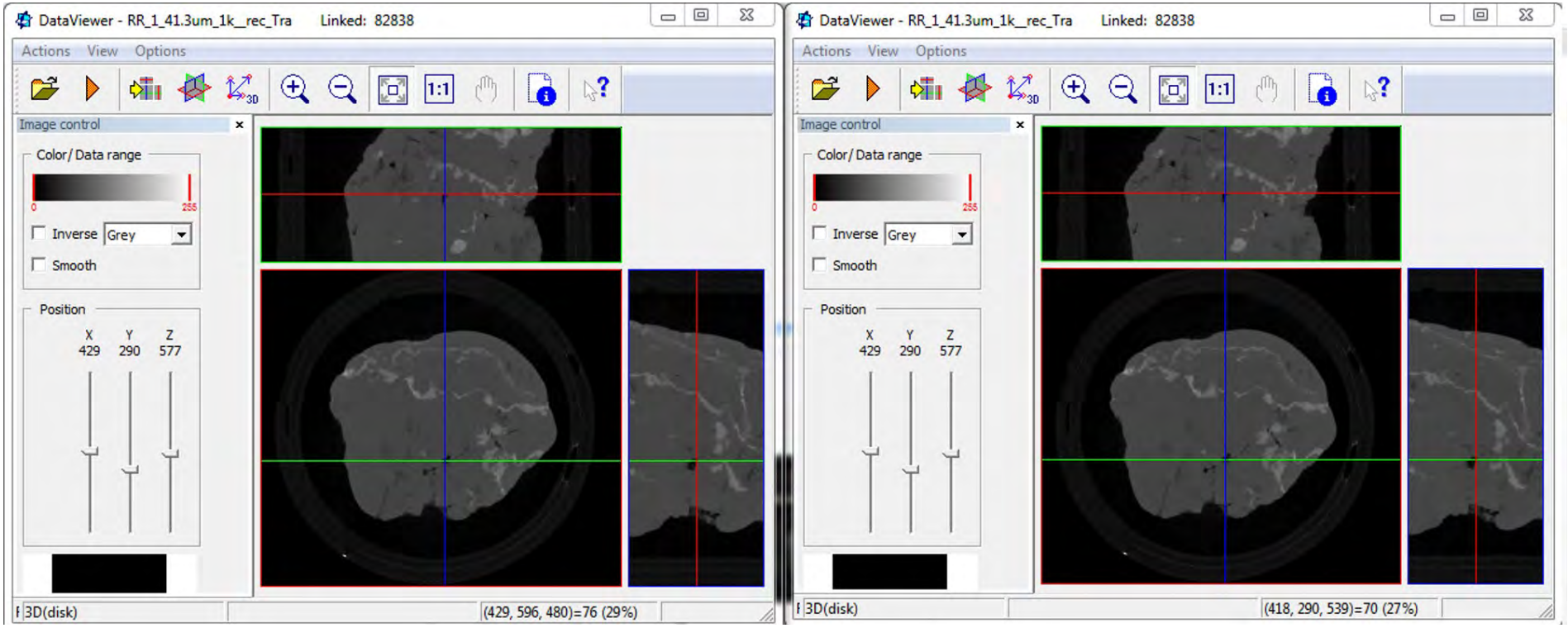

New Features in “CTVox”

Load Multiple Datasets

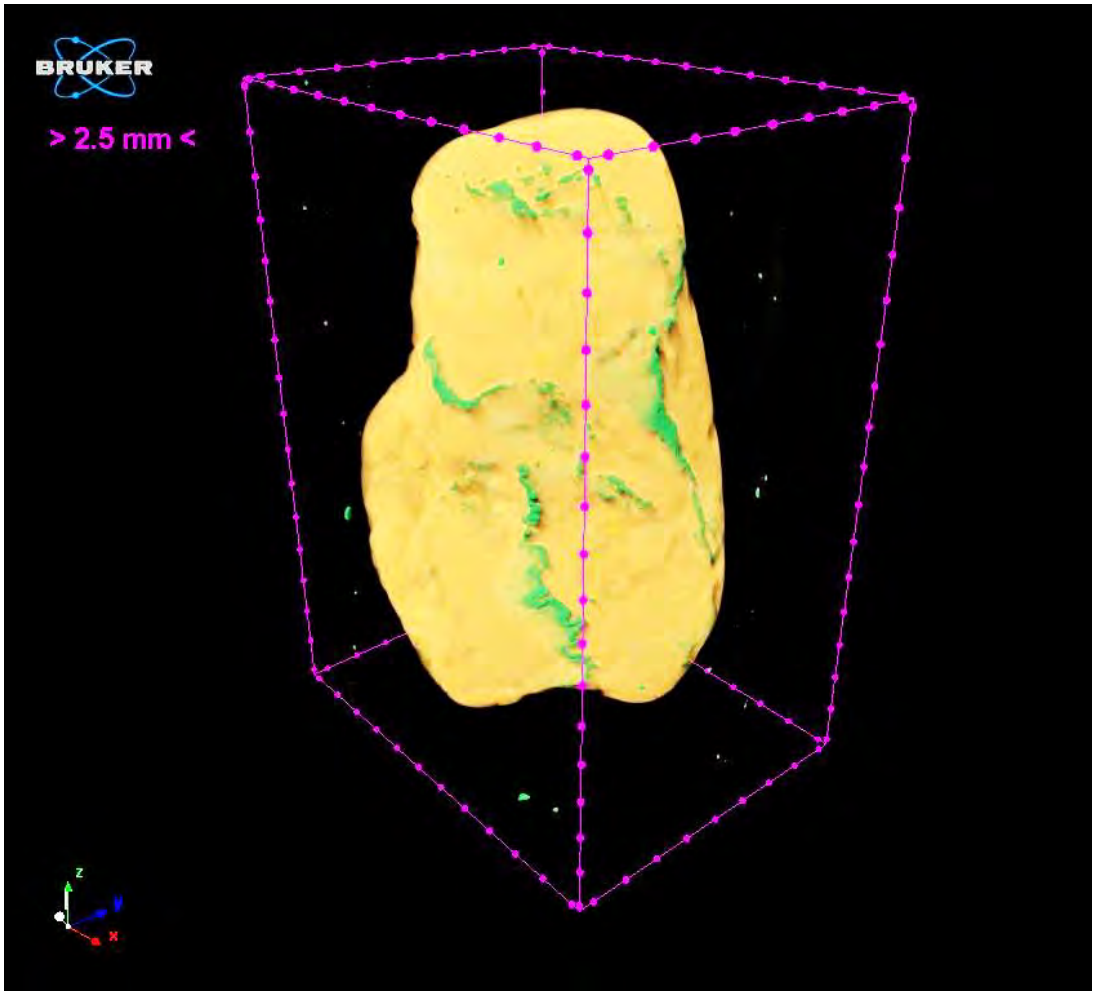

Possibility to load up to 10 different datasets in CTVOX.

New Features in “CT Analyzer”

Thickness Calculation

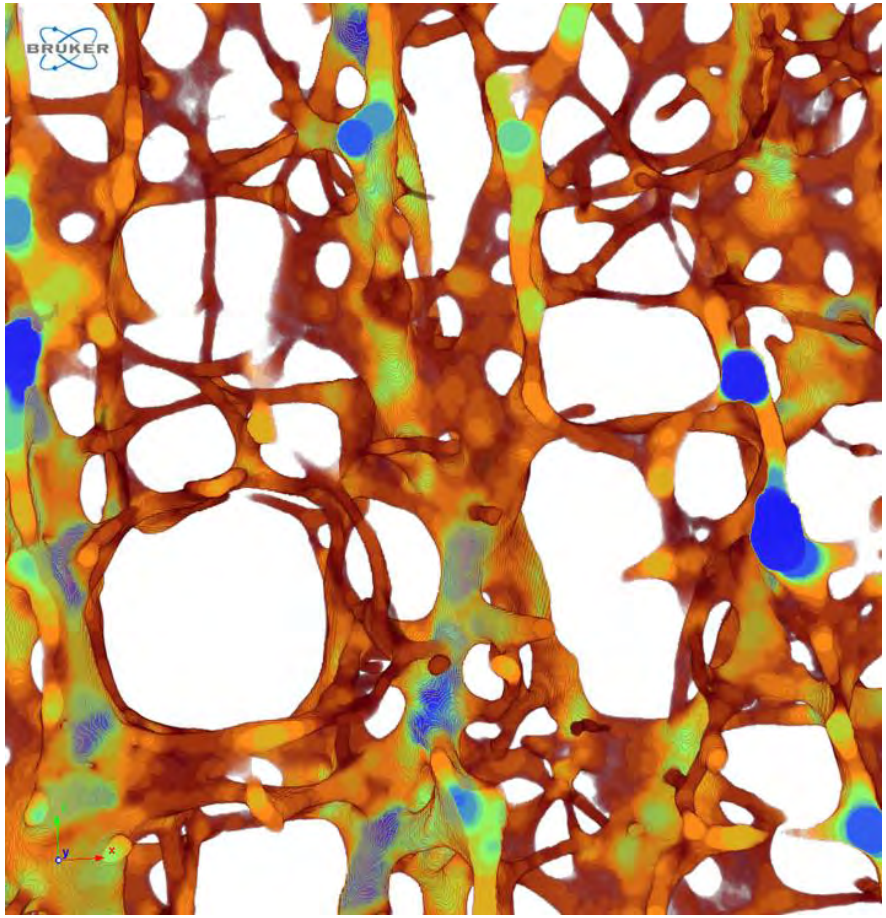

Mapping of spatially resolved local thickness in 3D, illustrated by this thickness-color image, is now 5-8 times faster in CTAn.

- 3D thickness and separation calculation is now 5-8 times faster than the previous versions.
- Slightly more acccurate
- Tb.Th and Tb.Sp results will be 1-2% different than in previous versions

New Features in “CT Analyzer”

Multiple ROIs and Add/Sub ROIs

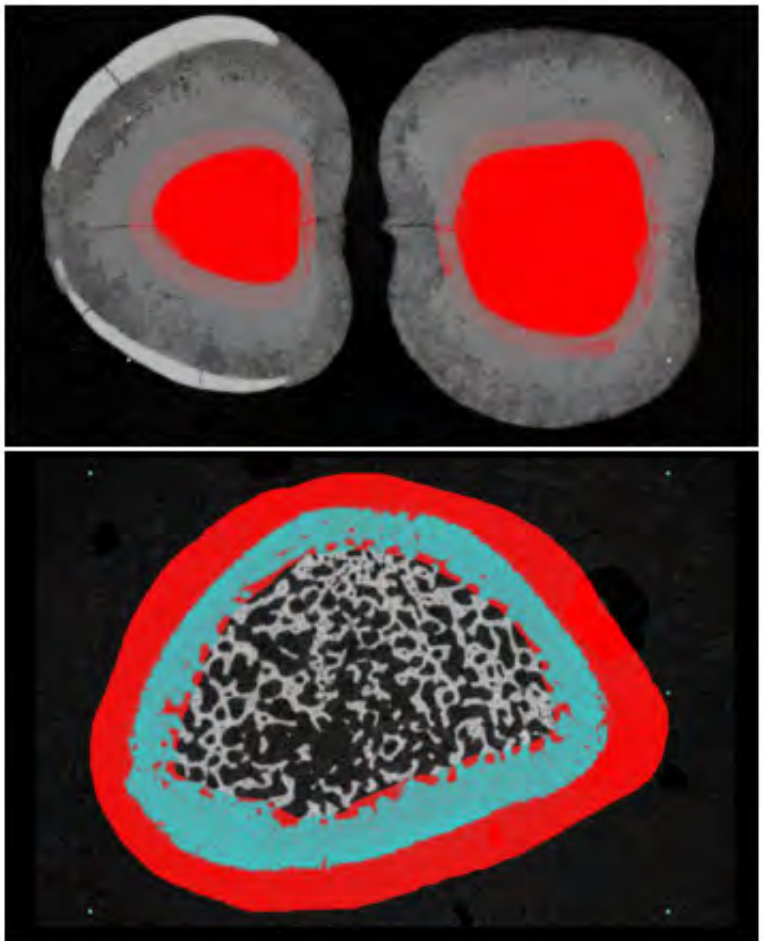

Multiple ROI shapes allow both molar tooth root canals to be delineated (above), and subtractive ROI shape drawing allows a hollow ROI for cortical bone to be drawn (below).

- 3D thickness and separation calculation is now 5-8 times faster than the previous versions.
- Slightly more acccurate
- Tb.Th and Tb.Sp results will be 1-2% different than in previous versions

New Features in “CT Analyzer”

Conditional Mean Filtering

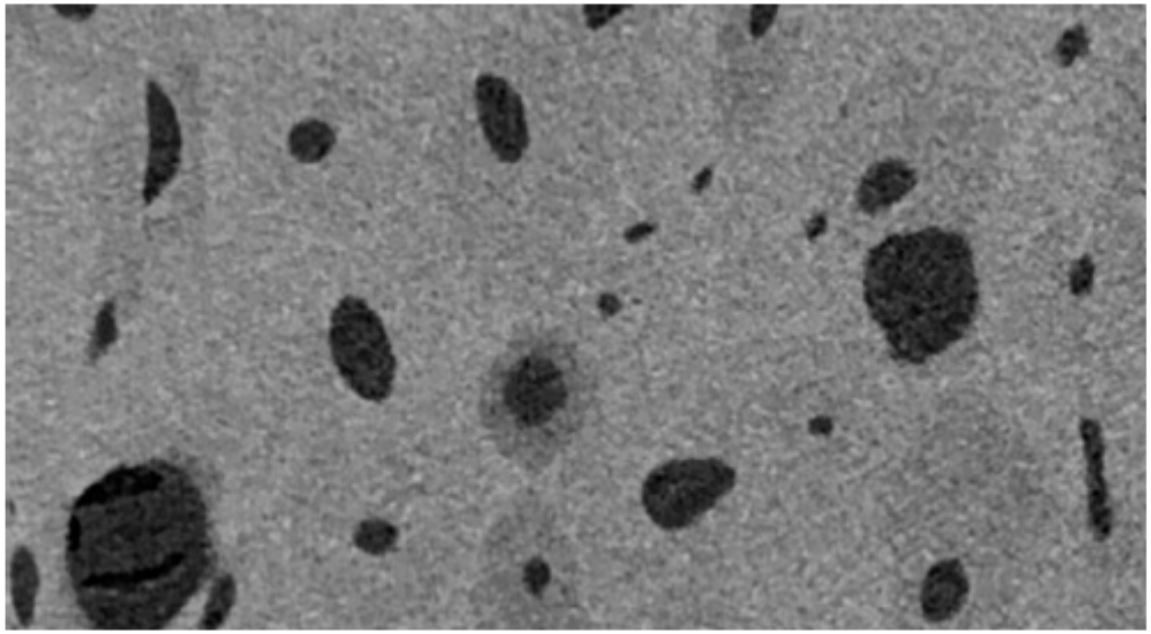

New Features in “CT Analyzer”

Conditional Mean Filtering

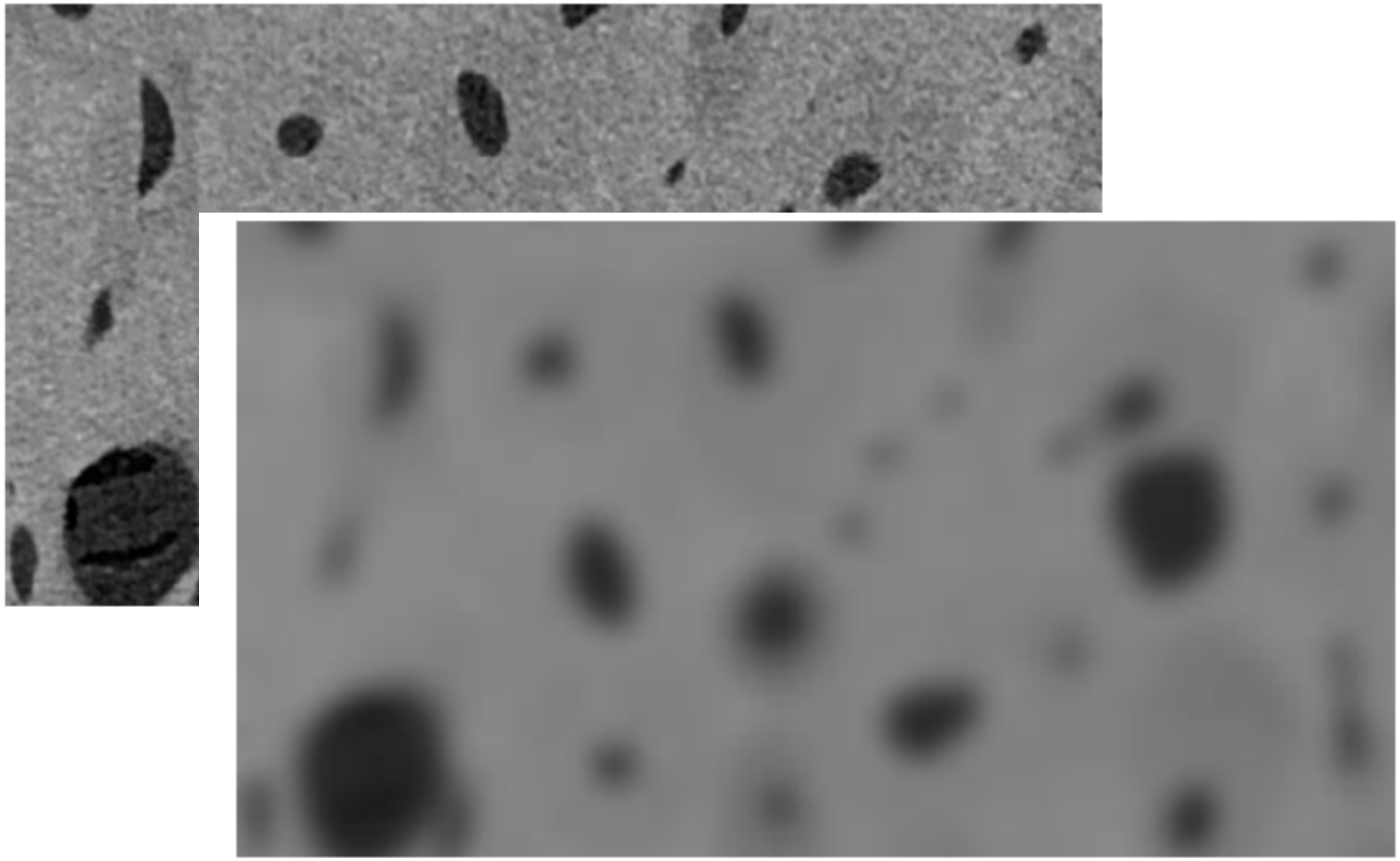

New Features in “CT Analyzer”

Conditional Mean Filtering

Neighboring voxels are smoothed if their greyscale difference is less than a certain value (“threshold“).

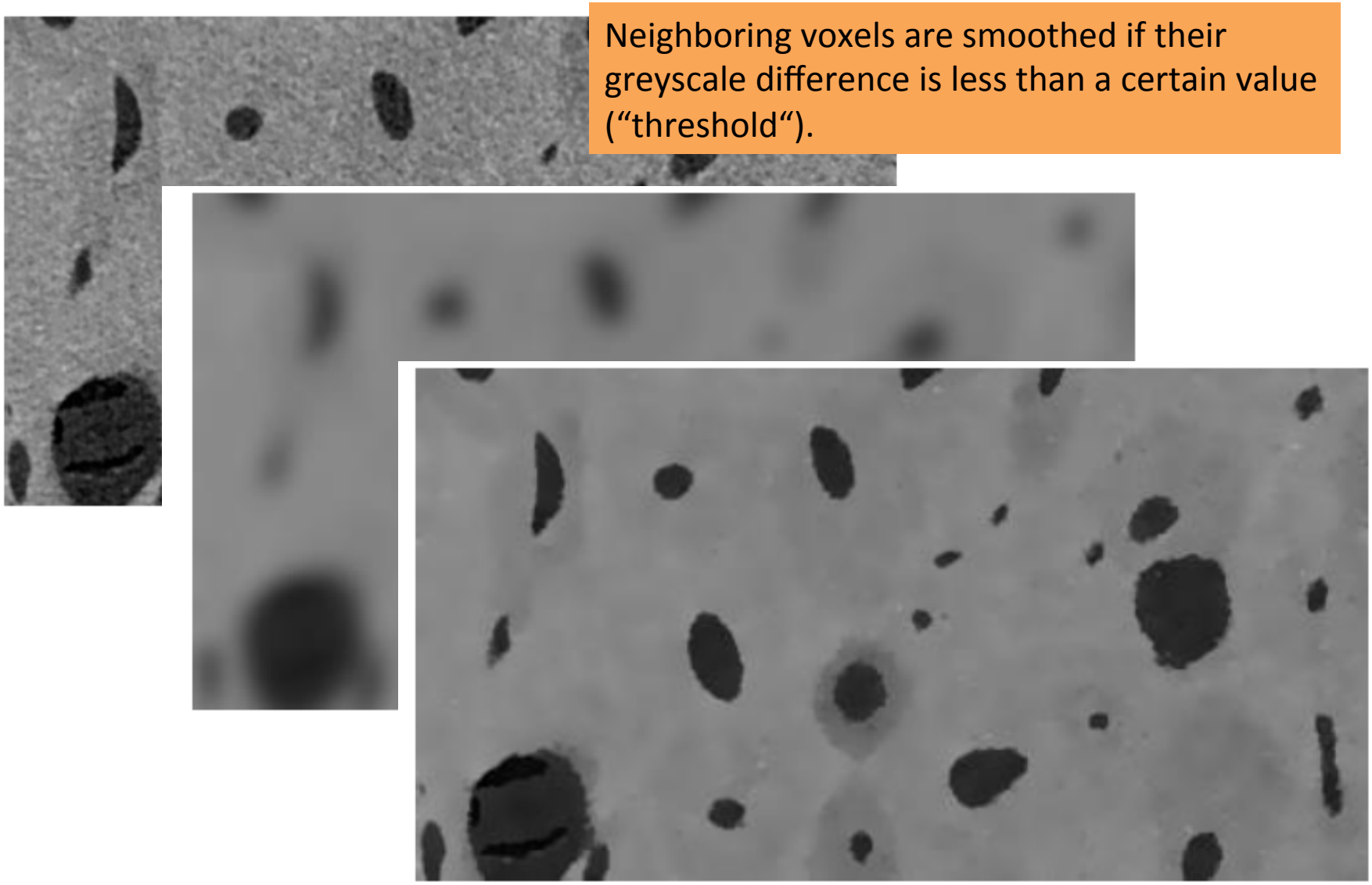

New Features in “CT Analyzer”

“Watershed” Separation

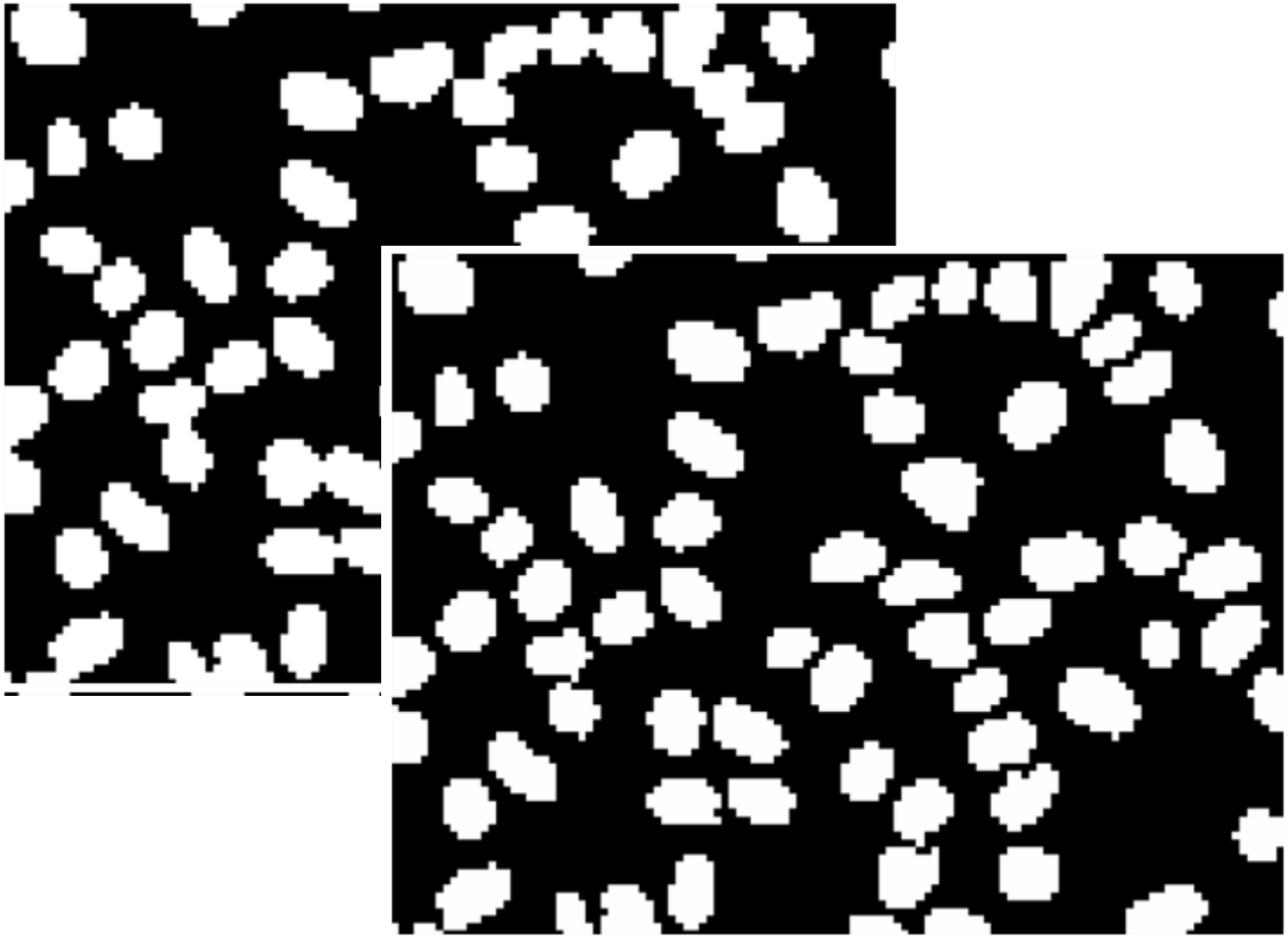

New Features in “CT Analyzer”

“Watershed” Separation

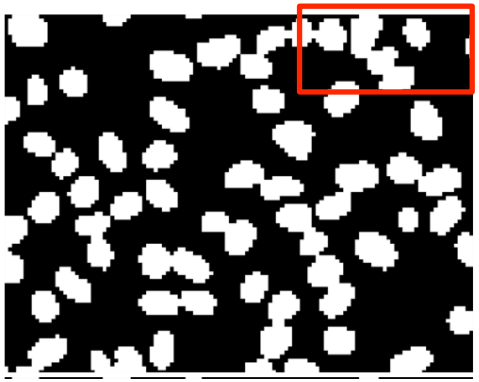

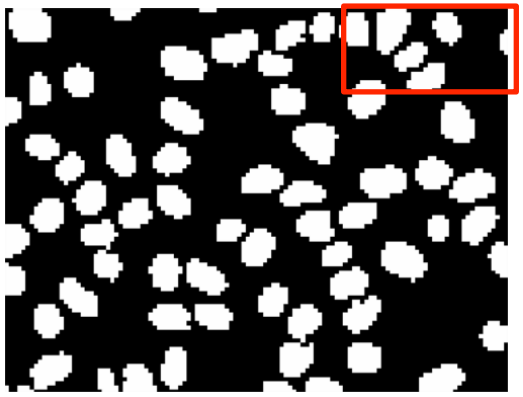

“Collection” Tab

Figure 6. The collections tab allows often-used task lists (e.g. “root canal”) to be available for quick access.

The new, fifth tab is added at the new first tab in the custom processing page. It is titled “collections” and its purpose is to allow the user to keep a list of frequently used task lists on hand for quick and easy call-up. Right-click “edit” on a task list in the collections tab to load it to the Task list tab – which now moves to second place just to the right of the collections tab

New Features in “CT Analyzer”

“Upside Down” Function for Reference Marker

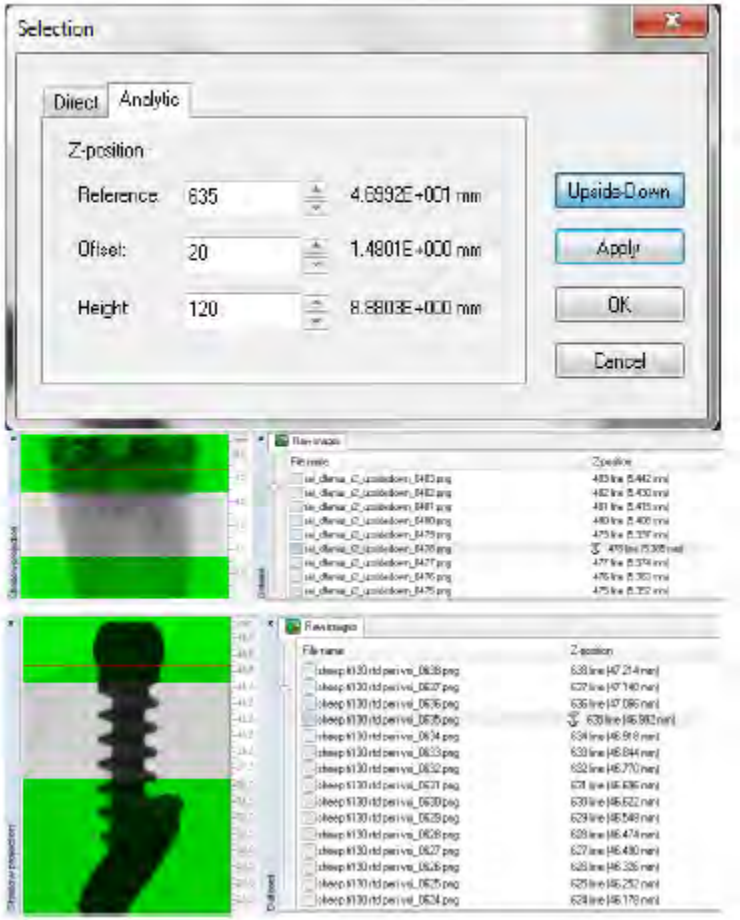

The button “Upside-Down” has been added in order to simplify use of the reference level where the landmark location is above, not below, the selected range of cross-sections in the “Z” (height) axis. VOI for a region of a rat distal femur for trabecular bone analysis, and bone around a metal implant, are selected relative to reference points above the analyzed region (the clear, non-colored band).

Excluding Top and Bottom Surfaces

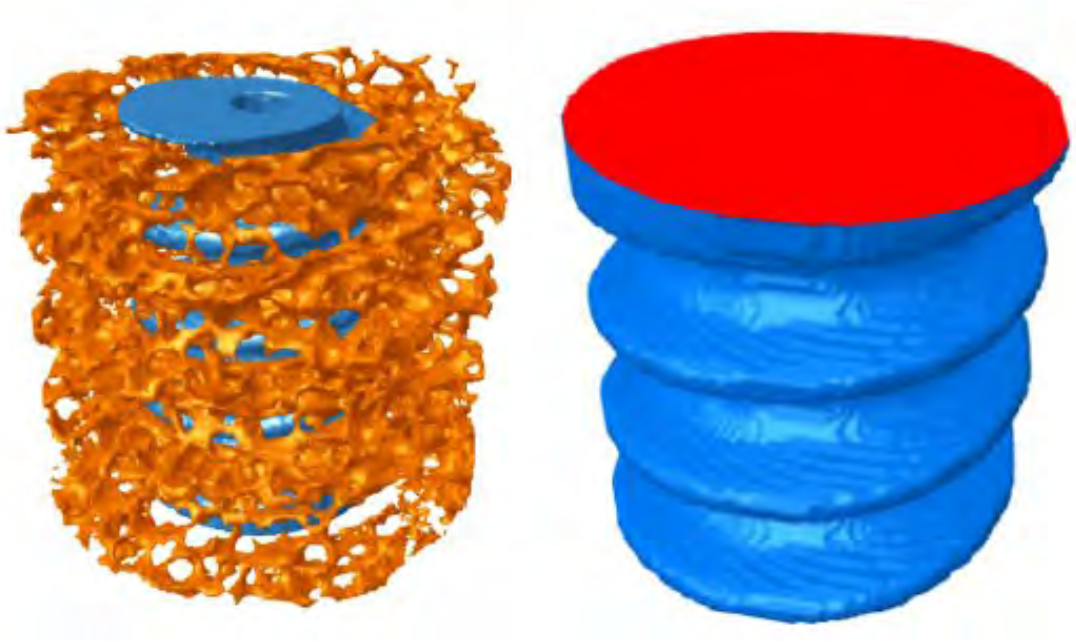

Peripheral object area (exclude VOI boundaries)

In some analyses you need to measure object surface area but exclude surfaces that are artificially cut in the cross-sectional plane by the top and bottom VOI boundaries. An example is the analysis of bone implant contact (BIC) around an orthopedic implant surface

The 2D slice-by-slice analysis not allows both intersection surface (BIC) and object surface to be measured while excluding these artificial cut surfaces.

THANK YOU